Efficacy and safety of metabolic interventions for the treatment of severe COVID-19: in vitro, Observational, and Non-Randomized Open Label Interventional Study

Avner Ehrlich[1,2], Konstantinos Ioannidis[1,2], Makram Nasar[3], Ismaeel Abu Alkian[3], Yuval Daskal[1,2], Nofar Atari[4], Limor Kliker[4], Nir Rainy[8], Matan Hofree[5], Sigal Shafran Tikva[7,8], Inbal Houri[9], Arrigo Cicero[10], Chiara Pavanello[11,12], Cesare R. Sirtori[12], Jordana B. Cohen[13], Julio A. Chirinos[13], Lisa Deutsch[14], Merav Cohen[1,2], Amichai Gottlieb[3], Adina Bar-Chaim[8], Oren Shibolet[9,15], Michal Mandelboim[4,15], Shlomo L. Maayan[3], Yaakov Nahmias[1,2,#]

1. Grass Center for Bioengineering, Benin School of Computer Science and Engineering, Jerusalem, Israel
2. Department of Cell and Developmental Biology, Silberman Institute of Life Sciences, Jerusalem, Israel
3. Division of Infectious Diseases, Barzilai Medical Center Ashkelon, Israel
4. Central Virology Laboratory, Public Health Services, Ministry of Health and Sheba Medical Center, Tel Hashomer, Israel
5. Klarman Cell Observatory, The Broad Institute of Harvard and MIT, Cambridge, MA
6. Hadassah Research and Innovation Center, Jerusalem, Israel
7. Department of Nursing, Faculty of School of Life and Health Sciences, The Jerusalem College of Technology – Lev Academic Center, Jerusalem, Israel
8. Laboratory Division, Shamir (Assaf Harofeh) Medical Center, Zerifin, Israel.
9. Department of Gastroenterology, Sourasky Medical Center, Tel Aviv, Israel
10. IRCSS S.Orsola-Malpighi University Hospital, Bologna, Italy
11. Centro Grossi Paoletti, Dipartimento di Scienze Farmacologiche e Biomolecolari, Università degli Studi di Milano, Milano, Italy
12. Centro Dislipidemie, Niguarda Hospital, Milano, Italy
13. Perelman School of Medicine, University of Pennsylvania, Philadelphia, PA
14. BioStats Statistical Consulting Ltd, Modiin, Israel
15. Sackler Faculty of Medicine, Tel-Aviv University, Tel-Aviv, Israel

Correspondence: ynahmias@cse.huji.ac.il

ABSTRACT

Background: Viral infection is associated with a significant rewire of the host metabolic pathways, presenting attractive metabolic targets for intervention. **Methods:** We chart the metabolic response of lung epithelial cells to SARS-CoV-2 infection in primary cultures and COVID-19 patient samples and perform *in vitro* metabolism-focused drug screen on primary lung epithelial cells infected with different strains of the virus. We perform observational analysis of Israeli patients hospitalized due to COVID-19 and comparative epidemiological analysis from cohorts in Italy and the Veteran's Health Administration in the United States. In addition, we perform a prospective non-randomized interventional open-label study in which 15 patients hospitalized with severe COVID-19 were given 145 mg/day of nanocrystallized fenofibrate added to the standard of care. **Results:** SARS-CoV-2 infection produced transcriptional changes associated with increased glycolysis and lipid accumulation. Metabolism-focused drug screen showed that fenofibrate reversed lipid accumulation and blocked SARS-CoV-2 replication through a PPARα-dependent mechanism in both alpha and delta variants. Analysis of 3,233 Israeli patients hospitalized due to COVID-19 supported *in vitro* findings. Patients taking fibrates showed significantly lower markers of immunoinflammation and faster recovery. Additional corroboration was received by comparative epidemiological analysis from cohorts in Europe and the United States. A subsequent prospective non-randomized interventional open-label study was carried out on 15 patients hospitalized with severe COVID-19. The patients were treated with 145 mg/day of nanocrystallized fenofibrate in addition to standard-of-care. Patients receiving fenofibrate

demonstrated a rapid reduction in inflammation and a significantly faster recovery compared to patients admitted during the same period. **Conclusions:** Taken together, our data suggest that pharmacological modulation of PPARα should be strongly considered as a potential therapeutic approach for SARS-CoV-2 infection and emphasizes the need to complete the study of fenofibrate in large randomized controlled clinical trials. **Funding:** Funding was provided by European Research Council Consolidator Grants OCLD (project no. 681870) and generous gifts from the Nikoh Foundation and the Sam and Rina Frankel Foundation (YN). The interventional study was supported by Abbott (project FENOC0003). **Clinical trial number:** NCT04661930.

INTRODUCTION

The severe acute respiratory syndrome coronavirus 2 (SARS-CoV-2) is a positive-strand RNA virus of the *sarbecovirus subgenus* that is related to SARS. SARS-CoV-2 infection leads to the development of coronavirus disease (COVID-19), an inflammatory lung condition resulting in acute respiratory distress and organ failure [1]. SARS-CoV-2 has infected over 265 million individuals worldwide, causing nearly 5.3 million deaths since its emergence. Like other viruses, SARS-CoV-2 must rely on the host machinery to propagate, rewiring cellular metabolism to generate macromolecules needed for virion replication, assembly, and egress.

Recent work suggests that COVID-19 progression is dependent on metabolic mechanisms. Elevated blood glucose, obesity, and hyperlipidemia were found to be risk factors for SARS-CoV-2-induced acute respiratory distress, independently from diabetes [2,3]. In fact, metabolic risk factors are associated with a more than 3-fold increase in COVID-19 severity risk, whereas inflammatory lung diseases, such as chronic obstructive pulmonary disease (COPD), and asthma are associated with less than a 1.5-fold increase in risk [4,5].

Metabolomics of COVID-19 patient sera showed alterations in circulating amino acids, glucose, and lipids, correlated with changes in inflammation and renal function [6]. Work on SARS-CoV-2 infected monocytes showed raised glycolysis [7,8], whereas proteomics of infected kidney and colon cells showed that SARS-CoV-2 proteins interact with mitochondria, glycolysis, and lipid metabolism [9,10]. Other transcriptional analyses showed SARS-CoV-2 induced significant changes in similar metabolic pathways [11-14]. These results support earlier observations that the closely related SARS and MERS infections are reliant on altered lipid metabolism [15-17]. However, recent clinical studies show conflicting results regarding the role of triglycerides in COVID-19 progression [18-20]. While these data suggest that lipid metabolic interventions should be studied in the context of COVID-19, the current reliance on animal experiments limits such efforts due to critical differences in lipid metabolism between humans and rodents [21,22].

Alarmingly, evidence from previous coronavirus outbreaks suggests that the metabolic rewiring induced by infection has detrimental and long-term effects post-recovery. MERS infection was associated with long-term immune dysregulation and enhanced susceptibility to metabolic diseases [23], while SARS infection was associated with long-term alterations in lipid metabolism, hyperlipidemia, and hyperglycemia even 12 years post-recovery [24,25]. Recent work points to similar post-sequelae effects of COVID-19 [26-28].

In this report, we charted the metabolic response of primary lung bronchiole and small airway epithelial cells to SARS-CoV-2 infection validating our results with multiple COVID-19 patient samples. We demonstrate intracellular lipid accumulation driven in part by the inhibition of PPARα-dependent lipid catabolism. Screening pharmacological modulators of the SARS-CoV-2 metabolic landscape showed that fenofibrate, and other PPARα-agonists that induce lipid catabolism, reversed metabolic changes and blocked SARS-CoV-2 replication *in vitro*. An observational study in 3,233 Israeli patients hospitalized due to COVID-19 was consistent with the *in vitro* observations, showing lower inflammation and faster recovery in patients taking fibrates, while those taking thiazolidinediones that lead to increased lipid accumulation in certain tissues [29-31] exhibited worse outcomes. Additional validation was received by comparative epidemiological analysis from cohorts in Italy and the Veteran's Health Administration in the United States.

Moreover, we performed a prospective non-randomized interventional open-label study in which 15 patients hospitalized with severe COVID-19 were given 145 mg/day of nanocrystallized fenofibrate added to the standard of care. These patients demonstrated a rapid reduction in inflammation and a significantly faster recovery compared to patients admitted during the same period and treated with the same standard-of-care. This work demonstrates that pharmacological modulations of PPARα may be an effective treatment for coronavirus infection. The clinical translation of these findings can only be determined following randomized placebo-controlled clinical studies, which are currently ongoing in several international centers.

METHODS

EXPERIMENTAL MODEL AND SUBJECT DETAILS

Human Subjects

All protocols involving human tissue were reviewed and exempted by the Hebrew University of Jerusalem, the Israeli Ministry of Health, Sheba medical center, and Icahn School of Medicine at Mount Sinai Institutional Review Boards.

Experiments using samples from human subjects were conducted in accordance with local regulations and with the approval of the institutional review board at the Icahn School of Medicine at Mount Sinai under protocol HS#12-00145 and the institutional review board at Sheba medical center under protocol SMC-7875-20.

All procedures performed in studies involving human participants were in accordance with the ethical standards of the institutional and/or national research committee and with the 1964 Helsinki Declaration and its later amendments or comparable ethical standards.
In the observational studies - the Israeli study was approved by the local institutional review board of the Hadassah Medical Center (IRB approval number no. HMO 0247-20) and the local institutional review board of the Ichilov Medical Center (IRB approval number no. 0282-20-TLV). The Italian study was reviewed by the local ethical board (AVEC) of the IRCSS S.Orsola-Malpighi University Hospital (approval number LLD-RP2018).

The interventional study was conducted in accordance with the Good Clinical Practice guidelines of the International Council for Harmonisation E6 and the principles of the Declaration of Helsinki or local regulations, whichever afforded greater patient protection.

The study was reviewed and approved by the Barzilai Medical Center Research Ethics Committee (0105-20-BRZ).

Cell Culture

Normal human bronchial epithelial (NHBE) cells (Lonza, CC-2540 Lot# 580580), isolated from a 79-year-old Caucasian female and were maintained at 37°C and 5% CO_2 in bronchial epithelial growth media (Lonza, CC-3171) supplemented with SingleQuots (Lonza, CC-4175) per manufacturer's instructions. Cells were maintained at the BSL3 facilities of the Icahn School of Medicine at Mount Sinai. NHBE cells (ATCC, PCS-300-010 Lot#63979089; #70002486), isolated from a 69-year-old Caucasian male and a 14-year-old Hispanic male were maintained in airway epithelial cell basal media (ATCC, PCS-300-030) supplemented with Bronchial Epithelial Growth Kit as per the manufacturer's instructions (ATCC, PCS-300-040) at 37°C and 5% CO_2. Cells were maintained at the BSL2 facilities of the Hebrew University of Jerusalem and the BSL-3 facility of the central virology laboratory of the ministry of health and Sheba medical center.

Cells were authenticated at the source and routinely screened for mycoplasma contamination using PCR.

Viruses

SARS-related coronavirus 2 (SARS-CoV-2), Isolate USA-WA1/2020 (NR-52281) was deposited by the Center for Disease Control and Prevention and obtained through BEI Resources, NIAID, NIH. SARS-CoV-2 was propagated in Vero E6 cells in DMEM supplemented with 2% Fetal Bovine Serum (FBS), 4.5 g/L D-glucose, 4 mM L-glutamine, 10 mM Non-Essential Amino Acids (NEAA), 1 mM Sodium Pyruvate, and 10 mM HEPES. Infectious titers of SARS-CoV-2 were determined by plaque assay in Vero E6 cells in Minimum Essential Media (MEM) supplemented with 4 mM L-glutamine, 0.2% Bovine Serum Albumin (BSA), 10 mM HEPES and 0.12% $NaHCO_3$, and 0.7% agar.

Isolate hCoV-19/Israel/CVL-45526-NGS/2020 (alpha) and hCoV-19/Israel/CVL-12806/2021 (delta) were isolated from nasopharyngeal samples of SARS-CoV-2 positive individuals which contained the alpha sub-lineage B.1.1.50 (hCoV-19/Israel/CVL-45526-NGS/2020) and Delta B.1.617.2 (hCoV-19/Israel/CVL-12804/2021) variants by the central virology laboratory of the ministry of health and Sheba medical center. Confluent Vero E6 cells were incubated for one hour at 33ºC with the nasopharyngeal samples, followed by the addition of MEM-EAGLE supplemented with 2% Fetal Bovine Serum (FBS). Upon cytopathic effect detection, supernatants were aliquoted and stored at -80ºC. Infectious titers of SARS-CoV-2 were determined by a 50% endpoint titer (TCID50) for each variant in Vero E6 cells. Approximately 1×10^5 Vero E6 cells were seeded and incubated at 37ºC for 24 hours. At that point, the cells were infected by 10-fold serial dilutions of each variant in MEM-EAGLE supplemented with 2% Fetal Bovine Serum (FBS). A Gentian Violet staining was used to determine the TCID50 of each variant, calculated using the Spearman-Karber method.

All work involving live SARS-CoV-2 was performed in the CDC/USDA-approved BSL-3 facility of the Global Health and Emerging Pathogens Institute at the Icahn School of Medicine at Mount Sinai or in the BSL-3 facility of the central virology laboratory of the ministry of health and Sheba medical center in accordance with institutional and national biosafety requirements

METHODS DETAILS

Analysis of gene expression by RNAseq

Expression count matrices were retrieved from GEO: GSE147507-Series1 (Bronchial; culture), GSE153970 (Small airway; culture), GSE147507-Series15 (Autopsy), GSE145926-(Lavage). Differential gene expression analysis was performed using a Poisson-Tweedie distribution model using the tweeDEseq Bioconductor package [32]. Count data from GEO were normalized using a trimmed-mean of M values (TMM) normalization with the edgeR Bioconductor packages [33]. Data from GSE153970 was previously normalized in GEO and was not further normalized. Genes with the following criteria were considered differentially expressed: (1) P-value adjusted by B&H method FDR < 0.05, (2) A fold change > 1.25, (3) Minimal mean expression > 20 in either condition (**Supplementary Table 2**).

Bronchial culture samples are 3 independent primary normal human bronchial epithelial cultures infected apically with SARS-CoV-2 (USA-WA1/2020; MOI 2) for 24 hours, compared with 3 independent primary normal human bronchial epithelial Mock-infected with PBS for 24 hours.

Small airway culture samples are 3 independent primary human airway epithelial cultures infected apically with SARS-CoV-2 (MOI 0.25) for 48 hours, compared with 3 independent primary human airway epithelial cultures Mock-infected with PBS for 48 hours.

The autopsy samples are of two old (age > 60) unidentified COVID-19 human subjects, who died due to COVID-19, had autopsy biopsy tissue acquisition post-mortem in Weill Cornell Medicine, and were provided as fixed samples for RNA extraction; the samples were compared with two old (age > 60) unidentified human biopsy lung samples, taken during lung surgery and stored at Mount Sinai Institutional Biorepository and Molecular Pathology Shared Resource Facility (SRF) in the Department of Pathology, similarly provided as fixed samples for RNA extraction.

COVID-19 patients' lung epithelial cells are bronchoalveolar lavage fluid isolates from one severe case and five critical cases. The median age of the patients was 62.5 years, and the participants included four male and two female patients. All patients had Wuhan exposure history and had a cough and/or fever as the first symptom. Diagnosis of SARS-CoV-2 was based on clinical symptoms, exposure history, chest radiography, and SARS-CoV-2 RNA-positive using commercial quantitative PCR with reverse transcription (qRT–PCR) assays. The samples were compared to three healthy donor controls. The median age was 24 years, and the participants included one female and three male patients. These donors were confirmed to be free of tuberculosis, tumor, and other lung diseases through CT imaging and other laboratory tests.

Analysis of Canonical Splice Variants

Reads were downloaded from SRA (GSE147507), and filtered and trimmed to remove low-quality reads and sequencing artifacts with fastp v20 [34] (https://github.com/OpenGene/fastp.git). Reads were pseudoaligned to the GRCh38 genecode human transcriptome (GRCh38.p13, version 32) using Kallisto version 0.46.1 [35] (https://github.com/pachterlab/kallisto) run with the default k-mer length of 31, in single-read, single-overhang mode, with fragment mean length of 400 and 100 SD. Differentially

expressed transcripts/genes were identified using Sleuth based on a likelihood ratio test comparing the condition of interest and 100 Kallisto bootstrap samples.

Assembly of Metabolic Categories

Aggregate metabolic categories were created as previously described [36]. Briefly, functional annotation gene-sets, taken from GO and KEGG, were merged into a set of glucose, lipid, mitochondrial, and amino acid gene-sets.

Processing, Analysis, and Graphic Display of Genomic Data

Hierarchical clustering, heat maps, correlation plots, and similarity matrices were created in Morpheus. Gene ontology enrichment analyses and clustering were performed using DAVID Informatics Resources 6.7 [37] and PANTHER Classification System [38]. Metabolic network maps were created using McGill's Network Analyst Tool using the KEGG database [39].

Quantification of Intracellular Glucose

To detect glucose uptake, we used 2-(N-(7-Nitrobenz-2-oxa-1,3-diazol-4-yl) Amino)-2-Deoxyglucose (2-NDBG) a fluorescent analog of glucose (Invitrogen, USA; N13195). 2-NDBG is transported through SGLT-1 and GLUT-2. Increased uptake leads to 2-NDBG accumulation in the cells. Cells infected with SARS-CoV-2 for 96 hours were exposed to 6 mM of 2-NDBG for 24 hours. Cells were then fixed, counterstained with 1 µg/mL Hoechst 33258. Staining intensity was normalized to Hoechst 33258 across multiple fields of view.

Quantification of Lipids

Lipid accumulation was measured using HCS LipidTOX™ Phospholipidosis and Steatosis Detection Kit according to the manufacturer's instructions (ThermoFisher, USA; H34158). Briefly, cells were incubated in complete bronchial epithelial growth media supplemented with 1x phospholipidosis detection reagent for 48 hours. Cells were subsequently fixed in 4% PFA and stained with 1X neutral lipid detected reagent for 30 min and counterstained with 1 µg mL-1 Hoechst 33258. Staining intensity was normalized to the amount of Hoechst 33258 positive nuclei across multiple fields of view.

Metabolic Analysis of Glucose, Lactate, and Glutamine

Metabolic analysis of SARS-CoV-2 infected culture media in the BSL3 facility was done using Accutrend Plus multiparameter meter (Roche Diagnostics). Culture media was collected every 48 hours and stored at -80 ºC prior to analysis. Measurements were carried out using Accutrend Plus Glucose and BM-Lactate Test Strips according to the manufacturer's instructions. Each measurement was done in 3 technical measurements for each sample, validated throughout the process using calibration media. Glucose uptake, as well as lactate production, were calculated based on the difference between sample and control media.

Metabolic analysis of SARS-CoV-2 proteins expressing culture media in the BSL2 facility was done using amperometric glucose, lactate, and glutamine sensor array (IST, Switzerland) as previously described [40]. Each measurement was done in 3 technical measurements for each

sample, calibrated periodically throughout the process using calibration media, according to the manufacturer's recommendations. Glucose and Glutamine uptake, as well as lactate production, were calculated based on the difference between sample and control media.

Generation Lentiviral SARS-CoV-2 Constructs

Plasmids encoding the SARS-CoV-2 open reading frames (ORFs) and eGFP control are a kind gift of Nevan Krogan (Addgene plasmid #141367-141395). Plasmids were acquired as bacterial LB-agar stabs and used per the provider's instructions. Briefly, each stab was first seeded into agar LB (Bacto Agar; BD, USA) in 10 cm plates. Then, single colonies were inoculated into flasks containing LB (BD Difco LB Broth, Lennox; BD, USA) and 100 µg/ml penicillin (BI, Israel). Transfection-grade plasmid DNA was isolated from each flask using the ZymoPURE II Plasmid Maxiprep Kit (Zymo Research, USA) according to the manufacturer's instructions.

HEK 293T cells (ATCC, USA) were seeded in 10 cm cell culture plates at a density of $4x10^6$ cells/plate. The cells were maintained in 293T medium composed of DMEM high glucose (4.5 g/l; Merck, USA) supplemented with 10% FBS (BI, Israel), 1x NEAA (BI, Israel), and 2 mM L-alanine-L-glutamine (BI, Israel).

The following day, cells were transfected with a SARS CoV 2 orf-expressing plasmid and the packaging plasmids using the TransIT-LT1 transfection reagent (Mirus Bio, USA) according to the provider's instructions. Briefly, 6.65 µg SARS CoV 2 lentivector plasmid, 3.3µg pVSV-G, and 5µg psPAX2 were mixed in Opti-MEM reduced serum medium (Gibco, USA), with 45µl of TransIT-LT1, kept at room temperature to complex and then added to each plate. Following 18h of incubation, the transfection medium was replaced with 293T medium and virus-rich supernatant was harvested after 48h and 96h. The supernatant was clarified by centrifugation (500×g, 5 min) and filtration (0.45 µm, Millex-HV, MerckMillipore). All virus stocks were aliquoted and stored at -80°C.

The packaging plasmids (psPAX2 and pVSV-G) are a kind gift from Prof. N. Benvenisti, Stem Cell Unit at the Hebrew University, Jerusalem, Israel.

SARS-CoV-2 Proteins Lentiviral Transduction

Approximately 1×10^5 cells were infected in two consecutive sessions of 12h each. A 50% dilution of the viral stock was used in both for a final transduction efficiency of about 60%. Transduction efficiency was validated by microscopy of the eGFP transduced culture.

Metabolic Flux Quantification (Seahorse)

Mitochondrial Stress Test (Agilent; 103010-100) assay was conducted per manufacturer instructions as previously described [36]. Briefly, cells were incubated in unbuffered DMEM supplemented with 2 mM glutamine, 1 mM sodium pyruvate, and 10 mM glucose (pH 7.4) for 1 hour at 37°C in a non-CO_2 incubator. Basal oxygen consumption rate (OCR) was measured for 30 min, followed by injection of 1.5 µM oligomycin, a mitochondrial Complex V inhibitor that blocks oxidative phosphorylation. The decrease in OCR due to oligomycin treatment is defined as the oxidative phosphorylation rate. 0.5 µM carbonyl cyanide-4 (trifluoromethoxy) phenylhydrazone (FCCP), an uncoupling agent, is added at 60 min to

measure maximal mitochondrial activity followed by complete inhibition at 90 min using a mixture of 0.5 μM antimycin A and rotenone, mitochondrial Complex III and Complex I inhibitors.

Free fatty acid oxidation was measured using XF Long Chain Fatty Acid Oxidation Stress Test Kit (Agilent; 103672-100) as previously described [36]. Briefly, cells were incubated overnight in a substrate-limited medium containing 0.5 mM glucose, 1 mM glutamine, and 0.5 mM L-Carnitine to prime cells for exogenous fatty acid utilization. Basal OCR was measured in the presence of BSA-palmitate (C16:0) or BSA-control for 30 minutes, followed by sequential exposure to 4 μM etomoxir, a carnitine palmitoyltransferase I (CPT1) inhibitor, or medium, 1.5 μM oligomycin, 0.5 μM carbonyl cyanide-4 (trifluoromethoxy) phenylhydrazone (FCCP), and a mixture of 0.5 μM antimycin A and rotenone at 30-minute intervals. Free fatty acid oxidation capacity was defined as the difference between spare capacity by etomoxir-treated and untreated conditions.

Generation PPARα CRISPR knock-out cells

The PPARα knock-out cells were created using a Cas9-based, CRISPR system. Two different sgRNA oligos from the human GeCKO v.2 Human CRISPR Knockout Pooled Library (Addgene; #1000000048), PPARa HGLibA_37838 and HGLibB_37787, were cloned into the lentiCRISPR v2 plasmid (Addgene; #52961). The sgRNA cloning was performed according to the human GeCKO v.2 system instructions as previously described [41]. Briefly, two oligos comprising each sgRNA insert were synthesized with BsmBI-compatible ends, and the vector plasmid was digested with BsmBI (FastDigest Esp3I, FD0454, Thermo), de-phosphorylated (FastAP thermosensitive alkaline phosphatase, EF0651, Thermo), and gel extracted (QiaQuick gel extraction, Qiagen). The sgRNA oligos were phosphorylated and annealed in a single session: first phosphorylation using T4 PNK (NEB-M0201S) followed by heating to 95°C for 5min and controlled cooling to allow annealing. The vector and insert fragments were ligated (T4 DNA ligase, EL0011) and transformed into chemically competent Stbl3 cells (Mix & Go! E.coli Transformation Kit, T3001, Zymo). Correctly ligated plasmids were used for lentiviral sgRNA vector production, as described before [41] . Approximately 1×10^6 cells were infected in two consecutive sessions of 12h each. The cells were then selected using 3 μM puromycin for 72 hours (Merck; P9620).

The lentiCRISPR v2 plasmid is a kind gift from Prof. N. Benvenisti, Stem Cell Unit at the Hebrew University, Jerusalem, Israel.

RNA-Seq of Viral Infections

Approximately 1×10^5 NHBE cells were infected with SARS-CoV-2 at a MOI of 2 (USA-WA1/2020) or TCID100 (hCoV-19/Israel/CVL-45526-NGS/2020 and hCoV-19/Israel/CVL-12806/2021) for 24 h in complete bronchial epithelial growth media. Total RNA from infected and mock-infected cells was extracted using TRIzol Reagent (Invitrogen) and Direct-zol RNA Miniprep kit (Zymo Research) according to the manufacturer's instructions and treated with DNase I. RNA-seq libraries of polyadenylated RNA were prepared using the TruSeq RNA Library Prep Kit v2 (Illumina) according to the manufacturer's instructions. RNA-seq libraries for total ribosomal RNA-depleted RNA were prepared using the TruSeq

Stranded Total RNA Library Prep Gold (Illumina) according to the manufacturer's instructions. cDNA libraries were sequenced using an Illumina NextSeq 500 platform**.**

Viral Load by Quantitative Real-Time PCR Analysis

In BSL3 experiments conducted in the BSL-3 facility at the Icahn School of Medicine at Mount Sinai, Genomic viral RNA was extracted from supernatants using TRIzol reagent according to the manufacturer's instructions (Thermo Fisher). RNA was reverse transcribed into cDNA using oligo d(T) primers and SuperScript II Reverse Transcriptase (Thermo Fisher). Quantitative real-time PCR was performed on a LightCycler 480 Instrument II (Roche) using KAPA SYBR FAST qPCR Master Mix Kit (KAPA biosystems) and primers specific for the SARS-CoV-2 nsp14 transcript as described previously [42,43]. The viral load for each sample was determined using genomic viral RNA purified from viral stocks to generate a standard curve. Error bars indicate the standard error from three biological replicates.

In BSL3 experiments conducted in the BSL-3 facility at the Sheba medical center, Total nucleic acids were extracted from all samples using MagNA Pure 96 DNA and Viral NA Small Volume Kit (Roche) according to the manufacturer protocol. Extracted RNA was transferred to 96 well PCR plate containing 20ul of TaqPath™ 1-step Multiplex Master Mix No ROX (Applied Bioscience, Cat number: A28523). This was followed by a one-step RT-PCR (TaqPath COVID-19 assay kit; Thermo-Fisher). Thereafter, the plate was sealed with MicroAmp clear adhesive strip (Applied Bioscience, Cat number: 4306311). The plate was loaded onto a QuantStudio™ 5 Real-Time PCR System (Applied Bioscience, Cat number: AB-A28574) and the following amplification program was used: 25°C for 2 minutes, X1 cycle 53°C for 10 minutes, X1 cycle 95°C for 2 minutes, X1 cycle 95°C for 3 seconds, followed by 60°C for 30 seconds, X40 cycles Ct threshold values were presented using the following values/parameters: MS2-15,000; by cycle 37; S gene- 20,000 by cycle 37; Orf1ab-20,000 by cycle 37; Ngene- 20,000 by cycle 37. Samples that passed the Threshold is a Ct value >37 were re-tested or considered weak positive. The viral load for each sample was determined using genomic viral RNA purified from viral stocks to generate a standard curve. Error bars indicate the standard error from three biological replicates.

Assembly of Metabolic Categories

Aggregate metabolic categories were created as previously described [36]. Briefly, functional annotation gene-sets, taken from GO and KEGG, were merged into a set of glucose, lipid, mitochondrial, and amino acid gene-sets.

Functional Annotations of Gene Expression

Differentially expressed genes were tested for enrichment overlap within functional gene sets. The general test for functional enrichment of the differentially expressed genes against various functional categories was done using the PANTHER tool [38]. Enrichment P values were calculated using Fisher's exact test and corrected with familywise (Bonferroni) multiple testing correction or the Benjamini-Hochberg False discovery method as indicated.

Drug Treatments

Approximately 5×10^5 NHBE or PPARα CRISPR-KO NHBE cells were infected with SARS-CoV-2. After 24h, the media was collected and changed to bronchial epithelial growth

media supplemented with 0.1% DMSO (vehicle control), 10 μM Cloperastine (Merck; C2040), 5 μM Empagliflozin (AG-CR1-3619), 1 mM Metformin (Merck; 317240), 20 μM Fenofibrate (Merck; F6020), 20 μM Rosiglitazone (Merck; R2408), 50 μM Bezafibrate (Merck; B7273), 2 μM Wy-14643 (Cayman Chemical; 70730), 50 μM Conjugated (9Z,11E)-Linoleic acid (Merck; 16413) in 50 μM Oleic Acid-Albumin (Merck; O3008) or 20 μM Fenofibrate and 4 μM Etomoxir (Cayman Chemical; 11969). Then, every 48 hours media was collected and replenished. The media was stored at -80ºC immediately after removal. Culture viability was assessed at the end of the experiment using Hoechst staining, compared with mock-infected cells.

Western blot

NHBE, PPARα CRISPR-KO NHBE cells or PPARα-OE HEK293T cells were washed in DPBS, lysed in 1x Laemmli Loading buffer, and boiled at 100ºC; 40 μl of cleared lysate were analyzed in a pre-cast gradient polyacrylamide gel (Bolt™ 4 to 12%, Bis-Tris, 1.0 mm, Mini Protein Gel/ NW04120BOX, Invitrogen) using SeeBlue™ Plus2 Pre-stained Protein Standard (LC5925, Invitrogen) in MES SDS running buffer (B0002, Invitrogen) according to manufacturer's instructions. The proteins were transferred to a PVDF membrane (iBlot™ 2 Transfer Stacks, PVDF, mini/ IB24002, Invitrogen) using iBlot2 (LifeSciences). The membrane was blocked with 5% BSA (160069, MPBio) in Tris-buffered saline plus 0.1% Tween 20 (TBST) for 1 h at room temperature. The membranes were incubated in primary antibodies overnight at 4 °C. The next day, the membranes were washed in TBST (3 × 10 min) and then incubated with horseradish peroxidase-conjugated secondary antibody for 2 h at room temperature. After the TBST washes (4 × 10 min), EZ-ECL kit (Sartorius; 20-500-1000A, 20-500-1000B) was used to detect the HRP activity. The membrane was imaged on a Vilber Fusion FX and band densitometry was performed on FIJI.

The following commercial primary antibodies were used: anti-PPARα (1:1000;ab24509, Abcam) and anti-α-tubulin (1:2000; T6074, Sigma). Commercial horseradish peroxidase--conjugated secondary antibodies were: anti-rabbit (111-035-003, Jackson) and anti-mouse (115-035-003, Jackson). All primary antibodies were used in 5% BSA in TBST. Secondary antibodies were used at a 1:8,000 dilution in TBST.

The gel, ladder, and equipment to run and transfer the gel were kindly provided by Prof. Eran Meshorer, Institute of Life Sciences, Hebrew University of Jerusalem. The anti-tubulin and both HRP conjugated antibodies, as well as the HRP detection kit, were kindly provided by Prof. Benjamin Aroeti, Institute of Life Sciences, Hebrew University of Jerusalem.

Quantification and Statistical Analysis

Work done in the BSL-3 facility at the Icahn School of Medicine at Mount Sinai was done on NHBE from a single donor, repeated in 3 experimental repeats with 3 or more technical repeats in each experiment. Work done in the BSL-3 facility at the Sheba medical center or in the BSL2 facility at the Hebrew University of Jerusalem was done on NHBE from two donors, repeated in 3 experimental repeats each (unless noted otherwise by the n value) with 3 or more technical repeats in each experiment. Work done in the BSL-3 facility at the Sheba medical center in different variants was done separately and independently for each variant and repeated as listed above.

Measurements were technically repeated 3 or 4 times for each sample, images were analyzed with 5 or more fields of view; Graphs show mean ± SEM; Continuous variables were compared with a Mann-Whitney U test or a two-sample t-test or ANOVA. Categorical variables were compared with a chi-squared or Fisher's exact test, as appropriate. FDR correction was used to adjust for multiple comparisons and RNA seq comparisons; Hypergeometric testing was used to assess statistically significant enrichments. * indicates $p < 0.05$, ** indicates $p < 0.01$, *** indicates $p < 0.001$, unless denoted otherwise**.**

OBSERVATIONAL STUDIES

Israeli Study

A retrospective, multi-center study was conducted in Hadassah and Ichilov medical centers. A total of 150,976 participants were diagnosed positive for SARS-COV-2 following WHO interim guidance (World Health Organization, 2020). Only patients hospitalized and diagnosed with COVID-19 were included. participants with incomplete electronic medical records, aged less than 18, with pregnancy or severe medical conditions, including acute lethal organ injury (i.e., acute coronary syndrome, acute stroke, and severe acute pancreatitis) were excluded. The flowchart for patient inclusion is illustrated in Supplementary **Figure S6**. Participants were admitted between March 1st, 2020, and January 31st, 2021 to either the Hadassah Medical Center in Jerusalem or the Tel Aviv Sourasky Medical Center. The final date of the follow-up was February 28th, 2021. The study protocols were approved by the institutional ethics committee. Patient informed consent was waived by each ethics committee. Demographic and clinical characteristics, vital signs, laboratory tests, medical history and comorbidities, therapeutic interventions, and outcome data were extracted from electronic medical records using a standardized data collection method. The laboratory data included routine blood tests, blood counts, and serum biochemical markers reflecting c-reactive protein, sepsis, liver injury, kidney injury, cardiac injury, glycemic status, and D-dimer were collected during hospitalization. In-hospital medication and respiratory intervention included the classification of the drugs, the dosage, the course of treatment, and using respiratory support were also extracted from medical records.

The retrospective study was designed to assess initial relationships between metabolic regulating drug use and COVID-19 clinical outcomes (28-day mortality and duration of hospitalization, ICU admission, mechanical ventilation, oxygen supplementation, disease severity at baseline, and inflammatory marker changes) versus a control group that did not take any drug of this type.

COVID-19 poses a significant risk in older patients and patients with comorbidities [44]. Hence, to account for the fact that metabolic drug users were older and had more comorbidities, we included metabolic regulating drug users and patients over 45 in the comparative analyses, creating a more comparable control group suitable for the between-treatment evaluations, as previously described [45]. Propensity score matching was avoided in this multi-drug comparison as it has been shown to increase model imbalance, inefficiency, model dependence, and bias in multiple group comparisons in small treatment groups. Significant differences in treatment group size and characteristics are expected to result in an underestimation of treatment effect and a high level of overt bias [46-49].

Comparisons were conducted between hospitalized COVID-19 patients using one or more metabolic regulating drugs (fibrates, thiazolidinediones, metformin, SGLT2 inhibitors,

statins, or telmisartan (IRE1α inhibitor)) versus control patients not taking any metabolic regulating drugs. Baseline values are defined as measurements taken upon hospital admission. Statistical analyses were performed using SAS® v9.4 (SAS®, SAS Institute Cary, NC USA) software and R-3.6.3 (R Foundation for Statistical Computing, Vienna, Austria). Continuous variables were summarized by a median and interquartile range (IQR) and categorical variables by a count and percentage. Statistical testing was two-sided. A p-value < 0.05 was considered statistically significant. Missing data was not imputed. Nominal p-values are presented since this was an exploratory study. Demographic and baseline clinical characteristics, comorbidities, and laboratory examinations, as well as initial univariate clinical outcomes, were compared between the groups (drugs versus no drugs) by data type using a two-sample t-test or Fisher's exact test as appropriate.

The relative risk of hospitalization, ICU admission, and 28-day all-cause-mortality of COVID-19 patients versus the general hospital population (1-year period, 5-year period, and 10-year period prior to study start date in patients 30 years and older) are presented with 95% confidence interval and level of significance (Wald test).

Dynamic changes of inflammatory markers were depicted using locally weighted scatterplot smoothing (Lowess) plotting [50] from day 1 to day 21 after admission, comparing each drug group to control patients that did not take metabolic regulators.

Time-to-event data is presented with Kaplan-Meier plots. Time-to-events are measured in days from the date of hospital admission to the date of in-hospital death, and release from the hospital or last follow-up or 28 days whichever is sooner. Cox regression was performed to compare time-to-event data between the groups adjusting for covariates that may have been imbalanced between the groups. We did not perform matching since Cox regression models applied to the entire study cohort can effectively address confounding attributable to observed covariates and maximize power by using all data available. Hazard ratios are comparing drug to control group, adjusted for covariates (age, sex, current smoker, asthma, chronic obstructive pulmonary disease, cerebrovascular accident, chronic heart disease, chronic liver disease, chronic kidney disease, obesity, diabetes, hypertension, and dyslipidemia) with a level of significance and 95% confidence interval. In cases of monotone likelihood (non-convergence of likelihood function), Firth's penalized maximum likelihood bias reduction method for Cox regression was implemented. Cox Regression with Firth's Penalized Likelihood has been shown to provide a solution in the case of monotone likelihood (non-convergence of likelihood function) and was shown to outperform Wald confidence intervals in these cases [51].

Italian Study

A validation study was conducted by phone interviews of the last 2,123 patients examined in the Outpatient Lipid Clinics of the University of Bologna and of the Niguarda Hospital in Milan during the last 12 months and on adequately dosed statins, fenofibrate, or both for at least three months. We excluded patients on lipid-lowering nutraceuticals (including polyunsaturated fatty acids), very low-dose or alternate-day statins, ezetimibe alone, PCSK9 inhibitors, and those on fibrates other than fenofibrate, in order to reduce the heterogeneity of the sample. Data were sampled based on comorbidities (obesity, chronic obstructive pulmonary disease, cardiovascular disease, managed as dummy variables), personal COVID history and severity, and contact with people affected by COVID. The study was carried out in adherence with the declaration of Helsinki. All participants were fully informed of the

objectives of the questionnaire and gave their oral authorization to use their data for research purposes. The telephone calls were recorded. Age was compared between groups with ANOVA followed by post-hoc testing using Tukey's method. Percentages were compared by a Chi-square test followed by Fisher's exact test.

US Study

A validation study was conducted using an existing observational cohort of 920,922 veterans with hypertension (defined by diagnostic codes for hypertension and at least two fills for antihypertensive medications from January 1, 2020, to October 25, 2020, and restricted to those veterans with evidence of using the Veterans Health Administration for their primary care). There were 5,144 (0.6%) veterans in the cohort who tested positive for SARS-CoV-2 between March 14, 2020, and October 25, 2020. Medication use was determined by confirmed pharmacy fills. The cohort contained a diverse, non-homogenous patient population with different disease severity. To minimize baseline differences between fenofibrate users and the three comparison groups (non-users, statin users, and TZD users), 1:5 propensity score matching was performed using Stata version 15.0. Baseline matching variables included age, sex, body mass index, race/ethnicity, and history of atherosclerotic cardiovascular disease, heart failure, diabetes mellitus, chronic lung disease, chronic liver disease, dementia, and current or former smoker. We performed nearest neighbor matching with a caliper of 0.1. We required a <10% standardized difference in each of the matched covariates between matched groups, as well as Rubin's B of ≤25% and Rubin's R between 0.5-2 to verify sufficient matching.

INTERVENTIONAL STUDY

Design and participants

The study was conducted as an open-label, phase 3a clinical trial, in the Barzilai Medical Center, Ashkelon, Israel. The study was approved by the Barzilai Medical Center Research Ethics Committee (0105-20-BRZ). The study enrolled adults (≥18 years of age) with severe Covid-19 pneumonia, as confirmed by positive polymerase-chain-reaction (PCR) and evidenced by bilateral chest infiltrates on chest radiography or computed tomography. Eligible patients had a disease severity score of 4 (Hospitalized, requiring supplemental oxygen), increased oxygen requirement compared to baseline at home, a blood oxygen saturation of 93% or less on room air, or a ratio of the partial pressure of oxygen to the fraction of inspired oxygen (PaO2/FiO2) of less than 300 mm Hg, respiratory rate >30 breaths/min, and lung infiltrates >50% on chest CT within 72 hours of hospital admission or within 72 hours of a positive test result.

Individuals who had respiratory failure, septic shock, and/or multiple organ dysfunction, SOFA >=5 or Disease Severity Score <=3 (requiring noninvasive mechanical ventilation, requiring extracorporeal membrane oxygenation (ECMO), invasive mechanical ventilation, or all) were excluded. Additionally, individuals with known hypersensitivity to fenofibrate, patient-reported history, or electronic medical record history of severe kidney disease (defined as any history of dialysis, history of chronic kidney disease stage IV or estimated Glomerular Filtration Rate (eGFR) of < 30ml/min/1.73 m2 at the time of enrollment), acute pre-renal azotemia at the time of enrollment in the opinion of the investigator or bedside clinician, most recent mean arterial blood pressure prior to enrollment <65 mmHg, patient-reported history or electronic medical record history of severe liver disease (defined as

cirrhosis, history of hepatitis B or C or documented AST or ALT > 10 times the upper limit of normal measured within 24 hours prior to enrollment), patient-reported history or electronic medical record history of gallbladder disease, potassium >5.0 within 24 hours prior to enrollment (unless a repeat value was <=5.0), treatment with coumarin anticoagulants, immunosuppressants or bile acid resins or female subjects breastfeeding or undergoing fertility treatments were also excluded.

All participants provided written informed consent signed by the participant or legally authorized representative. Standard care according to local practice (supplemental oxygen, antiviral treatment, anticoagulants, vitamin D3, low-dose glucocorticoids, convalescent plasma, and supportive care) was provided. However, concomitant treatment with another investigational agent (except antiviral drugs) or any immunomodulatory agent, was prohibited. Written informed consent was obtained from all the patients or, if written consent could not be provided, the patient's legally authorized representative could provide oral consent with appropriate documentation by the investigator. The primary analysis was performed on day 14, a follow-up was done 28 days post-admission.

Procedures

Participants who met the inclusion criteria were assigned to intervention with nanocrystallized fenofibrate (TriCor®, AbbVie Inc., North Chicago, IL USA) at a dose of 145 mg (1 tablet) once per day. Standard care for severe-hospitalized COVID-19 patients was provided according to local practice: antiviral treatment, vitamin D3, low-dose glucocorticoids, convalescent plasma, and supportive care as well as antipyretics for symptoms of fever (products containing paracetamol, or non-steroidal anti-inflammatories such as aspirin and ibuprofen) and dextromethorphan for symptoms of cough. Standard chronic treatments were continued unless COVID-19, clinical status, or fenofibrate treatment was a contraindication for treatment. Control patients were collected from the observational study's database and filtered to patients that met the inclusion criteria, admitted with low immunoinflammatory stress (NLR<10 at admission), and treated according to the standard care used in the interventional study.

Valuations

For the evaluation of patients in this trial, the baseline was defined as the last observation before the administration of fenofibrate on day 0. The patients' disease severity was assessed on an ordinal scale according to the following categories: The scale is as follows: 1) Death; 2) Hospitalized, on invasive mechanical ventilation or extracorporeal membrane oxygenation (ECMO); 3) Hospitalized, on non-invasive ventilation or high flow oxygen devices; 4) Hospitalized, requiring supplemental oxygen; 5) Hospitalized, not requiring supplemental oxygen; 6) Not hospitalized, limitation of activities; 7) Not hospitalized, no limitations of activities. Clinical status was recorded at baseline and every day during hospitalization.

Viral RNA and S-gene target failure (SGTF) Detection by Real-Time PCR

Extracted RNA was transferred to 96 well PCR plate containing 20ul of TaqPath™ 1-step Multiplex Master Mix No ROX (Applied Bioscience, Cat number: A28523). This was followed by a one-step RT-PCR (TaqPath COVID-19 assay kit; Thermo-Fisher). Thereafter, the plate was sealed with MicroAmp clear adhesive strip (Applied Bioscience, Cat number: 4306311). The plate was loaded onto a QuantStudio™ 5 Real-Time PCR System (Applied

Bioscience, Cat number: AB-A28574) and the following amplification program was used: 25°C for 2 minutes, X1 cycle 53°C for 10 minutes, X1 cycle 95°C for 2 minutes, X1 cycle 95°C for 3 seconds, followed by 60°C for 30 seconds, X40 cycles Ct threshold values were preset using the following values/parameters: MS2-15,000; by cycle 37; S gene- 20,000 by cycle 37; Orf1ab- 20,000 by cycle 37; Ngene- 20,000 by cycle 37. Samples that passed the Threshold is a Ct value >37 were re-tested or considered weak positive. Above threshold values of MS2, Orf1ab, and Ngene, but not S gene was considered S-gene target failure (SGTF). SGTF serves as a proxy for identifying B.1.1.7 cases [52,53].

Variant Detection by Real-Time PCR

Allplex™ SARS-CoV-2 Variants I Assay from Seegene Inc. was used according to the manufacturer protocol to perform rRT-PCR. Briefly, Extracted RNA (5ul) was transferred to 96 well PCR plate containing 15ul of the master mix. Plates were then spun down at 2500 rpm for 5 s and analyzed on a CFX96 Touch Real-Time PCR from BioRad. Reverse Transcription reaction 1 cycle: 50 °C/20 min – 95 °C/15 min. PCR reaction 45 cycles: 94 °C/15 s – 58 °C/30 sec. Gene amplifications were analyzed by FAM (E484K mutation on S-Gene), HEX (RdRP), Cal Red 610 (N501Y mutation on S-Gene), Quasar 705 (69-70del on S-Gene), and Quasar 670 (Human Endo Internal control) fluorophores. Results were compiled and analyzed using the 2019-nCoV viewer from Seegene Inc. according to the manufacturer's instructions.

Statistical analysis

Demographic data were summarized, continuous variables with non-normal distributions were expressed as median [IQR] and categorical variables were expressed as numbers and percentages (%). The sample size is detailed in each display item. Comparisons between groups were performed with Mann-Whitney U test for continuous variables and Fisher's exact test or chi-squared test for categorical variables.

Analysis of weighted differences in hospitalization duration, mortality, and incidence of oxygen weaning was done using the Mantel–Haenszel test. The cumulative rates of death and hospital discharge were compared using Kaplan-Meier curves, a log-rank test, and cause-specific Cox regression analysis. The hazard ratio (HR) was calculated using the Cox proportional hazard model comparing the treatment group versus the non-treatment group as previously described [54,55]. In the Cox regression models, individuals discharged were treated as "0-at risk" but not as censored data since individuals with COVID-19 would not be discharged unless their symptoms were significantly relieved and two continuous viral PCR negatives were achieved. Additionally, a clinic or electronic (medical records) follow-up at 28 days was conducted to register out-of-hospital death, need for supplemental oxygen, and/or rehospitalization. Since no deaths were recorded in the intervention group, Cox proportional hazard regression for mortality was performed using Firth's penalized maximum likelihood bias reduction method. Cox Regression with Firth's Penalized Likelihood has been shown to provide a solution in the case of monotone likelihood (non-convergence of likelihood function) and was shown to outperform Wald confidence intervals in these cases [51]. Regression adjustment was applied to remove residual confounding bias where it included the covariates with a standardized difference greater than 0.10. Multi-variable adjusted residual imbalances including age, gender, clinical characteristics on admission, indicators of disease severity and organ injuries on admission, and pre-existing medical conditions were adjusted in the analysis of the association between treatment and clinical outcomes. The

proportional hazard assumptions were verified using correlation testing based on the Schoenfeld residuals.

Dynamic changes of inflammatory factors tracking from day 0 to day 8 after treatment were depicted using the Lowess model [50,56]. A two-side α less than 0.05 was considered statistically significant. Data were analyzed in R-3.6.3 (R Foundation for Statistical Computing, Vienna, Austria) and SPSS Statistics (version 23.0, IBM, Armonk, NY, USA). Day 0 was determined to be the first day of treatment with nanocrystallized fenofibrate in the intervention group or first-day disease severity has reached 4 (but not higher) and at least 3 MOH indicators (increased oxygen requirement compared to baseline among those on home, a blood oxygen saturation of 93% or less on room air, or a ratio of the partial pressure of oxygen to the fraction of inspired oxygen (PaO2/FiO2) of less than 300 mm Hg, respiratory rate >30 breaths/min, and lung infiltrates >50% on chest CT) were recorded.

ETHICS AND OVERSIGHT

All procedures performed in studies involving human participants were in accordance with the ethical standards of the institutional and/or national research committee and with the 1964 Helsinki Declaration and its later amendments or comparable ethical standards.
In the observational studies - the Israeli study was approved by the local institutional review board of the Hadassah Medical Center (IRB approval number no. HMO 0247-20) and the local institutional review board of the Ichilov Medical Center (IRB approval number no. 0282-20-TLV). The Italian study was reviewed by the local ethical board (AVEC) of the IRCSS S.Orsola-Malpighi University Hospital (approval number no. code LLD-RP2018).
The American study was reviewed by the local institutional review board of Corporal Michael J. Crescenz VA Medical Center (IRB approval number 01654).

The interventional study was conducted in accordance with the Good Clinical Practice guidelines of the International Council for Harmonisation E6 and the principles of the Declaration of Helsinki or local regulations, whichever afforded greater patient protection. The study was reviewed and approved by the Barzilai Medical Center Research Ethics Committee (0105-20-BRZ).

Statistical analysis of the Israeli studies was done by BioStats Statistical Consulting Ltd. (Maccabim, Israel), funded by the sponsor. Data management is performed in compliance with GCP and 21 CFR part 1. Statistical analyses and reporting are performed in compliance with E6 GCP, E9, and ISO 14155. Independently validated by the author. Statistical analysis of the Italian study was done by Prof. Arrigo Cicero and Dr. Chiara Pavanello. Statistical analysis of the US study was done by Prof. Jordana Cohen.

Software resources

Our custom Cell Analysis CellProfiler® Pipeline is available at https://github.com/avnere/Single-Cell-Analysis-CellProfiler-Pipeline.

RESULTS

The metabolic fingerprint of SARS-CoV-2 infection

To elucidate the metabolic effects of SARS-CoV-2 we infected primary human bronchial epithelial cells with the virus (***methods***). Infected cells became noticeably smaller, showing vacuolization. RNA-Seq analysis of infected primary cells identified 535 differentially expressed genes (FDR<0.05). Enrichment analysis identified the regulation of viral transcription (FDR<$3x10^{-2}$), immune processes (FDR<$9x10^{-4}$), and cellular response to stress (FDR<$5x10^{-11}$). An analysis was also carried out on RNA-Seq data obtained from primary small airway epithelial cells infected with SARS-CoV-2 [57], lung biopsies obtained from COVID-19 autopsies, and lung epithelial cells obtained from bronchoalveolar lavage of COVID-19 patients [58]. All four sample groups showed similar enrichment patterns (**Figure 1A**). These four sample groups also display significant enrichment in metabolic processes (FDR<$4x10^{-4}$), particularly lipid (FDR<$2x10^{-5}$) and carbohydrate metabolic processes (FDR<0.05; **Figure 1A**).

Further transcriptional analysis shows that 58±3% of differentially expressed genes are metabolism-related, with about 15±2% of the genes associated with lipid metabolism (**Figure 1B; Figure 1-Figure Supplement 1**). Mapping of the SARS-CoV-2-induced transcriptional changes on the metabolic landscape of lung epithelial cells showed induction of a glycolytic phenotype (*i.e. Warburg-like effect*) and significant changes to lipid metabolism (**Figure 1C**). The shift to anaerobic metabolism is suggested to provide nucleotides for viral replication [59], while changes in lipid metabolism support palmitoylation of viral proteins as well as supply lipid components of the viral replication complex [17] (**Figure 1C**). However, in contrast to other viruses [36], SARS-CoV-2 infection appears to downregulate lipid catabolism (**Figure 1C; Figure 1-Figure Supplement 1**).

Mapping differentially expressed genes on the central carbon metabolism pathway showed that SARS-CoV-2 induces key glycolysis genes (**Figure 1D**) including rate-limiting enzymes such as hexokinase 2 (HK2) and pyruvate kinase isozyme (PKM). Interestingly, while core genes of the citric acid cycle did not change significantly, ATP citrate lyase (ACLY) was up-regulated suggesting a shift toward fatty acid synthesis. Mapping of differentially expressed genes on lipid metabolism (**Figure 1D**) showed induction of HMG-CoA synthase (HMGCS) and squalene monooxygenase (SQLE), rate-limiting steps in cholesterol synthesis [60]. Surprisingly, we found only a few significantly up-regulated lipogenesis genes, but rather significant down-regulation of lipid catabolism genes CPT1A and ACSL1 (n=3, FDR<0.01) (**Figure 1D**).

To confirm these transcriptional signatures we validated our results in SARS-CoV-2-infected primary lung cells (**Figure 1E-G**). Microscopic analysis showed an 85% increase in intracellular glucose in infected cells (**Figure 1E**; ***methods***). Concurrent metabolic analysis showed a 50% increase (n=6, p<0.001) in lactate production (**Figure 1-Figure Supplement 1**) and a shift in the lactate over glucose ratio (glycolytic index) from 1 to 1.7 indicating a Warburg-like effect (**Figure 1F**). Alterations in lipid metabolism were confirmed by fluorescence microscopy, showing an increase of neutral lipids (n=3, p<0.05) and a significant accumulation of phospholipids (n=3, p<0.001) in SARS-CoV-2 infected primary lung cells (**Figure 1G**).

Metabolic changes are often linked to endoplasmic stress. Indeed, SARS-CoV-2 infection of primary cells induced the dsRNA-activated protein kinase R (PKR/PERK) and IRE1 pathways leading to differential expression of ATF4 and splicing of XBP1. The ATF6 pathway of ER stress was seemingly unaffected by infection. Induction of PKR/PERK and IRE1 pathways were previously shown to lead to a Warburg-like shift to anaerobic glycolysis [61], increased lipogenesis [62,63], and decreased lipid catabolism [64] (**Figure 1-Figure Supplement 1**).

SARS-CoV-2 proteins cause direct modulation of metabolic pathways

To explore the role of viral proteins in the host metabolic response to SARS-CoV-2 we expressed a large protein panel [9] in primary bronchial epithelial cells (***methods;*** **Figure 2-Figure Supplement 1A**). Microscopic analysis of intracellular glucose retention showed the involvement of a small subset of viral proteins including N, ORF3a, NSP7, ORF8, NSP5, and NSP12 in glucose accumulation (n=6; **Figure 2A**). Direct measurement of glucose uptake and lactate production showed a marked increase in lactate production in cells expressing the same viral protein subset (n=6, $p<0.01$; **Figure 2B**) confirming a viral protein-driven shift to glycolysis (n=6, $p<0.01$; **Figure 2C**). Independent measurement of extracellular acidification rate (ECAR), a surrogate measurement for glycolysis [65], confirmed the activity of these viral proteins (n=6; **Figure 2D**). Mitochondrial stress test analysis (***methods***) showed a marked disruption in oxidative phosphorylation, induced by expression of N, ORF3a, and NSP7 (n=6, $p<0.05$; **Figure 2E-F**).

To study the role of viral proteins in lipid metabolism, we measured the exogenous fatty acid oxidation using Seahorse™ (***methods***) showing marked disruption in fatty acid oxidation, induced by expression of ORF9c, M, N, ORF3a, NSP7, ORF8, NSP5, and NSP12 (n=4, $p<0.05$; **Figure 2G; Figure 2-Figure Supplement 1B**). While triglyceride accumulation did not change, microscopic analysis confirmed a significant accumulation of phospholipids induced by expression of the same viral proteins (n=6, $p<0.01$; **Figure 2F**) supporting the significance of lipid accumulation for SARS-CoV-2 infection.

The inhibition of lipid catabolism by SARS-CoV-2 infection of primary lung epithelial cells and associated lipid accumulation is a unique host response [36] that might offer a distinct metabolic intervention. These data suggest that fibrates and other metabolic interventions that increase lipid catabolism [66,67] and reduce inflammatory stress [68-71] might interfere with the virus lifecycle.

Pharmacological modulation of SARS-CoV-2-induced metabolic pathways

The metabolic pathways induced by SARS-CoV-2 infection can be pharmacologically modulated at multiple points (**Figure 3A; Figure 3-Figure Supplement 1**). Pharmacological modulation of host metabolism was shown to block replication in other viruses [36,72-75]. SGLT inhibitors can block glucose absorption, while metformin can modulate mitochondrial activity potentially reversing a Warburg-like effect [76,77]. Cholesterol synthesis can be blocked by statins, while lipid oxidation can be induced by fibrates. Telmisartan could act by decreasing ER stress through IRE1 inhibition [78]. Thiazolidinediones are PPARγ agonists that modulate lipid content in certain tissues and are thought to reduce lung inflammation [29,79].

Exposing primary cells infected with the alpha variant of SARS-CoV-2 to therapeutic concentrations (C_{max}) of these drugs produced mixed effects (**Figure 3B-E**). Rosiglitazone, empagliflozin, and metformin showed no effect at the concentrations studied. Cloperastine, a recently identified SGLT1 inhibitor [80], reduced viral load by 3-fold (n=3, $p<0.01$) without affecting cell number but did not result in a reduction of lipid content or change in the glycolytic index. However, the PPARα agonist fenofibrate blocked phospholipid accumulation (n=3, $p<0.001$) and the increase in glycolysis (**Figure 3B-C**). Treatment of infected primary cells with the usual therapeutic concentration of fenofibrate reduced viral load by 2-logs (n=3, $p<0.001$) without affecting cell number (**Figure 3D-E**).

Since the online deposition of these initial findings [81], more recent work suggested a role for fenofibrate in blocking viral entry receptors [82]. To address this effect, we studied the effect of several structurally different PPARα agonists, including bezafibrate, WY14643, and conjugated linoleic acid (CLA). All four PPARα agonists showed a similar effect in both alpha and delta strains of the virus (***method***), blocking phospholipid accumulation (n=6, $p<0.05$; **Figure 3F; Figure 3-Figure Supplement 2**) and reducing viral load by 2 to 4-logs, indicating a class effect (n=6, $p<0.05$; **Figure 3G; Figure 3-Figure Supplement 2**).

To demonstrate the role of PPARα-induced fatty acid oxidation in our mechanism, we used etomoxir an irreversible inhibitor of CPT1A a rate-limiting enzyme in the pathway (**Figure 3A**). The addition of etomoxir reversed the fenofibrate effect restoring phospholipid accumulation (n=6; **Figure 3H; Figure 3-Figure Supplement 2**) and viral propagation (n=6; **Figure 3I**) in both alpha and delta strains of the virus. To further validate this pathway, we used genetic inactivation of PPARα by CRISPR KO (***methods***). Knockout of PPARα made the primary lung epithelial cells refractive to the effects of fenofibrate and etomoxir. Cells show phospholipid accumulation (n=6; **Figure 3J; Figure 3-Figure Supplement 3**) and viral propagation (n=6; **Figure 3K**) similar to untreated cells in both alpha and delta strains of the virus. Together, these data suggest that PPARα-dependent fatty acid oxidation inhibits the proliferation of SARS-CoV-2 in primary lung epithelial cells.

Metabolic regulators affect COVID-19 severity and progression

To assess the clinical relevance of these findings we collected a total of 3,233 cases of confirmed COVID-19 patients admitted to Hadassah and Ichilov Medical Centers between March 2020 to February 2021. 1,156 of these patients (35.8%) were registered with in-hospital use of different metabolic regulators (**Supplementary Table 2**). Participants treated with metabolic regulators were older and had a higher prevalence of chronic medical conditions, including hypertension, diabetes mellitus, dyslipidemia, obesity, coronary heart disease, cerebrovascular diseases, and chronic kidney diseases than those without these treatments (**Supplementary Table 2**) and thus were expected to be over-represented in ICU admissions and COVID-19 related deaths. Comparison between 2,806 COVID-19 patients above the age of 30 and 532,493 recent unique hospital patient records showed a significant over-representation of patients taking thiazolidinediones, metformin, SGLT2 inhibitors, statins, or telmisartan (IRE1α inhibitor) across all COVID-19 severity indicators (**Figure 4; Figure 4-Figure Supplement 1; Supplementary Table 2**). However, patients taking fibrates (n=21) were significantly underrepresented in hospital admissions ($p=0.02$) and not over-represented in other severity indicators (**Supplementary Table 2**). The same trends are conserved regardless of the comparison period (**Supplementary Table 2**).

Reports suggest that severe COVID-19 is characterized by early inflammation, marked by elevated C-reactive protein (CRP) [83], followed by distinct changes in neutrophils and lymphocytes marking the onset of the immunoinflammatory response [84,85]. To further investigate the effect of metabolic regulators on COVID-19 progression, we tracked a sub-cohort of high-risk COVID-19 patients above the age of 45 that were hospitalized for 3 or more days (n = 1,438**; Supplementary Table 2**, ***methods***). In general, fibrates use was associated with significantly shorter hospitalization duration (p=0.03; **Figure 4B, Supplementary Table 2**). Patients taking other metabolic regulators exhibited similar or worse clinical outcomes compared to the control (**Supplementary Table 2**).

To track disease progression, we followed changes in CRP during the first 21-days of hospitalization. Data were fitted using locally weighted scatterplot smoothing (Lowess) comparing each drug group to all other high-risk patients that did not take metabolic regulators (n=648; **Figure 4C-D; Supplementary Table 2**, ***methods***). Both groups had similar clinical characteristics upon admission, while comorbidities were higher in patients taking metabolic regulators (**Supplementary Table 2**). High CRP levels marking systemic inflammation gradually declined after admission in the control group, reaching a plateau 14-days post-admission (**Figure 4C**). No significant differences were noted for patients taking statins, metformin, or SGLT-2 inhibitors compared with controls. CRP levels in patients taking thiazolidinediones, which is thought to increase lipid synthesis in certain tissues [29,30], failed to decline. IRE1α inhibitor users exhibited slightly lower CRP levels than control patients throughout their hospitalization. Importantly, patients taking fibrates showed a significant decline in inflammation within 5-days post-admission (**Figure 4C**). The neutrophil-to-lymphocyte ratio (NLR) marking immunoinflammatory stress, rose in the control group to peak around day 10 post-admission (**Figure 4D; Figure 4-Figure Supplement 2**). Treatment with SGLT2 inhibitors, metformin, or thiazolidinediones was associated with similar responses compared to controls, albeit with higher maxima for the thiazolidinedione group. Patients taking IRE1α inhibitors exhibited significantly elevated NLR post-day 10, due to decreased lymphocyte counts during recovery (**Figure 4D; Figure 4-Figure Supplement 2**). However, patients taking fibrates showed consistently low NLR throughout their hospitalization, suggesting minimal immunoinflammatory stress. Analysis of 28-day all-cause mortality showed that no deaths were reported for the small group of patients taking fibrates (n=16, **Figure 4E**). Mortality did not appear to differ for statins, IRE1α inhibitors, or metformin, but was significantly higher in patients taking SGLT2 inhibitors (aHR=2.6; 95% CI, 1.1 to 6.2; p=0.034) or thiazolidinedione (aHR=3.6; 95% CI, 1.0 to 12.4; p=0.043; **Figure 4E**; **Supplementary Table 2;** ***methods***).

Analysis of an additional observational cohort of 2,123 patients examined in the Outpatient Lipid Clinics of the University of Bologna and the Niguarda Hospital in Milan during the last 12 months and on adequately dosed statins, fenofibrate, or both for at least three months (**Supplementary Table 3**) indicates that fenofibrate users regardless of additional treatment had significantly less COVID-19 history and severe illness (**Supplementary Table 3**). Additionally, in the sub-cohort of patients reporting contact with affected people, analysis indicates that statin users are significantly more likely to develop COVID-19 (p=0.02), while fenofibrate users, regardless of additional treatment are less likely to develop COVID-19 (**Supplementary Table 3**). Parallel analysis of an observational cohort of 920,922 veterans with hypertension in the US Veteran's Health Administration, comparing fenofibrate to matched non-users, statins users, or thiazolidinediones users (VHA; **Supplementary Table 3**), showed that fenofibrate users have shorter hospitalization duration (**Supplementary**

Table 3) and fairly better outcomes across several severity indicators (**Supplementary Table 3**).

Pilot study of prospective administration of nanocrystallized fenofibrate in humans with COVID-19 treated with standard-of-care

To further assess the clinical relevance of our findings, we performed an interventional single-arm clinical study in severe, hospitalized COVID-19 patients, who exhibited respiratory deterioration and severe pneumonia (NCT04661930; ***methods***) [86]. Fifteen patients (**Figure 5-Figure Supplement 1; Supplementary Table 4**) were treated with 145 mg/day of nanocrystallized fenofibrate added to standard-of-care for 10 days or until discharge (**Figure 5A)** tracking multiple parameters to demonstrate differences in disease progression as observational studies by our group (**Figure 4**) and others [87] are not powered to show differences in endpoints such as mortality. Nanocrystallized fenofibrate was selected due to its improved lung bioavailability [88] and short T_{max} [89,90] enabling rapid intervention (**Figure 5B)**.

Enrolled participants exhibited a higher prevalence of chronic medical conditions compared to other hospitalized patients admitted with severe COVID-19 during the same period and treated under the same standard-of-care, who were used as historical controls (**Supplementary Table 4**). Despite these comorbidities, patients treated with nanocrystallized fenofibrate exhibited a significantly shorter hospitalization (weighted difference of 2.8 days; 95% CI, 1 to 5.7; $p<0.001$; **Figure 5C**), were significantly more likely to be discharged within 28 days of hospital admission (HR=3.6; 95% CI, 2.1 to 6.4; $p<0.001$; **Figure 5C**) and demonstrated lower rates of ICU admission and rehospitalization (**Figure 5C; Supplementary Table 4**).

Dynamic changes in serum levels of CRP and NLR, which mark the immunoinflammatory progression of the disease, also demonstrated favorable trends (**Figure 5D-E)**. Patients treated with nanocrystallized fenofibrate showed a rapid decline in CRP levels within 48 hours of treatment, with significantly lower CRP levels by day 3-5 post-treatment ($p<0.001$; **Figure 5D**). Immunoinflammatory stress, indicated by NLR remained muted throughout the treatment period, showing significantly lower stress by day 3-5 post-treatment ($p=0.002$; **Figure 5E**).

Patients treated with nanocrystallized fenofibrate also exhibited lower mortality, lower respiratory intervention rates, and significantly increased withdrawal rate from supplemental oxygen by day 7 (weighed difference of 26.1 percentage points; 95% CI, 7.0 to 45.2; $p=0.003$; **Figure 5F; Supplementary Table 4**). COVID-19 progression was investigated as a time-varying outcome using a Cox model accounting for baseline variance, which also suggests a difference in COVID-19-related risk (**Figure 5G; Supplementary Table 4**).

Novaplex™ SARS-CoV-2 variant analysis showed a dominant presence of 69/70 deletion and N501Y substitution mutation correlating to the B.1.1.7 (UK) variant of the virus in the patient population (**Figure 5H**), a similar variant distribution to the one seen in other clinical centers in Israel during the same period (**Figure 5-Figure Supplement 2**). Investigation into post-acute sequelae of COVID-19 in these patients, 6 months post-admission, revealed that only one patient suffered from respiratory symptoms and fatigue (IR 6.67; 95% CI, 0.1 to 32.0),

without any additional post-acute sequelae in any of the other patients (**Figure 5I; Supplementary Table 4)**

Discussion

Viruses are dependent on host metabolism to obtain macromolecules essential for their lifecycle. While metabolic interventions of host pathways offer promise, the current reliance on animal models and cell lines limits our ability to identify targets for intervention due to critical metabolic and genetic differences between animal models, cell lines, and patients. In this work we utilized primary human cells and clinical samples to chart SARS-CoV-2 metabolic response, to identify metabolic targets that could rapidly translate to the treatment of severe COVID-19.

Glycolysis is often upregulated to supply nucleotides for virus replication [36,72,91], as part of a Warburg-like effect. We show that SARS-CoV-2 infection induced a Warburg-like effect in both bronchial and small airway primary cells, as well as COVID-19 patient samples (Figs. 1). Recent work in Vero and Caco-2 cell lines, showed direct binding of some viral proteins to mitochondrial and glycolysis-related proteins [9,10], with electron microscopy studies confirming mitochondrial disruption [92], and PET/CT studies revealing increased glycolytic activity in lungs of COVID-19 patients [93]. These results brought several groups to assess different glucose modulators as pharmacological interventions. For example, 2-Deoxyglucose (2-DG) blocked SARS-CoV-2 replication, but at concentrations 20-fold higher than C_{max} while causing cellular damage [10]. Our results showed a minimal effect of the SGLT1 inhibitor cloperastine and no effect of SGLT2 inhibitor empagliflozin or metformin in blocking virus replication or affecting the patient outcome (**Figure 3-4**). Recent observational studies support our findings [54,94], suggesting that while glycolysis is part of the virus lifecycle, it may not be a viable target to treat SARS-CoV-2 infection.

Our study demonstrates coordinated changes in lipid metabolism, such as the upregulation of palmitoylation and cholesterol synthesis (**Figure 1**) both critical to the virus lifecycle. SARS-CoV-2 inhibition of PPARα-dependent lipid oxidation is surprising, as the pathway was up-regulated in other viral infections [36]. Histological analysis of COVID-19 patient biopsies confirms our findings, showing enlarged lung epithelial cells with amphophilic granular cytoplasm [95], while electron microscopy images of infected cells showed lipid droplet accumulation [92,96]. As lipogenesis is poorly tolerated in thin epithelial tissue, it might lead to pulmonary lipotoxicity [97]. Indeed, several groups looked at lipid modulators as possible pharmaceutical interventions. Triacsin C and VPS34 inhibitors blocked viral replication at concentrations 1000-fold higher than C_{max} [98], with similar effects shown for statins at concentrations 100-fold higher than C_{max} [99]. This gap might explain why observational studies on the effect of statins show an inconsistent reduction of 28-days all-cause-mortality and mixed effect regarding secondary outcomes [55]. Our study confirms these earlier observations (**Figure 4**).

Fibrates are a family of amphipathic carboxylic acids that are ligands of PPARα, known to up-regulate lipid oxidation and lower serum triglycerides [66,67]. Fibrates have also been shown to produce an anti-inflammatory and immunomodulatory effect in multiple tissues [68-71]. We show that fenofibrate inhibits viral replication in primary human lung cells, reversing phospholipid accumulation at 20 μM concentration (**Figure 3**), lower than its effective physiological concentration (C_{max}) recorded as 25-30 μM with a standard dose of 145 mg/day

[100,101]. Fenofibrate was detected at an effective plasma concentration of 15-20 μM range hours after administration [102].

Our work shows that several structurally different ligands of PPARα have a similar anti-viral effect (**Figure 3**). Additionally, we show that inhibition of fatty acid oxidation reversed the antiviral effect of fenofibrate, while knockout of PPARα made the cells refractive to the drug (**Figure 3**). Recent work suggested that fenofibrate might also block viral entry receptors [82]. These results suggest that a combination of mechanisms might be responsible for the proposed anti-viral effect of fenofibrate.

One challenge in the investigation of host metabolic pathways *in vitro* is the difficulty to study lipid metabolism in proliferating cell lines and stem-cell-derived models [36 103], that in addition to the *Warburg effect,* also show differences in PPARα expression and activity compared to primary cells and tissue [104-107]. These differences result in an effective concentration above clinical relevance, at sub-millimolar ranges [82], far above the levels tested in standard high content screens [108,109]. Thus, our work focused on primary human lung cells. In contrast to cell lines, we do not observe significant cell death in primary cell cultures even after 5 days, while the virus is clearly still replicating at this point (**Figure 3**). This is consistent with other studies in primary tissue and clinical data [110-112].

One challenge in the validation of our findings is that hamster models are unresponsive to fibrates [113,114], requiring human clinical data to support these *in vitro* observations. Thus, our work was directed to observational studies. We show that patients taking bezafibrate or ciprofibrate were significantly underrepresented in COVID-19-related hospitalizations (**Figure 4**). Compared to hospitalized patients that are not treated with metabolic drugs, those taking fibrates showed a minimal inflammatory response and improved disease outcomes (**Figure 4**). Other observational studies in the US and Italy showed similarly improved outcomes and disease-related complications (**Figure 4)**.

The clinical importance of understanding the role of lipid metabolism in COVID-19 is further emphasized by the negative response induced by thiazolidinediones (TZD) in our study. Thiazolidinediones are ligands of PPARγ that upregulate lipogenesis in certain tissues [29]. Our study showed that Israeli COVID-19 patients taking rosiglitazone were overrepresented in ICU admissions and death (**Figure 4**), had a worse immunoinflammatory response, and had higher mortality (**Figure 4**). These results correlate with recent data showing that long-term thiazolidinedione use is associated with an increased risk of pneumonia in patients with type 2 diabetes [115].

To validate our findings, we carried out a prospective non-randomized interventional study of 15 severe hospitalized COVID-19 patients (NCT04661930). Severe COVID-19 patients treated with 145 mg/day of nanocrystallized fenofibrate in addition to standard-of-care showed dramatic improvement in inflammation and faster recovery compared to patients admitted during the same period in neighboring hospitals and treated with the same standard of care (**Figure 5)**. This favorable course was observed despite the presence of a higher comorbidity burden in fenofibrate-treated patients. Patients treated with fenofibrate showed significantly decreased CRP levels 72 hours post-treatment suggesting a rapid decrease in inflammation, possibly due to PPARα anti-inflammatory effect. The patients NLR remained stable indicating low immunoinflammatory stress. In a 6-month follow-up, these patients report post-acute sequelae far below the rates reported in the literature [27] (**Figure 5**).

Clinical Limitations

While our clinical results are highly encouraging, baseline differences between the groups and lack of randomization must be noted. Therefore, confounding and/or random error cannot be excluded. For instance, the higher comorbidity burden in the fenofibrate group may have conditioned a lower threshold for the initial hospital admission, with consequent favorable differences in outcomes relative to controls.

In addition, it must be noted that the study controls were assigned from neighboring clinical centers serving the same diverse and mixed ethnic population, as clinical outcomes of non-consenting patients at the Barzilai Medical Center were significantly worse than the treatment group as these patients often refused or had difficulties in adhering to treatment. Thus, the best control that replicated the clinical characteristics of the patients and course of treatment, were patients that were qualified for the study but were not included simply because they were in another local hospital. Standard of care during this time period was identical for all clinical centers in Israel.

Our work demonstrates the importance of weaving primary human cells, with clinical samples, and observational data for the rapid clinical translation of new metabolic interventions. Additional work is needed to confirm the specific activation of biochemical pathways and validate our findings in pathology samples. Still, this mechanistic understanding allowed us to design an ad hoc preliminary prospective clinical study and showed significant differences from the control group despite the small number of patients.

Our work charts the metabolic response of human lung epithelium to SARS-CoV-2 infection. Our data suggest that the up-regulation of lipid oxidation might be an effective therapeutic target in the treatment of COVID-19. A definitive answer regarding the efficacy of fenofibrate for the treatment of COVID-19 will require the execution of large randomized controlled clinical trials with meaningful clinical outcomes. Two randomized placebo-controlled trials are ongoing, including a large international trial in the US, Mexico, Greece, and several South American countries (FERMIN trial; NCT04517396), and a clinical trial in Israel (FENOC trial; NCT04661930).

ACKNOWLEDGMENTS

Funding was provided by European Research Council Consolidator Grants OCLD (project no. 681870) and generous gifts from the Nikoh Foundation and the Sam and Rina Frankel Foundation (YN). The interventional study was supported by Abbott (project FENOC0003). The funders had no role in study design, data collection, and interpretation, or the decision to submit the work for publication. The authors would like to thank Prof. Benjamin R. tenOever and his team at the Icahn School of Medicine for providing viral load quantifications (**Figure 3D**) and fixed drug-treated SARS-CoV-2 infected primary cell cultures at their BSL3 facility at the request of the study authors.

EXPERIMENTAL MODEL AND SUBJECT DETAILS

Human Subjects

All protocols involving human tissue were reviewed and exempted by the Hebrew University of Jerusalem, the Israeli Ministry of Health, Sheba medical center, and Icahn School of Medicine at Mount Sinai Institutional Review Boards.

Experiments using samples from human subjects were conducted in accordance with local regulations and with the approval of the institutional review board at the Icahn School of Medicine at Mount Sinai under protocol HS#12-00145 and the institutional review board at Sheba medical center under protocol SMC-7875-20.

All procedures performed in studies involving human participants were in accordance with the ethical standards of the institutional and/or national research committee and with the 1964 Helsinki Declaration and its later amendments or comparable ethical standards.
In the observational studies - the Israeli study was approved by the local institutional review board of the Hadassah Medical Center (IRB approval number no. HMO 0247-20) and the local institutional review board of the Ichilov Medical Center (IRB approval number no. 0282-20-TLV). The Italian study was reviewed by the local ethical board (AVEC) of the IRCSS S.Orsola-Malpighi University Hospital (approval number LLD-RP2018).

The interventional study was conducted in accordance with the Good Clinical Practice guidelines of the International Council for Harmonisation E6 and the principles of the Declaration of Helsinki or local regulations, whichever afforded greater patient protection. The study was reviewed and approved by the Barzilai Medical Center Research Ethics Committee (0105-20-BRZ).

Cell Culture

Normal human bronchial epithelial (NHBE) cells (Lonza, CC-2540 Lot# 580580), isolated from a 79-year-old Caucasian female and were maintained at 37°C and 5% CO_2 in bronchial epithelial growth media (Lonza, CC-3171) supplemented with SingleQuots (Lonza, CC-4175) per manufacturer's instructions. Cells were maintained at the BSL3 facilities of the Icahn School of Medicine at Mount Sinai. NHBE cells (ATCC, PCS-300-010 Lot#63979089; #70002486), isolated from a 69-year-old Caucasian male and a 14-year-old Hispanic male were maintained in airway epithelial cell basal media (ATCC, PCS-300-030) supplemented with Bronchial Epithelial Growth Kit as per the manufacturer's instructions (ATCC, PCS-300-040) at 37°C and 5% CO_2. Cells were maintained at the BSL2 facilities of the Hebrew University of Jerusalem and the BSL-3 facility of the central virology laboratory of the ministry of health and Sheba medical center.

Viruses

SARS-related coronavirus 2 (SARS-CoV-2), Isolate USA-WA1/2020 (NR-52281) was deposited by the Center for Disease Control and Prevention and obtained through BEI Resources, NIAID, NIH. SARS-CoV-2 was propagated in Vero E6 cells in DMEM supplemented with 2% Fetal Bovine Serum (FBS), 4.5 g/L D-glucose, 4 mM L-glutamine, 10 mM Non-Essential Amino Acids (NEAA), 1 mM Sodium Pyruvate, and 10 mM HEPES. Infectious titers of SARS-CoV-2 were determined by plaque assay in Vero E6 cells in

Minimum Essential Media (MEM) supplemented with 4 mM L-glutamine, 0.2% Bovine Serum Albumin (BSA), 10 mM HEPES and 0.12% $NaHCO_3$, and 0.7% agar.

Isolate hCoV-19/Israel/CVL-45526-NGS/2020 (alpha) and hCoV-19/Israel/CVL-12806/2021 (delta) were isolated from nasopharyngeal samples of SARS-CoV-2 positive individuals which contained the alpha sub-lineage B.1.1.50 (hCoV-19/Israel/CVL-45526-NGS/2020) and Delta B.1.617.2 (hCoV-19/Israel/CVL-12804/2021) variants by the central virology laboratory of the ministry of health and Sheba medical center. Confluent Vero E6 cells were incubated for one hour at 33ºC with the nasopharyngeal samples, followed by the addition of MEM-EAGLE supplemented with 2% Fetal Bovine Serum (FBS). Upon cytopathic effect detection, supernatants were aliquoted and stored at -80ºC. Infectious titers of SARS-CoV-2 were determined by a 50% endpoint titer (TCID50) for each variant in Vero E6 cells. Approximately 1×10^5 Vero E6 cells were seeded and incubated at 37ºC for 24 hours. At that point, the cells were infected by 10-fold serial dilutions of each variant in MEM-EAGLE supplemented with 2% Fetal Bovine Serum (FBS). A Gentian Violet staining was used to determine the TCID50 of each variant, calculated using the Spearman-Karber method.

All work involving live SARS-CoV-2 was performed in the CDC/USDA-approved BSL-3 facility of the Global Health and Emerging Pathogens Institute at the Icahn School of Medicine at Mount Sinai or in the BSL-3 facility of the central virology laboratory of the ministry of health and Sheba medical center in accordance with institutional and national biosafety requirements

FIGURE LEGENDS

Figure 1. Metabolic fingerprint of SARS-CoV-2 infection. (**A**) Bubble plot visualization of GO terms enriched by SARS-CoV-2 infection. Epithelial cells were isolated by bronchoalveolar lavage from 6 severe COVID-19 patients compared to 4 healthy patients (lavage). Post-mortem lung biopsies from 2 severe COVID-19 patients compared to surgical biopsies from 2 non-COVID patients (autopsy). Culture sample groups include primary small airway epithelial cells (n=3; alveoli) and primary bronchial epithelial cells (n=3; bronchial) infected with SARS-CoV-2. Enrichment analysis shows immunoinflammatory response, cellular stress ($FDR<10^{-22}$), and lipid metabolism ($FDR<10^{-5}$). (**B**) Venn diagram describing the relationship between differentially expressed genes (DEG), metabolic genes (GO:0008152), and lipid metabolism genes (GO:0006629) in SARS-CoV-2 infection of primary bronchial epithelial cells and COVID-19 patient samples. Across all four sample groups 58±3% of the differentially expressed genes were metabolism-related, with 15±2% of the genes associated with lipid metabolism. (**C**) Schematic depicting the metabolic landscape of SARS-CoV-2 infection superimposed with a heat map of pathway-associated genes. Red and green boxes indicate gene expression changes following infection in primary bronchial epithelial cells. * marks differentially regulated genes (n=3, FDR<0.05). (**D**) Schematic of central carbon metabolism and lipid metabolism fluxes superimposed with flux-associated genes. Differentially expressed genes (n=3, FDR <0.01) are marked with *. Genes and associated fluxes are highlighted in red or green for up- or down-regulation, respectively. (**E**) Microscopic evaluation of primary bronchial epithelial cells infected with SARS-CoV-2 virus or mock control shows an 85% increase in the intracellular accumulation of fluorescent glucose analog (n=3). (**F**) The ratio of lactate production to glucose uptake (glycolytic index) in SARS-CoV-2 and mock-infected primary cells. Index increases from 1.0 to 1.7 out of 2.0 indicating a transition to glycolysis (*i.e., Warburg effect*). (**G**) Microscopic evaluation of

primary bronchial epithelial cells infected with SARS-CoV-2 virus or mock control. Neutral lipids (triglycerides) are dyed green while phospholipids are dyed red. Image analysis shows a 23% increase in triglycerides (n=3, $p<0.05$) and a 41% increase in phospholipids (n=3, $p<0.001$) following SARS-CoV-2 infection indicating abnormal lipid accumulation in lung epithelium. * $p<0.05$, ** $p<0.01$, *** $p<0.001$. # indicates a small sample size. Bar = 20 μm. Error bars indicate S.E.M.

Figure 2. SARS-CoV-2 proteins modulate host metabolic pathways. Analysis of primary bronchial epithelial cells expressing different SARS-CoV-2 proteins for 72 hours using multiple independent assays. (**A**) Microscopic analysis shows an increased abundance of fluorescent glucose analog (2-NDBG) by a small set of viral proteins. Quantification shows a significant increase in intracellular glucose in bronchial cells expressing N, ORF3a, NSP7, ORF8, NSP5, and NSP12 (n=6, $p<0.05$). (**B**) Direct sensor measurement of lactate production of bronchial epithelial cells shows significantly higher lactate production (n=6, $p<0.01$) in cells expressing the abovementioned protein subset. (**C**) The ratio of lactate production to glucose uptake (glycolytic index) in bronchial cells expressing viral proteins. Index significantly increases from 1.1 to 1.7 marking a shift to glycolysis (n=6, $p<0.01$) induced by the viral proteins. (**D**) Seahorse™ analysis of extracellular acidification rate (ECAR) surrogate measurement for lactate production, shows independent confirmation of increased glycolysis. (**E**) Seahorse™ mitochondrial stress analysis of bronchial cells expressing the viral proteins. Oxygen consumption rate (OCR) is shown as a function of time. Oligomycin, FCCP, and antimycin/rotenone were injected at 25, 55, and 85 minutes, respectively. Orange lines indicate viral protein-expressing cells. (n=6) (**F**) Quantification of oxidative phosphorylation (OXPHOS) shows a decrease of mitochondrial function following expression of N, ORF3a, and NSP7 (n=6, $p<0.05$). (**G**) Seahorse™ XF long-chain fatty acid oxidation stress analysis, a surrogate measurement for lipid catabolism, shows virus protein-induced significant decrease in lipid catabolism by ORF9c, M, N, ORF3a, NSP7, ORF8, NSP5, and NSP12 (n=4, $p<0.05$). (**H**) Microscopic analysis of triglycerides (neutral lipids) and phospholipids shows a virus protein-induced perinuclear lipid accumulation. Quantification shows a significant accumulation of phospholipids in cells expressing the same panel of viral proteins that induced lipid catabolism inhibition (n=6, $p<0.01$). * $p<0.05$, ** $p<0.01$, *** $p<0.001$ in a 2-sided heteroscedastic student's t-test against control. Bar = 50 μm. Error bars indicate S.E.M.

Figure 3. Metabolic intervention of SARS-CoV-2 shows the antiviral effect of PPARα activation. (**A**) *Left:* Schematic depicting potential drug interactions with the metabolic landscape of SARS-CoV-2 infection. *Right:* Schematic of the relationship between PPARα and fatty acid oxidation in our model. (**B**) Microscopic analysis of lipid accumulation in lung cells infected by SARS-CoV-2 (USA-WA1/2020) at MOI 2 exposed to different drugs for 96 hours compared to DMSO-treated (vehicle) and mock-infected controls. Cells treated with PPARα agonist fenofibrate showed a significant decrease in phospholipid content (n=3, $p<0.001$). (**C**) Lactate over glucose ratio of SARS-CoV-2 infected primary lung cells treated with various drugs. Fenofibrate significantly reduced the lactate-to-glucose ratio by 60% (n=3; $p<0.01$) normalizing the metabolic shift induced by infection. (**D**) Quantification of SARS-CoV-2 viral RNA over treatment with a physiological concentration of various drugs or DMSO (vehicle). Treatment with 20 μM fenofibrate (C_{max}) reduced SARS-CoV-2 viral load by 2-logs (n=3; $p<0.001$). Treatment with 10 μM cloperastine reduced viral load by 2.5 to 3-fold (n=3; $p<0.05$). (**E**) Cell number post-treatment was unaffected by all drugs tested. (n=3). (**F**) Microscopic analysis of lipid accumulation in lung cells infected by SARS-CoV-2 (hCoV-19/Israel/CVL-45526-NGS/2020) and B.1.617.2 variant of concern (hCoV-

19/Israel/CVL-12806/2021) exposed to structurally different PPARα agonists for 5 days compared to DMSO-treated cells (vehicle). Cells treated with any PPARα agonists showed a significant decrease in phospholipid content in both viruses (n=6, $p<0.001$). (**G**) Quantification of SARS-CoV-2 viral RNA over treatment with a physiological concentration of various PPARα agonists or DMSO (vehicle). Treatment with 20 μM fenofibrate, 50 μM bezafibrate, or 1 μM WY-14643 reduced SARS-CoV-2 viral load by 3-5-logs (n=6; $p<0.001$). Treatment with 50 μM conjugated (9Z,11E)-linoleic acid and 50 μM oleic acid reduced viral load by 2.5-logs (n=6; $p<0.01$ in alpha variant). (**H**) Microscopic analysis of lipid accumulation in lung cells infected by SARS-CoV-2 and B.1.617.2 variant of concern (delta) exposed to PPARα agonist fenofibrate with 4 μM of lipid catabolism inhibitor, etomoxir (ETO) for 5 days compared to DMSO-treated (vehicle). Cells treated with fenofibrate showed a significant decrease in phospholipid content in both viruses (n=6, $p<0.001$). Phospholipid decrease was reversed by the addition of etomoxir. (**I**) Quantification of SARS-CoV-2 viral RNA exposed to the PPARα agonist fenofibrate with or without 4 μM of lipid catabolism inhibitor, etomoxir, or DMSO (vehicle). Treatment with 20 μM fenofibrate reduced SARS-CoV-2 viral load by 4-5-logs (n=6; $p<0.001$). Fenofibrate antiviral effect was reversed by the addition of etomoxir. (**J**) Microscopic analysis of lipid accumulation in PPARα or NT CRISPR-knockout lung cells (***methods***) infected by SARS-CoV-2 and B.1.617.2 variant of concern (delta) exposed to PPARα agonist fenofibrate with 4 μM of lipid catabolism inhibitor, etomoxir compared to DMSO-treated (vehicle). PPARα or NT CRISPR-knockout cells treated with fenofibrate did not show a decrease in phospholipid content in either virus and was unaffected by etomoxir (n=6). (**K**) Quantification of SARS-CoV-2 viral RNA after treatment with the PPARα agonist fenofibrate with or without 4 μM of lipid catabolism inhibitor, etomoxir, or DMSO (vehicle). Genetic inhibition of PPARα causes cells to be refractory to fenofibrate treatment and the addition of etomoxir (n=6). * $p<0.05$, ** $p<0.01$, *** $p<0.001$ in a 2-sided heteroscedastic student's t-test against control. Bar = 30 μm. Error bars indicate S.E.M.

Figure 4. Observational study shows differential immunoinflammatory response to metabolic intervention. (**A**) Comparative representation of Israeli patients above the age of 30 taking different metabolic regulators. 532,493 unique general hospital medical records were compared with 2,806 confirmed COVID-19 patients. COVID-19 patients treated with metabolic regulators were older and had a higher prevalence of chronic medical conditions and risk factors than other COVID-19 patients (**Table S1).** Patients taking thiazolidinediones (n=37; $p<0.001$), metformin (n=321; $p<0.01$), SGLT2 inhibitors (n=54; $p<0.001$), statins (n=924; $p<0.001$), or telmisartan (IRE1α inhibitor; n = 278; $p<0.001$) were over-represented across all severity indicators (**Table S2**). Patients taking fibrates (n=21) were significantly underrepresented in hospital admissions ($p=0.02$) and were not over-represented in other severity indicators. * $p<0.05$, ** $p<0.01$, *** $p<0.001$ in a Wald test compared to the proportion of these drug users in medical records. Error bars indicate S.E.M. (**B**) Box and whisker plot of length of hospitalization in treatment and non-treatment groups (Control). Israeli patients taking bezafibrate or ciprofibrate (fibrates) were associated with significantly lower hospitalization duration ($p=0.03$). The numbers in parentheses indicate the number of patients. (**C-D**) Dynamic changes in the inflammation marker CRP and neutrophil-to-lymphocyte ratio (NLR) marking immunoinflammatory stress in treatment and non-treatment groups (Control) during 21-day hospitalization. The centerline shows the mean value while the 95% confidence interval is represented by the shaded region. (**C**) CRP levels gradually declined in the control group reaching a plateau by day 14 post-hospitalization. The fibrates group showed a significantly faster decline in inflammation, while the thiazolidinedione

group showed marked elevation in CRP level above control. (**D**) NLR rose in the control group above normal values (dotted red line) stabilizing after 7-14 days and then declining as recovery begins. The fibrates group showed only mild stress, and maintain normal levels of NLR throughout hospitalization. Patients taking statins or IRE inhibitors showed elevated NLR post-day 10 of hospitalization. (**E**) Kaplan–Meier survival curves of 28-day in-hospital mortality for treatment and non-treatment groups (Control). The small group of patients taking fibrates did not report any deaths, while thiazolidinedione and SGLT2 inhibitor users had a significantly higher risk of mortality (HR: 3.6, 2.5; p = 0.04, 0.03 respectively, Table S4). * p<0.05, ** p<0.01, *** p<0.001. In boxplots, x is the mean; center line is the median; box limits are 25th and 75th percentiles; whiskers extend to 1.5× the interquartile range (IQR) from the 25th and 75th percentiles; dots are outliers. [#] indicates that the hazard ratios were calculated using Firth's correction for monotone likelihood with profile likelihood confidence limits.

Figure 5. Inflammation and speed recovery in severe COVID-19 patients treated with standard-of-care plus nanocrystallized fenofibrate. (A) Schematic depicting interventional study design in 15 severe hospitalized COVID-19 patients receiving remdesivir, dexamethasone, and enoxaparin. Patients received 145 mg/day of nanocrystallized fenofibrate for 10 days with blood samples taken every 48-72 hours until discharge. **(B)** Chemical, clinical, and pharmacokinetic characteristics of nanocrystallized fenofibrate. Lower T_{max} compared to other fibrates enables rapid intervention in deteriorating COVID-19 patients. (**C**) box and whisker plot of hospitalization duration (left) and Cox accumulative estimated hospital time to discharge by day 28 analysis, plotted as 1 minus the Cox estimator (right). Patients treated with nanocrystallized fenofibrate had a significantly lower hospitalization duration (n=15; p<0.001), and a higher likelihood of discharge (HR: 3.6, 95% CI 2.1 to 6.4; n=15; p < 0.001). (**D-E**) Dynamic changes (*right*) and box and whisker plots (*left*) of immunoinflammatory indicators CRP and neutrophil-to-lymphocyte ratio (NLR) in treatment and non-treatment groups (Control) over hospitalization duration (***methods***). The centerline shows the mean value while the 95% confidence interval is shaded. (**D**) High CRP levels gradually declined in the control group reaching a plateau by day 7. Nanocrystallized fenofibrate-treated patients showed a faster decline in inflammation, resulting in significantly lower CRP levels 3-5 days post-treatment (n=15; p<0.001). (**E**) NLR in the control group increased during hospitalization indicating severe immunoinflammatory stress. Patients treated with nanocrystallized fenofibrate showed no increase in NLR, suggesting minimal immune response, resulting in a significantly lower NLR 3-5 days post-treatment (n=15; p=0.002). (**F**) Withdrawal from oxygen support plotted as cumulative incidence at day 7 (left; OR: 3.2, 95% CI 1.3 to 7.9; n=15; p = 0.005) Kaplan-Meier estimated time to discharge by day 28, plotted as 1 minus the survival estimator (right; HR: 2.9, 95% CI 1.7 to 5.0; n=15; p < 0.001). (**G**) Kaplan–Meier survival curves of 28-days mortality in treatment and non-treatment groups (Control) and Cox regression modeling presenting hazard ratio estimate, 95% CI, and p-value. (**H**) Novaplex™ SARS-CoV-2 qPCR variant analysis (***methods***), showing a dominant presence of 69/70 deletion and N501Y substitution mutation correlating to the B.1.1.7 (UK) variant of the virus in the patient population. (**I**) Assessment of significant post-acute incident diagnoses in people who had been hospitalized with COVID-19 (long COVID) in patients taken from Al-Aly and colleagues [27] compared to those treated with 145 mg fenofibrate in this study at 6 months after hospital discharge. Incident rate (IR) per 1000 at 6 months in hospitalized COVID-19 was ascertained from day 30 after hospital admission until 6 months or end of follow-up. For each outcome, cohort participants without

a history of the outcome in the past year were included in the analysis. Hazard ratios (HR) and the related p-values were calculated by a Cox regression model. Odds ratios (ORs) and the related p-values were calculated using Fisher's exact test (methods). * $p<0.05$, ** $p<.$ 0.01, *** $p<0.001$. In boxplots, x is the mean; center line is the median; box limits are the 25th and 75th percentiles; whiskers extend to 1.5× the interquartile range (IQR) from the 25th and 75th percentiles; dots are outliers. # indicates that the hazard ratios were calculated using Firth's correction for monotone likelihood with profile likelihood confidence limits.

Supporting Information

Supplementary Figures Legends

Figure 1-Figure Supplement 1. Metabolic signature of infection in COVID-19 patients' samples and SARS-CoV-2 infected primary cells. (**A**) Venn diagrams describing the relationship between differentially expressed genes (DEG), metabolic genes (GO:0008152), and lipid metabolism genes (GO:0006629) in COVID-19 patient sample groups including epithelial cells isolated by bronchoalveolar lavage (lavage) and post-mortem lung biopsies (autopsy), as well as primary small airway epithelial cells (alveoli) and primary bronchial epithelial cells (bronchial) infected with SARS-CoV-2. (**B**) Sunburst graphs showing the coverage of composite metabolic terms[36] on general metabolic response induced by SARS-CoV-2 infection. Lipid and mitochondrial metabolism dominate the transcriptional metabolic signature of infection across all four sample groups. (**C**) Heat map of metabolic genes (**Figure 1D**) across four sample groups. Red and green boxes are up and downregulated by infection, respectively. # Indicates small sample size. (**D**) Metabolic analysis of SARS-CoV-2 and mock-infected primary bronchial epithelial cells confirms a 50% increase ($n=6$, $p<0.001$) in lactate production 48 hours post-infection. (**E**) The ratio of lactate production to glucose uptake (glycolytic index) in SARS-CoV-2 and mock-infected primary cells. Index increases from 1.0 to 1.7 out of 2.0 indicating a transition to glycolysis (*i.e., Warburg effect*). (**F**) Schematic depicting ER stress pathways superimposed with pathway-associated genes. Red and green boxes are up and downregulated by infection, respectively. * marks differentially regulated genes ($n=3$, $FDR<0.05$). Red and green arrows schematically note interactions based on the transcriptional response. XBP1S is the IRE1 spliced form of XBP1. (**G**) Heat map of ER stress pathway-associated genes (**Figure S1G**) across four sample groups. Red and green boxes are up and downregulated by infection, respectively. # Indicates small sample size.

Figure 2-Figure Supplement 1. Gene expression patterns of SARS-CoV-2 proteins. (**A**) Gene expression analysis of SARS-CoV-2 genes in primary bronchial epithelial cells expressing different SARS-CoV-2 proteins for 72 hours. (**B**) Gene expression analysis of PPARα and CPT1α genes in primary bronchial epithelial cells expressing different SARS-CoV-2 proteins for 72 hours. * $p<0.05$, ** $p<0.01$, *** $p<0.001$ in a 2-sided heteroscedastic student's t-test against control. Error bars indicate S.E.M.

Figure 3-Figure Supplement 1. **Metabolic regulators in SARS-CoV-2 infection *in vitro*.** (**A**) Schematic depicting the metabolic landscape of SARS-CoV-2 infection. Potential drugs (white boxes) and their therapeutic targets are marked on the chart. (**B**) Table summarizing FDA-approved drugs that interfere with SARS-CoV-2-induced metabolic alterations. (**C**) Microscopic analysis of lipid accumulation and cell number in alpha variant (USA-

WA1/2020) infected bronchial epithelial cells at MOI 2 after treatment with different metabolic regulators, compared to mock-infected bronchial epithelial cells. Bar = 30 μm.

Figure 3-Figure Supplement 2. **PPARα agonism anti-viral mechanism is ligand-wide and fatty oxidation dependent in SARS-CoV-2 infection *in vitro.*** (**A**) Microscopic analysis of lipid accumulation and cell number in alpha variant (hCoV-19/Israel/CVL-45526-NGS/2020) infected bronchial epithelial cells at TCID100 after treatment with different PPARα agonists (**B**) Quantification of alpha variant SARS-CoV-2 viral RNA before treatment with a physiological concentration of various PPARα agonists or DMSO (vehicle). (**C**) Microscopic analysis of lipid accumulation and cell number in delta variant (hCoV-19/Israel/CVL-12806/2021) infected bronchial epithelial cells at TCID50 after treatment with different PPARα agonists. (**D**) Quantification of delta variant SARS-CoV-2 viral RNA before treatment with a physiological concentration of various PPARα agonists or DMSO (vehicle). (**E-F**) Microscopic analysis of lipid accumulation and cell number in (**E**) alpha variant (hCoV-19/Israel/CVL-45526-NGS/2020) infected bronchial epithelial cells at TCID50 after 5 days of treatment with 20 μM fenofibrate or 20 μM fenofibrate and 4 μM CPT1α inhibitor etomoxir. (**F**) delta variant (hCoV-19/Israel/CVL-12806/2021) infected bronchial epithelial cells at TCID50 after treatment with 20 μM fenofibrate or 20 μM fenofibrate and 4 μM CPT1α inhibitor etomoxir. (**G**) Quantification of alpha and delta variant SARS-CoV-2 viral RNA before treatment with 20 μM fenofibrate or 20 μM fenofibrate and 4 μM CPT1α inhibitor etomoxir. * $p<0.05$, ** $p<0.01$, *** $p<0.001$. Bar = 50 μm. Error bars indicate S.E.M.

Figure 3-Figure Supplement 3. **PPARα is required for fenofibrate rescue and etomoxir reversal in SARS-CoV-2 infection *in vitro.*** (**A**) Gene expression of PPARα and CPT1α by qRT-PCR in bronchial epithelial cells or PPARα CRISPR-KO bronchial epithelial cells. Analysis shows a significant decrease in PPARα expression and its target gene CPT1α (n=6, $p<0.001$). (**B**) Western blot analysis of PPARα protein in bronchial epithelial cells or PPARα CRISPR-KO bronchial epithelial cells. Microscopic analysis of lipid accumulation and viability in (**C**) alpha variant (hCoV-19/Israel/CVL-45526-NGS/2020) infected PPARα K/O bronchial epithelial cells at TCID50 after 5 days of treatment with 20 μM fenofibrate or 20 μM fenofibrate and 4 μM CPT1α inhibitor etomoxir. (**D**) Delta (hCoV-19/Israel/CVL-12806/2021) infected PPARα K/O bronchial epithelial cells at TCID50 after 5 days of treatment with 20 μM fenofibrate or 20 μM fenofibrate and 4 μM CPT1α inhibitor etomoxir. (**E**) Quantification of alpha and delta variant SARS-CoV-2 viral RNA in infected PPARα K/O bronchial before treatment with 20 μM fenofibrate or 20 μM fenofibrate and 4 μM CPT1α inhibitor etomoxir. * $p<0.05$, ** $p<0.01$, *** $p<0.001$. Bar = 50 μm. Error bars indicate S.E.M.

Figure 4-Figure Supplement 1. **Observational study flow diagram.**

Figure 4-Figure Supplement 2. **The host-immune response in hospitalized COVID-19 patients in different metabolic interventions.** (**A-D**) Dynamic changes in (**A**) neutrophils, (**B**) lymphocytes, (**C**) monocytes, and (**D**) platelet levels during 21-day hospitalization in treatment and non-treatment groups (Control). The centerline shows the mean value while the 95% confidence interval is represented by the shaded region. **(E)** Microscopic analysis of lipid accumulation in lung cells induced by 10 μM of PPARγ agonist rosiglitazone and 100 μM oleic acid with or without 20 μM fenofibrate for 5 days. Lipogenic induction resulted in a 65% increase in triglycerides (n=6, $p<0.05$) and a 75% increase in phospholipids (n=6, $p<0.001$). Lipid increase in lung cells is reversed upon treatment with fenofibrate. (**F**)

Analysis of CCL20, CXCL1, CXCL2, CXCL5, GCSF, IL-1b, IL-6, IL-8, NFKB, SAA2, and TNFα by qRT-PCR as markers of immunoinflammatory stress. Lipogenic induction results in significant upregulation of chemokines, cytokines, and inflammation markers, which is reversed by fenofibrate (n=6, $p<0.05$). * $p<0.05$, ** $p<0.01$, *** $p<0.001$ in a 2-sided heteroscedastic student's t-test against control. Bar = 30 μm. Error bars indicate S.E.M.

Figure 5-Figure Supplement 1. **Interventional study CONSORT flow diagram.**

Figure 5-Figure Supplement 2. **Analysis of variant emergence dynamics and distribution during the study period in participants and other hospitalized patients.** (**A)** sample distribution (left) and relative abundance (left), with and without SGTF by day from 30 November 2020 to 28 February 2021. **(B)** Stratified relative abundance of samples with and without SGTF of patients in the interventional study (left) and other hospitalized patients (right) from 16 December 2020 to 28 February 2021. **(C)** Pie chart representation of variant distribution between the patient in the interventional study and other patients in other clinical centers in Israel during the same period (OR: 1.36, 0.59 to 3.1; p = 0.44). SGTF, S-gene target failure, serves as a proxy for identifying B.1.1.7 cases [52,53]. **(D)** Distribution comparison of sample distribution with and without SGTF in stratified periods. Odds ratios (ORs) and the related p-values were calculated using Fisher's exact test (methods). SGTF, S-gene target failure, serves as a proxy for identifying B.1.1.7 cases [52,53]. **(E)** Assessment of significant post-acute incident diagnoses in people who had been hospitalized with COVID-19 (long COVID) in patients registered in the VA database [27] vs. those treated with 145 mg fenofibrate in this study at 6 months after hospital discharge. Incident rates per 1000 at 6-months in hospitalized COVID-19 were ascertained from day 30 after hospital admission until 6 months or end of follow-up. A p-value less than 0.001 was considered statistically significant and included in the analysis. For each outcome, cohort participants without a history of the outcome in the past year were included in the analysis.

Supplementary Files

Supplementary File 1. Differentially expressed genes (DEG) analysis in SARS-CoV-2 infected human lung epithelium. (**Tab 2)** Normal bronchial epithelial cells (**Tab 3**) Lung Biopsies (**Tab 4**) Small airway (**Tab 5-6**) Epithelial cells in bronchial alveolar lavage fluid. (**Tab 7**) Primer list used for qPCR gene expression validations.

Supplementary File 2. Observational study descriptive statistics. (**Tab 1-8**) **Characteristics of COVID-19 patients in the cohort.** SBP, systolic blood pressure; DBP, diastolic blood pressure; COPD, chronic obstructive pulmonary disease; SpO2, oxygen saturation; ECMO, extracorporeal membrane oxygenation; IQR, interquartile range. Continuous variables were compared with a two-sample t-test and categorical variables with Fisher's exact test. (**Tab 9-11**) **Observational comparison between unique patients' visits to Hadassah medical center taking metabolic regulators and unique patients in various hospitalization conditions in patients with COVID-19 taking metabolic regulators in different periods**. Patients taking thiazolidinediones (n=37; $p<0.001$), metformin (n=321; $p<0.01$), SGLT2 inhibitors (n=54; $p<0.001$), statins (n=924; $p<0.001$), or telmisartan (IRE1α inhibitor; n = 278; $p<0.001$) were over-represented across all severity indicators, while patients taking fibrates (n=21) were significantly underrepresented in hospital admissions

(p=0.02) and were not over-represented in other severity indicators regardless of the period examined. Observational comparison between unique patients visiting Hadassah medical center during (**Tab 9**) 11/2018-2019, (**Tab 10**) 11/2015-2020, or (**Tab 11**) 11/2010-2020 taking metabolic regulators and unique patients in various hospitalization conditions in patients with COVID-19 taking metabolic regulators. (**Tab 12-20**) **Characteristics of patients included in the study.** Patients included in the study were between the age of 45-100, that were hospitalized for more than 3 days (N=1,438). SBP, systolic blood pressure; DBP, diastolic blood pressure; COPD, chronic obstructive pulmonary disease; SpO2, oxygen saturation; ECMO, extracorporeal membrane oxygenation; IQR, interquartile range Continuous variables were compared with a two-sample t-test and categorical variables with Fisher's exact test. (**Tab 21**) **Cox regression model of 28-days mortality in the treatment groups versus control.** Adjusted HR and p-values were calculated based using a Cox regression model adjusting for age, gender, and pre-existing comorbidities (smoking, asthma, COPD, DM, hypertension, diabetes, coronary heart disease, obesity, dyslipidemia, cerebrovascular disease, chronic liver disease, and chronic kidney disease). There were no deaths recorded in fibrate patients, resulting in monotone likelihood (non-convergence of likelihood function, Firth's penalized maximum likelihood bias reduction method was implemented to calculate hazard ratios and confidence intervals. Thiazolidinediones and SGLT2 inhibitors users show a significantly higher risk of death within 28 days of hospitalization (adjusted risk). # indicates that the hazard ratios were calculated using Firth's correction for monotone likelihood with profile likelihood confidence limits.

Supplementary File 3. International comparative validation cohorts descriptive statistics. (**Tab 1**) **Comparative Cohort of the Outpatient Lipid Clinics of the University of Bologna and of the Niguarda Hospital in Milan.** (**A**) Characteristics of included patients stratified by lipid-lowering treatment. A cohort of 2,123 patients (M: 48.1%, F: 51.9%) on statins (1,791, mean age 59,2±15.2 years), fenofibrate (220, mean age 60,7±15.4 years) or both (112, mean age 62,9±16.3 years) were interviewed. Patients on statins were significantly younger than those on both drugs (p=0.023). 177 patients received a diagnosis of COVID by molecular swab: 9.2% of statin-treated subjects, 3.2% of fenofibrate-treated ones, and 5.4% of those treated with both statins and fenofibrate (p=0.005) without differences in the source of exposition (family members, co-workers; p=0.648). (**B**) Disease severity stratified by lipid-lowering treatment. 134 reported mild COVID-19 symptoms and 31 patients reported severe COVID-19 symptoms, requiring hospitalization: 1.7% of statin-treated subjects, 0.5% of fenofibrate-treated ones, and 0% of those treated with both statins and fenofibrate (p=0.022) without differences in the source of exposure. (**C**) Characteristics of included patients according to the personal history of COVID. Patients affected by COVID were more frequently obese, with COPD and/or cardiovascular diseases, and had strict contact with COVID-affected subjects, independent of the lipid-lowering treatment. (**D**) Characteristics of patients exposed to contact with affected people (n=254). Out of 254 patients reporting contact with affected people, 45 became positive for COVID. 93.3% were in treatment with statins 4.4% with fenofibrate and 4.5% with both (p=0.059). Affected to exposed to positive contacts ratio according to background lipid-lowering was 20.5% in patients treated with statins 7.4% with fenofibrate and 4.5% with both (p=0.059). (**Tab 2**) **Comparative cohort in the American veteran's health administration (VHA) registry.** (**A**) Characteristics of fenofibrate users compared with non-users before and after PSM. (**B**) The median duration of hospitalization among fenofibrate users vs. non-users. (**C**) SARS-CoV-2 infection and COVID-19 severity among fenofibrate users vs. non-users.

Supplementary File 4. Interventional study descriptive statistics. (**Tab 1**) **Characteristics of patients compared in the patients in the interventional study** 15 Participants who met the inclusion criteria were assigned to intervention with nanocrystallized fenofibrate (TriCor®, AbbVie Inc., North Chicago, IL USA) at a dose of 145 mg (1 tablet) once per day. Standard care for severe-hospitalize COVID-19 patients was provided according to local practice: antiviral treatment, vitamin D3, low-dose glucocorticoids, convalescent plasma, and supportive care as well as antipyretic for symptoms of fever (products containing paracetamol, or non-steroidal anti-inflammatories such as aspirin and ibuprofen) and dextromethorphan for symptoms of cough. Standard chronic treatments were continued unless COVID-19, clinical status, or fenofibrate treatment was a counterindication for the treatment. Control patients were collected from the observational study's database and filtered to patients that meet the inclusion criteria, were admitted with low immunoinflammatory stress (NLR<10 at admission), and were treated according to the standard care used in the interventional study. SBP, systolic blood pressure; DBP, diastolic blood pressure; COPD, chronic obstructive pulmonary disease; SpO2, oxygen saturation; ECMO, extracorporeal membrane oxygenation; IQR, interquartile range. Continuous variables were expressed as median [IQR] and were compared with a Mann-Whitney U test. Categorical variables were expressed as a count and percentage (%) and compared with a chi-squared test or Fisher's exact test. The sample size is detailed in each display item. (**Tab 2**) **Cox regression model of 28-days mortality in the treatment group versus control.** Adjusted HR and p-values were calculated based using an unadjusted Cox regression model, a Cox regression model adjusting for age, gender, and pre-existing comorbidities (smoking, asthma, COPD, DM, hypertension, diabetes, coronary heart disease, obesity, dyslipidemia, cerebrovascular disease, chronic liver disease, and chronic kidney disease) or a Cox regression model adjusting for significantly different patient characteristics, obesity, chronic kidney disease, and SpO2. (**A**) Cox regression model of 28-days hospital discharge. (**B**) Cox regression model of 28-days oxygen withdrawal. (**C**) Cox regression model of 28-days mortality. There were no deaths recorded in the treatment patients, resulting in monotone likelihood (non-convergence of likelihood function, Firth's penalized maximum likelihood bias reduction method was implemented to calculate hazard ratios and confidence intervals.

Source Data Files

Figure 1-Source data. Raw measurements, mean, standard error, and student t-test values were used to create the display items in Figure 1.

Figure 2-Source data. Raw measurements, mean, standard error, and student t-test values were used to create the display items in Figure 2.

Figure 3-Source data. Raw measurements, mean, standard error, and student t-test values were used to create the display items in Figure 3.

Figure 3-Figure Supplement 3-Source data. (1) original and (2) inverted files of the full raw unedited alpha tubulin blot. (3) original and (4) inverted files of the full raw unedited PPAR alpha blot. (5) The uncropped blots with the relevant bands are clearly labeled.

REFERENCES

1 Grasselli, G. *et al.* Pathophysiology of COVID-19-associated acute respiratory distress syndrome: a multicentre prospective observational study. *The Lancet Respiratory Medicine* **8**, 1201-1208 (2020). https://doi.org:10.1016/S2213-2600(20)30370-2

2 Bornstein, S. R., Dalan, R., Hopkins, D., Mingrone, G. & Boehm, B. O. Endocrine and metabolic link to coronavirus infection. *Nature Reviews Endocrinology* (2020). https://doi.org:10.1038/s41574-020-0353-9

3 Zhu, L. *et al.* Association of Blood Glucose Control and Outcomes in Patients with COVID-19 and Pre-existing Type 2 Diabetes. *Cell Metabolism* (2020). https://doi.org:https://doi.org/10.1016/j.cmet.2020.04.021

4 Ko, J. Y. *et al.* Risk Factors for COVID-19-associated hospitalization: COVID-19-Associated Hospitalization Surveillance Network and Behavioral Risk Factor Surveillance System. *Clin Infect Dis* (2020). https://doi.org:10.1093/cid/ciaa1419

5 Williamson, E. J. *et al.* Factors associated with COVID-19-related death using OpenSAFELY. *Nature* **584**, 430-436 (2020). https://doi.org:10.1038/s41586-020-2521-4

6 Thomas, T. *et al.* COVID-19 infection alters kynurenine and fatty acid metabolism, correlating with IL-6 levels and renal status. *JCI Insight* **5** (2020). https://doi.org:10.1172/jci.insight.140327

7 Codo, A. C. *et al.* Elevated Glucose Levels Favor SARS-CoV-2 Infection and Monocyte Response through a HIF-1α/Glycolysis-Dependent Axis. *Cell Metabolism* **32**, 437-446.e435 (2020). https://doi.org:https://doi.org/10.1016/j.cmet.2020.07.007

8 Ajaz, S. *et al.* Mitochondrial metabolic manipulation by SARS-CoV-2 in peripheral blood mononuclear cells of patients with COVID-19. *American Journal of Physiology-Cell Physiology* **320**, C57-C65 (2021). https://doi.org:10.1152/ajpcell.00426.2020

9 Gordon, D. E. *et al.* A SARS-CoV-2-Human Protein-Protein Interaction Map Reveals Drug Targets and Potential Drug-Repurposing. *bioRxiv*, 2020.2003.2022.002386 (2020). https://doi.org:10.1101/2020.03.22.002386

10 Bojkova, D. *et al.* Proteomics of SARS-CoV-2-infected host cells reveals therapy targets. *Nature* **583**, 469-472 (2020). https://doi.org:10.1038/s41586-020-2332-7

11 Delorey, T. M. *et al.* COVID-19 tissue atlases reveal SARS-CoV-2 pathology and cellular targets. *Nature* (2021). https://doi.org:10.1038/s41586-021-03570-8

12 Melms, J. C. *et al.* A molecular single-cell lung atlas of lethal COVID-19. *Nature* (2021). https://doi.org:10.1038/s41586-021-03569-1

13 Islam, A. B. M. M. K. & Khan, M. A.-A.-K. Lung transcriptome of a COVID-19 patient and systems biology predictions suggest impaired surfactant production which may be druggable by surfactant therapy. *Scientific reports* **10**, 19395-19395 (2020). https://doi.org:10.1038/s41598-020-76404-8

14 Singh, K. *et al.* Network Analysis and Transcriptome Profiling Identify Autophagic and Mitochondrial Dysfunctions in SARS-CoV-2 Infection. *Front Genet* **12**, 599261-599261 (2021). https://doi.org:10.3389/fgene.2021.599261

15 Yuan, S. *et al.* SREBP-dependent lipidomic reprogramming as a broad-spectrum antiviral target. *Nature Communications* **10**, 120 (2019). https://doi.org:10.1038/s41467-018-08015-x

16 McBride, C. E. & Machamer, C. E. Palmitoylation of SARS-CoV S protein is necessary for partitioning into detergent-resistant membranes and cell-cell fusion but not

interaction with M protein. *Virology* **405**, 139-148 (2010). https://doi.org:10.1016/j.virol.2010.05.031

17 Yan, B. *et al.* Characterization of the Lipidomic Profile of Human Coronavirus-Infected Cells: Implications for Lipid Metabolism Remodeling upon Coronavirus Replication. *Viruses* **11**, 73 (2019). https://doi.org:10.3390/v11010073

18 Barberis, E. *et al.* Large-Scale Plasma Analysis Revealed New Mechanisms and Molecules Associated with the Host Response to SARS-CoV-2. *Int J Mol Sci* **21** (2020). https://doi.org:10.3390/ijms21228623

19 Wang, L. *et al.* Serum triglyceride level and hypertension are highly associated with the recovery of COVID-19 patients. *Am J Transl Res* **12**, 6646-6654 (2020).

20 Masana, L. *et al.* Low HDL and high triglycerides predict COVID-19 severity. *Sci Rep* **11**, 7217 (2021). https://doi.org:10.1038/s41598-021-86747-5

21 Bergen, W. G. & Mersmann, H. J. Comparative Aspects of Lipid Metabolism: Impact on Contemporary Research and Use of Animal Models. *The Journal of Nutrition* **135**, 2499-2502 (2005). https://doi.org:10.1093/jn/135.11.2499

22 Demetrius, L. Of mice and men. When it comes to studying ageing and the means to slow it down, mice are not just small humans. *EMBO Rep* **6 Spec No**, S39-S44 (2005). https://doi.org:10.1038/sj.embor.7400422

23 Kulcsar, K. A., Coleman, C. M., Beck, S. E. & Frieman, M. B. Comorbid diabetes results in immune dysregulation and enhanced disease severity following MERS-CoV infection. *JCI insight* **4**, e131774 (2019). https://doi.org:10.1172/jci.insight.131774

24 Wu, Q. *et al.* Altered Lipid Metabolism in Recovered SARS Patients Twelve Years after Infection. *Scientific Reports* **7**, 9110 (2017). https://doi.org:10.1038/s41598-017-09536-z

25 Yang, J. K., Lin, S. S., Ji, X. J. & Guo, L. M. Binding of SARS coronavirus to its receptor damages islets and causes acute diabetes. *Acta Diabetol* **47**, 193-199 (2010). https://doi.org:10.1007/s00592-009-0109-4

26 Akter, F. *et al.* Clinical characteristics and short term outcomes after recovery from COVID-19 in patients with and without diabetes in Bangladesh. *Diabetes Metab Syndr* **14**, 2031-2038 (2020). https://doi.org:10.1016/j.dsx.2020.10.016

27 Al-Aly, Z., Xie, Y. & Bowe, B. High-dimensional characterization of post-acute sequelae of COVID-19. *Nature* **594**, 259-264 (2021). https://doi.org:10.1038/s41586-021-03553-9

28 Li, G. *et al.* Follow-up study on serum cholesterol profiles and potential sequelae in recovered COVID-19 patients. *BMC Infectious Diseases* **21**, 299 (2021). https://doi.org:10.1186/s12879-021-05984-1

29 Ahmadian, M. *et al.* PPARγ signaling and metabolism: the good, the bad and the future. *Nature medicine* **19**, 557-566 (2013). https://doi.org:10.1038/nm.3159

30 Todd, M. K., Watt, M. J., Le, J., Hevener, A. L. & Turcotte, L. P. Thiazolidinediones enhance skeletal muscle triacylglycerol synthesis while protecting against fatty acid-induced inflammation and insulin resistance. *Am J Physiol Endocrinol Metab* **292**, E485-493 (2007). https://doi.org:10.1152/ajpendo.00080.2006

31 Phan, A. N. H. *et al.* PPARγ sumoylation-mediated lipid accumulation in lung cancer. *Oncotarget* **8**, 82491-82505 (2017). https://doi.org:10.18632/oncotarget.19700

32 Esnaola, M., Puig, P., Gonzalez, D., Castelo, R. & Gonzalez, J. R. A flexible count data model to fit the wide diversity of expression profiles arising from extensively

replicated RNA-seq experiments. *BMC Bioinformatics* **14**, 254 (2013). https://doi.org:10.1186/1471-2105-14-254

33 Robinson, M. D., McCarthy, D. J. & Smyth, G. K. edgeR: a Bioconductor package for differential expression analysis of digital gene expression data. *Bioinformatics* **26**, 139-140 (2009). https://doi.org:10.1093/bioinformatics/btp616

34 Chen, S., Zhou, Y., Chen, Y. & Gu, J. fastp: an ultra-fast all-in-one FASTQ preprocessor. *Bioinformatics* **34**, i884-i890 (2018). https://doi.org:10.1093/bioinformatics/bty560

35 Bray, N. L., Pimentel, H., Melsted, P. & Pachter, L. Near-optimal probabilistic RNA-seq quantification. *Nature Biotechnology* **34**, 525-527 (2016). https://doi.org:10.1038/nbt.3519

36 Levy, G. *et al.* Nuclear receptors control pro-viral and antiviral metabolic responses to hepatitis C virus infection. *Nature Chemical Biology* **12**, 1037-1045 (2016). https://doi.org:10.1038/nchembio.2193

37 Huang, D. W., Sherman, B. T. & Lempicki, R. A. Systematic and integrative analysis of large gene lists using DAVID bioinformatics resources. *Nature Protocols* **4**, 44-57 (2009). https://doi.org:10.1038/nprot.2008.211

38 Mi, H., Muruganujan, A., Ebert, D., Huang, X. & Thomas, P. D. PANTHER version 14: more genomes, a new PANTHER GO-slim and improvements in enrichment analysis tools. *Nucleic Acids Research* **47**, D419-D426 (2018). https://doi.org:10.1093/nar/gky1038

39 Xia, J., Gill, E. E. & Hancock, R. E. W. NetworkAnalyst for statistical, visual and network-based meta-analysis of gene expression data. *Nature Protocols* **10**, 823-844 (2015). https://doi.org:10.1038/nprot.2015.052

40 Ehrlich, A. *et al.* Microphysiological flux balance platform unravels the dynamics of drug induced steatosis. *Lab Chip* **18**, 2510-2522 (2018). https://doi.org:10.1039/c8lc00357b

41 Liu, J. *et al.* Sequential CRISPR-Based Screens Identify LITAF and CDIP1 as the Bacillus cereus Hemolysin BL Toxin Host Receptors. *Cell Host & Microbe* **28**, 402-410.e405 (2020). https://doi.org:https://doi.org/10.1016/j.chom.2020.05.012

42 Chu, D. K. W. *et al.* Molecular Diagnosis of a Novel Coronavirus (2019-nCoV) Causing an Outbreak of Pneumonia. *Clin Chem* **66**, 549-555 (2020). https://doi.org:10.1093/clinchem/hvaa029

43 Corman, V. M. *et al.* Detection of 2019 novel coronavirus (2019-nCoV) by real-time RT-PCR. *Euro Surveill* **25**, 2000045 (2020). https://doi.org:10.2807/1560-7917.ES.2020.25.3.2000045

44 Rosenthal, N., Cao, Z., Gundrum, J., Sianis, J. & Safo, S. Risk Factors Associated With In-Hospital Mortality in a US National Sample of Patients With COVID-19. *JAMA Network Open* **3**, e2029058-e2029058 (2020). https://doi.org:10.1001/jamanetworkopen.2020.29058

45 Cummings, M. J. *et al.* Epidemiology, clinical course, and outcomes of critically ill adults with COVID-19 in New York City: a prospective cohort study. *The Lancet* **395**, 1763-1770 (2020). https://doi.org:10.1016/S0140-6736(20)31189-2

46 King, G. & Nielsen, R. Why Propensity Scores Should Not Be Used for Matching. *Political Analysis* **27**, 435-454 (2019). https://doi.org:10.1017/pan.2019.11

47 Wang, J. To use or not to use propensity score matching? *Pharmaceutical Statistics* **20**, 15-24 (2021). https://doi.org:https://doi.org/10.1002/pst.2051

48 Fullerton, B. *et al.* The Comparison of Matching Methods Using Different Measures of Balance: Benefits and Risks Exemplified within a Study to Evaluate the Effects of German Disease Management Programs on Long-Term Outcomes of Patients with Type 2 Diabetes. *Health Serv Res* **51**, 1960-1980 (2016). https://doi.org:10.1111/1475-6773.12452

49 Ali, M. S. *et al.* Propensity Score Methods in Health Technology Assessment: Principles, Extended Applications, and Recent Advances. *Frontiers in Pharmacology* **10** (2019). https://doi.org:10.3389/fphar.2019.00973

50 Cleveland, W. S. Robust Locally Weighted Regression and Smoothing Scatterplots. *Journal of the American Statistical Association* **74**, 829-836 (1979). https://doi.org:10.1080/01621459.1979.10481038

51 Heinze, G. & Schemper, M. A solution to the problem of monotone likelihood in Cox regression. *Biometrics* **57**, 114-119 (2001). https://doi.org:10.1111/j.0006-341x.2001.00114.x

52 Brown, K. A. *et al.* S-Gene Target Failure as a Marker of Variant B.1.1.7 Among SARS-CoV-2 Isolates in the Greater Toronto Area, December 2020 to March 2021. *JAMA* (2021). https://doi.org:10.1001/jama.2021.5607

53 Davies, N. G. *et al.* Increased mortality in community-tested cases of SARS-CoV-2 lineage B.1.1.7. *Nature* **593**, 270-274 (2021). https://doi.org:10.1038/s41586-021-03426-1

54 Cheng, X. *et al.* Metformin Is Associated with Higher Incidence of Acidosis, but Not Mortality, in Individuals with COVID-19 and Pre-existing Type 2 Diabetes. *Cell metabolism* **32**, 537-547.e533 (2020). https://doi.org:10.1016/j.cmet.2020.08.013

55 Zhang, X.-J. *et al.* In-Hospital Use of Statins Is Associated with a Reduced Risk of Mortality among Individuals with COVID-19. *Cell metabolism* **32**, 176-187.e174 (2020). https://doi.org:10.1016/j.cmet.2020.06.015

56 Shyu, W. M. in *Statistical models in S* 309-376 (Routledge, 2017).

57 Vanderheiden, A. *et al.* Type I and Type III Interferons Restrict SARS-CoV-2 Infection of Human Airway Epithelial Cultures. *J Virol* **94** (2020). https://doi.org:10.1128/jvi.00985-20

58 Liao, M. *et al.* Single-cell landscape of bronchoalveolar immune cells in patients with COVID-19. *Nature Medicine* **26**, 842-844 (2020). https://doi.org:10.1038/s41591-020-0901-9

59 Mayer, K. A., Stöckl, J., Zlabinger, G. J. & Gualdoni, G. A. Hijacking the Supplies: Metabolism as a Novel Facet of Virus-Host Interaction. *Frontiers in Immunology* **10** (2019). https://doi.org:10.3389/fimmu.2019.01533

60 Sharpe, L. J. & Brown, A. J. Controlling cholesterol synthesis beyond 3-hydroxy-3-methylglutaryl-CoA reductase (HMGCR). *The Journal of biological chemistry* **288**, 18707-18715 (2013). https://doi.org:10.1074/jbc.R113.479808

61 Yu, Y., Maguire, T. G. & Alwine, J. C. ChREBP, a glucose-responsive transcriptional factor, enhances glucose metabolism to support biosynthesis in human cytomegalovirus-infected cells. *Proc Natl Acad Sci U S A* **111**, 1951-1956 (2014). https://doi.org:10.1073/pnas.1310779111

62 Han, J. & Kaufman, R. J. The role of ER stress in lipid metabolism and lipotoxicity. *J Lipid Res* **57**, 1329-1338 (2016). https://doi.org:10.1194/jlr.R067595

63 Yu, Y., Pierciey, F. J., Jr., Maguire, T. G. & Alwine, J. C. PKR-like endoplasmic reticulum kinase is necessary for lipogenic activation during HCMV infection. *PLoS Pathog* **9**, e1003266 (2013). https://doi.org:10.1371/journal.ppat.1003266

64 Rutkowski, D. T. *et al.* UPR Pathways Combine to Prevent Hepatic Steatosis Caused by ER Stress-Mediated Suppression of Transcriptional Master Regulators. *Developmental Cell* **15**, 829-840 (2008). https://doi.org:https://doi.org/10.1016/j.devcel.2008.10.015

65 Mookerjee, S. A., Gerencser, A. A., Nicholls, D. G. & Brand, M. D. Quantifying intracellular rates of glycolytic and oxidative ATP production and consumption using extracellular flux measurements. *The Journal of biological chemistry* **292**, 7189-7207 (2017). https://doi.org:10.1074/jbc.M116.774471

66 Lalloyer, F. & Staels, B. Fibrates, glitazones, and peroxisome proliferator-activated receptors. *Arterioscler Thromb Vasc Biol* **30**, 894-899 (2010). https://doi.org:10.1161/ATVBAHA.108.179689

67 Fruchart, J. C. & Duriez, P. Mode of action of fibrates in the regulation of triglyceride and HDL-cholesterol metabolism. *Drugs Today (Barc)* **42**, 39-64 (2006). https://doi.org:10.1358/dot.2006.42.1.963528

68 Bocher, V., Chinetti, G., Fruchart, J. C. & Staels, B. [PPARs activators and regulation of lipid metabolism, vascular inflammation and atherosclerosis]. *Journ Annu Diabetol Hotel Dieu*, 23-32 (2001).

69 Sheu, M. Y. *et al.* Topical peroxisome proliferator activated receptor-alpha activators reduce inflammation in irritant and allergic contact dermatitis models. *J Invest Dermatol* **118**, 94-101 (2002). https://doi.org:10.1046/j.0022-202x.2001.01626.x

70 Price, E. T., Welder, G. J. & Zineh, I. Modulatory effect of fenofibrate on endothelial production of neutrophil chemokines IL-8 and ENA-78. *Cardiovasc Drugs Ther* **26**, 95-99 (2012). https://doi.org:10.1007/s10557-011-6368-7

71 Ann, S. J. *et al.* PPARα agonists inhibit inflammatory activation of macrophages through upregulation of β-defensin 1. *Atherosclerosis* **240**, 389-397 (2015). https://doi.org:10.1016/j.atherosclerosis.2015.04.005

72 Gualdoni, G. A. *et al.* Rhinovirus induces an anabolic reprogramming in host cell metabolism essential for viral replication. *Proc Natl Acad Sci U S A* **115**, E7158-e7165 (2018). https://doi.org:10.1073/pnas.1800525115

73 Kilbourne, E. D. Inhibition of influenza virus multiplication with a glucose antimetabolite (2-deoxy-D-glucose). *Nature* **183**, 271-272 (1959). https://doi.org:10.1038/183271b0

74 Fujita, N. *et al.* Effects of bezafibrate in patients with chronic hepatitis C virus infection: combination with interferon and ribavirin. *J Viral Hepat* **13**, 441-448 (2006). https://doi.org:10.1111/j.1365-2893.2005.00718.x

75 Ikeda, M. *et al.* Different anti-HCV profiles of statins and their potential for combination therapy with interferon. *Hepatology* **44**, 117-125 (2006). https://doi.org:10.1002/hep.21232

76 Andrzejewski, S., Gravel, S.-P., Pollak, M. & St-Pierre, J. Metformin directly acts on mitochondria to alter cellular bioenergetics. *Cancer Metab* **2**, 12-12 (2014). https://doi.org:10.1186/2049-3002-2-12

77 Tang, D. *et al.* Metformin facilitates BG45-induced apoptosis via an anti-Warburg effect in cholangiocarcinoma cells. *Oncol Rep* **39**, 1957-1965 (2018). https://doi.org:10.3892/or.2018.6275

78 Tong, Q. *et al.* Inhibition of endoplasmic reticulum stress-activated IRE1α-TRAF2-caspase-12 apoptotic pathway is involved in the neuroprotective effects of telmisartan in the rotenone rat model of Parkinson's disease. *Eur J Pharmacol* **776**, 106-115 (2016). https://doi.org:10.1016/j.ejphar.2016.02.042

79 Belvisi, M. G. & Mitchell, J. A. Targeting PPAR receptors in the airway for the treatment of inflammatory lung disease. *British Journal of Pharmacology* **158**, 994-1003 (2009). https://doi.org:https://doi.org/10.1111/j.1476-5381.2009.00373.x

80 Burggraaff, L. *et al.* Identification of novel small molecule inhibitors for solute carrier SGLT1 using proteochemometric modeling. *Journal of Cheminformatics* **11**, 15 (2019). https://doi.org:10.1186/s13321-019-0337-8

81 Ehrlich, A. *et al.* The SARS-CoV-2 Transcriptional Metabolic Signature in Lung Epithelium. *SSRN Electronic Journal* (2020). https://doi.org:10.2139/ssrn.3650499

82 Davies, S. P. *et al.* The Hyperlipidaemic Drug Fenofibrate Significantly Reduces Infection by SARS-CoV-2 in Cell Culture Models. *Frontiers in Pharmacology* **12** (2021). https://doi.org:10.3389/fphar.2021.660490

83 Mueller, A. A. *et al.* Inflammatory Biomarker Trends Predict Respiratory Decline in COVID-19 Patients. *Cell Reports Medicine* **1**, 100144 (2020). https://doi.org:10.1016/j.xcrm.2020.100144

84 Feng, X. *et al.* Immune-Inflammatory Parameters in COVID-19 Cases: A Systematic Review and Meta-Analysis. *Frontiers in Medicine* **7** (2020). https://doi.org:10.3389/fmed.2020.00301

85 Zhu, Z. *et al.* Clinical value of immune-inflammatory parameters to assess the severity of coronavirus disease 2019. *International Journal of Infectious Diseases* **95**, 332-339 (2020). https://doi.org:https://doi.org/10.1016/j.ijid.2020.04.041

86 World Health, O. COVID-19 clinical management: living guidance, 25 January 2021. (World Health Organization, Geneva, 2021).

87 Feher, M. *et al.* Fenofibrate as a COVID-19 modifying drug: Laboratory success versus real-world reality. *Atherosclerosis* **339**, 55-56 (2021). https://doi.org:10.1016/j.atherosclerosis.2021.11.012

88 Chapman, M. J. Pharmacology of fenofibrate. *Am J Med* **83**, 21-25 (1987). https://doi.org:10.1016/0002-9343(87)90867-9

89 Ling, H., Luoma, J. T. & Hilleman, D. A Review of Currently Available Fenofibrate and Fenofibric Acid Formulations. *Cardiol Res* **4**, 47-55 (2013). https://doi.org:10.4021/cr270w

90 Maciejewski, S. & Hilleman, D. Effectiveness of a fenofibrate 145-mg nanoparticle tablet formulation compared with the standard 160-mg tablet in patients with coronary heart disease and dyslipidemia. *Pharmacotherapy* **28**, 570-575 (2008). https://doi.org:10.1592/phco.28.5.570

91 Smallwood, H. S. *et al.* Targeting Metabolic Reprogramming by Influenza Infection for Therapeutic Intervention. *Cell Rep* **19**, 1640-1653 (2017). https://doi.org:10.1016/j.celrep.2017.04.039

92 Zhu, N. *et al.* Morphogenesis and cytopathic effect of SARS-CoV-2 infection in human airway epithelial cells. *Nature Communications* **11**, 3910 (2020). https://doi.org:10.1038/s41467-020-17796-z

93 Setti, L., Kirienko, M., Dalto, S. C., Bonacina, M. & Bombardieri, E. FDG-PET/CT findings highly suspicious for COVID-19 in an Italian case series of asymptomatic

patients. *European Journal of Nuclear Medicine and Molecular Imaging* **47**, 1649-1656 (2020). https://doi.org:10.1007/s00259-020-04819-6

94 Turabian, J. L. A Case Control-Study of Cloperastine Treatment in Covid-19. Potential Drug, Clinical Observation and Common Sense. *Epidemiology International Journal* **4**, 13 (2020). https://doi.org:https://doi.org/10.23880/eij-16000S1-009

95 Xu, Z. *et al.* Pathological findings of COVID-19 associated with acute respiratory distress syndrome. *The Lancet Respiratory Medicine* **8**, 420-422 (2020). https://doi.org:10.1016/S2213-2600(20)30076-X

96 Pizzorno, A. *et al.* Characterization and treatment of SARS-CoV-2 in nasal and bronchial human airway epithelia. *bioRxiv*, 2020.2003.2031.017889 (2020). https://doi.org:10.1101/2020.03.31.017889

97 Plantier, L. *et al.* Activation of sterol-response element-binding proteins (SREBP) in alveolar type II cells enhances lipogenesis causing pulmonary lipotoxicity. *J Biol Chem* **287**, 10099-10114 (2012). https://doi.org:10.1074/jbc.M111.303669

98 Silvas, J. A., Jureka, A. S., Nicolini, A. M., Chvatal, S. A. & Basler, C. F. Inhibitors of VPS34 and lipid metabolism suppress SARS-CoV-2 replication. *bioRxiv*, 2020.2007.2018.210211 (2020). https://doi.org:10.1101/2020.07.18.210211

99 Hao Zhang, J. S., Heng Xu, Jing Sun, Wen Yin, Yu Zuo, Zhangzhao Wang, Fengmin Xiong, Yuqi Zhang, Hua Lin, Jingqiu Liu, Yiluan Ding, Naixia Zhang, Hualiang Jiang, & Kaixian Chen, W. J. Z., Kehao Zhao, Jincun Zhao, Xiangyang Xie and Cheng Luo. Activation of Peroxiredoxin 1 by Fluvastatin Effectively Protects from Inflammation and SARS-CoV-2. *SSRN Electronic Journal* (2020). https://doi.org:https://dx.doi.org/10.2139/ssrn.3606782

100 Wei Qiu, P. D. C. F. D. E. A. R. (ed OFFICE OF CLINICAL PHARMACOLOGY AND BIOPHARMACEUTICS; FDA) (U.S. Food and Drug Administration, 2004).

101 Godfrey, A. R., Digiacinto, J. & Davis, M. W. Single-dose bioequivalence of 105-mg fenofibric acid tablets versus 145-mg fenofibrate tablets under fasting and fed conditions: a report of two phase I, open-label, single-dose, randomized, crossover clinical trials. *Clin Ther* **33**, 766-775 (2011). https://doi.org:10.1016/j.clinthera.2011.05.047

102 Sonet, B., Vanderbist, F., Streel, B. & Houin, G. Randomised crossover studies of the bioequivalence of two fenofibrate formulations after administration of a single oral dose in healthy volunteers. *Arzneimittelforschung* **52**, 200-204 (2002). https://doi.org:10.1055/s-0031-1299880

103 Alsabeeh, N., Chausse, B., Kakimoto, P. A., Kowaltowski, A. J. & Shirihai, O. Cell culture models of fatty acid overload: Problems and solutions. *Biochim Biophys Acta Mol Cell Biol Lipids* **1863**, 143-151 (2018). https://doi.org:10.1016/j.bbalip.2017.11.006

104 Uhlén, M. *et al.* Proteomics. Tissue-based map of the human proteome. *Science* **347**, 1260419 (2015). https://doi.org:10.1126/science.1260419

105 Berglund, L. *et al.* A genecentric Human Protein Atlas for expression profiles based on antibodies. *Mol Cell Proteomics* **7**, 2019-2027 (2008). https://doi.org:10.1074/mcp.R800013-MCP200

106 Karlsson, M. *et al.* A single-cell type transcriptomics map of human tissues. *Sci Adv* **7** (2021). https://doi.org:10.1126/sciadv.abh2169

107 Uhlen, M. *et al.* A genome-wide transcriptomic analysis of protein-coding genes in human blood cells. *Science* **366** (2019). https://doi.org:10.1126/science.aax9198

108 Riva, L. *et al.* Discovery of SARS-CoV-2 antiviral drugs through large-scale compound repurposing. *Nature* **586**, 113-119 (2020). https://doi.org:10.1038/s41586-020-2577-1

109 Bakowski, M. A. *et al.* Drug repurposing screens identify chemical entities for the development of COVID-19 interventions. *Nat Commun* **12**, 3309 (2021). https://doi.org:10.1038/s41467-021-23328-0

110 Liu, Y. *et al.* Cell-Type Apoptosis in Lung during SARS-CoV-2 Infection. *Pathogens* **10** (2021). https://doi.org:10.3390/pathogens10050509

111 Rosa, R. B. *et al.* In Vitro and In Vivo Models for Studying SARS-CoV-2, the Etiological Agent Responsible for COVID-19 Pandemic. *Viruses* **13** (2021). https://doi.org:10.3390/v13030379

112 Chu, H. *et al.* Comparative Replication and Immune Activation Profiles of SARS-CoV-2 and SARS-CoV in Human Lungs: An Ex Vivo Study With Implications for the Pathogenesis of COVID-19. *Clin Infect Dis* **71**, 1400-1409 (2020). https://doi.org:10.1093/cid/ciaa410

113 Guo, Q. *et al.* Regulation of lipid metabolism and gene expression by fenofibrate in hamsters. *Biochim Biophys Acta* **1533**, 220-232 (2001). https://doi.org:10.1016/s1388-1981(01)00156-1

114 Srivastava, R. A. & He, S. Anti-hyperlipidemic and insulin sensitizing activities of fenofibrate reduces aortic lipid deposition in hyperlipidemic Golden Syrian hamster. *Mol Cell Biochem* **345**, 197-206 (2010). https://doi.org:10.1007/s11010-010-0573-8

115 Singh, S., Loke, Y. K. & Furberg, C. D. Long-term use of thiazolidinediones and the associated risk of pneumonia or lower respiratory tract infection: systematic review and meta-analysis. *Thorax* **66**, 383-388 (2011). https://doi.org:10.1136/thx.2010.152777

A

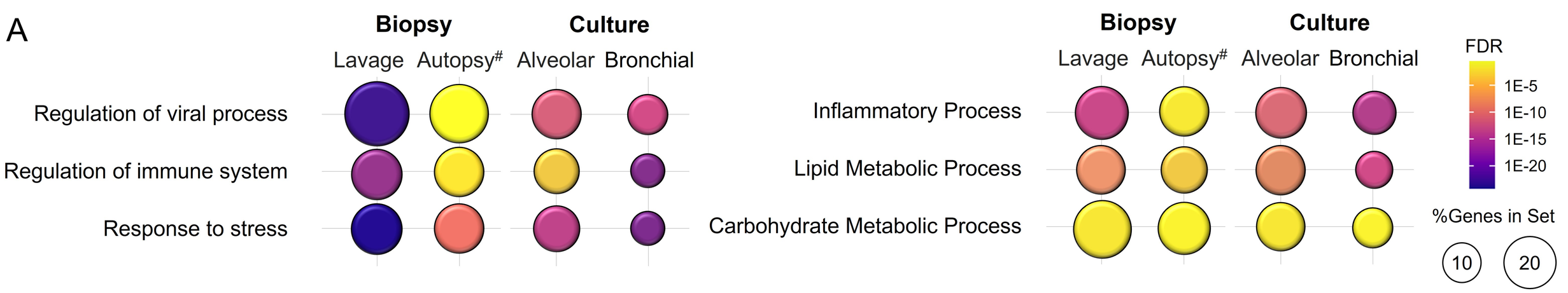

C

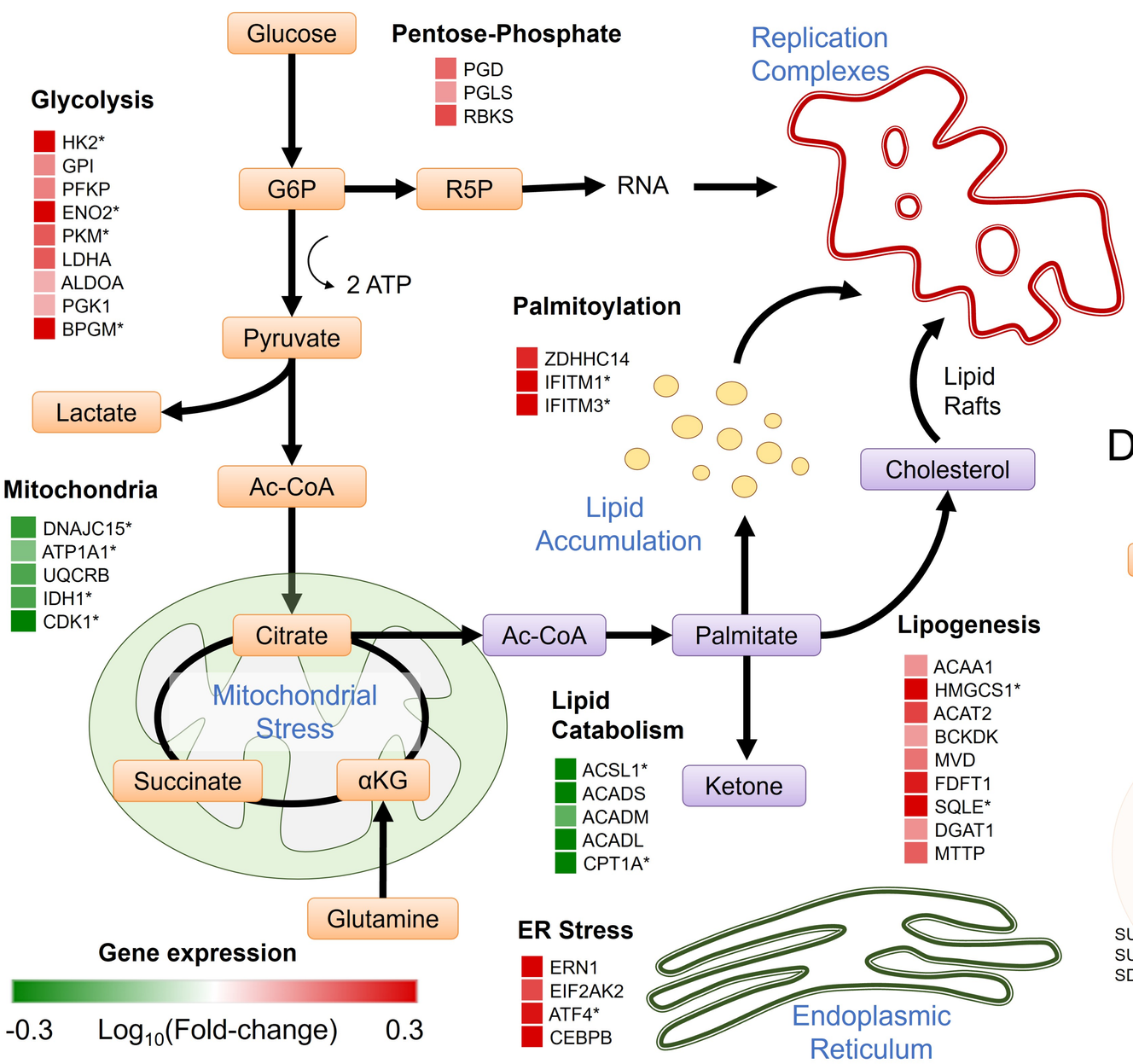

B

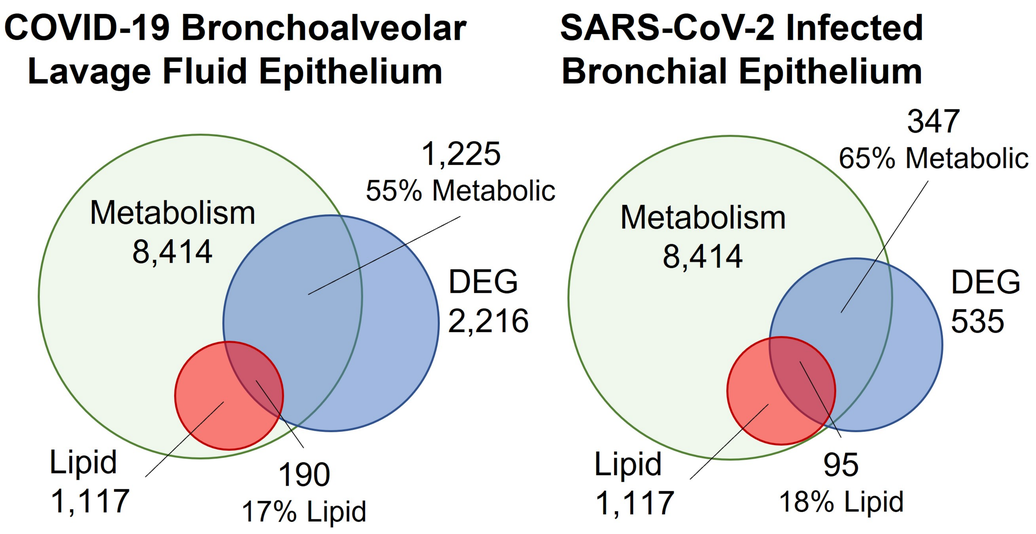

D

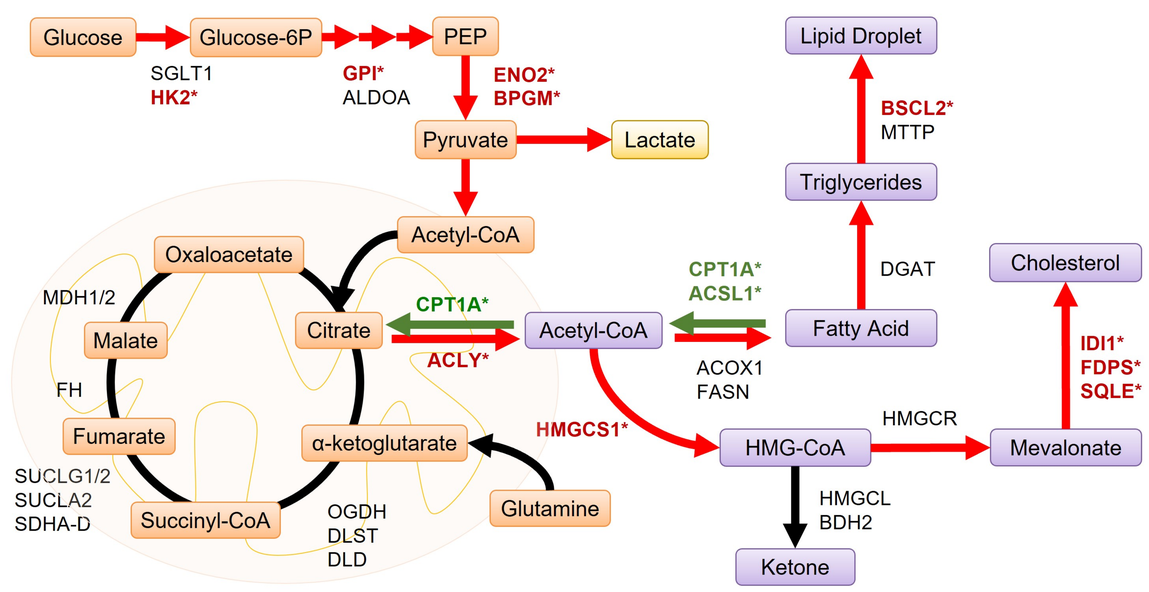

Warburg Effect and Altered Lipid Metabolism in SARS-CoV-2 Infected Bronchial Epithelial Cells

E

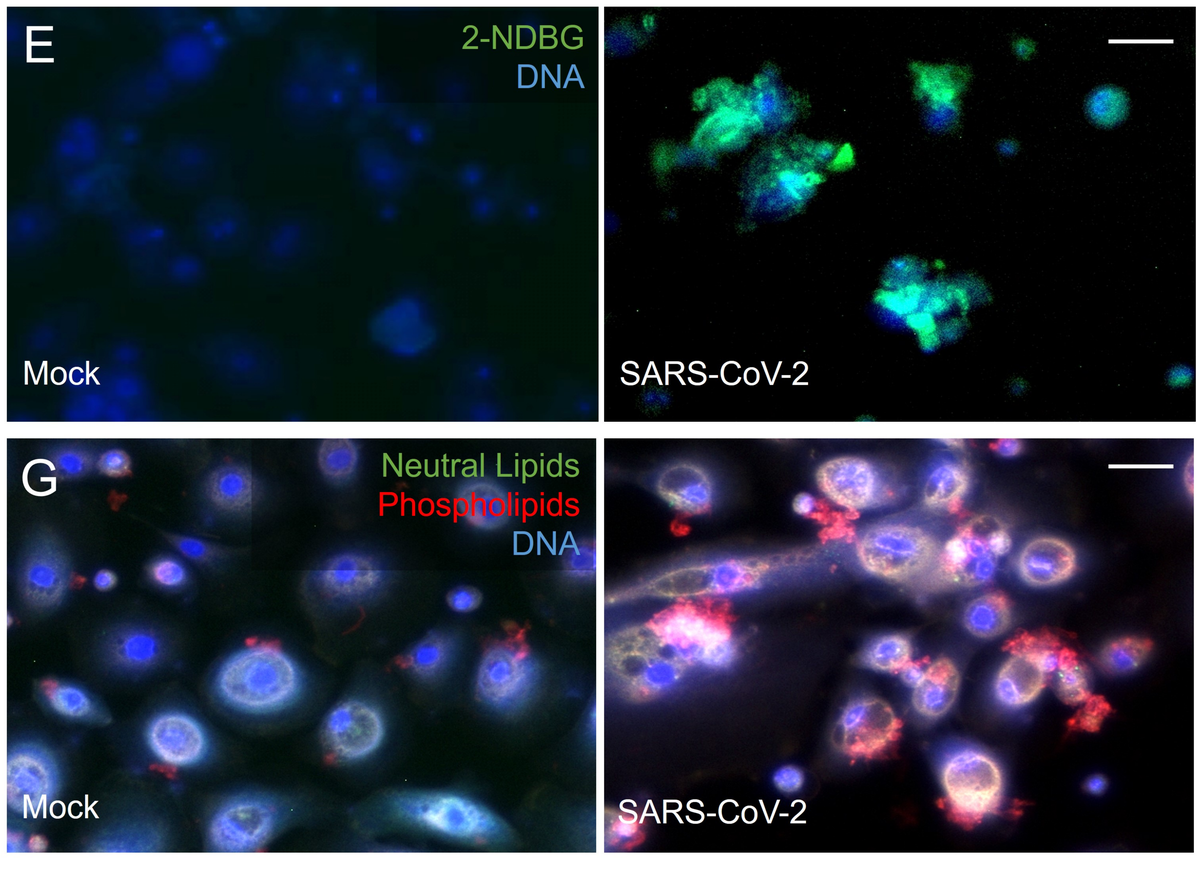

G

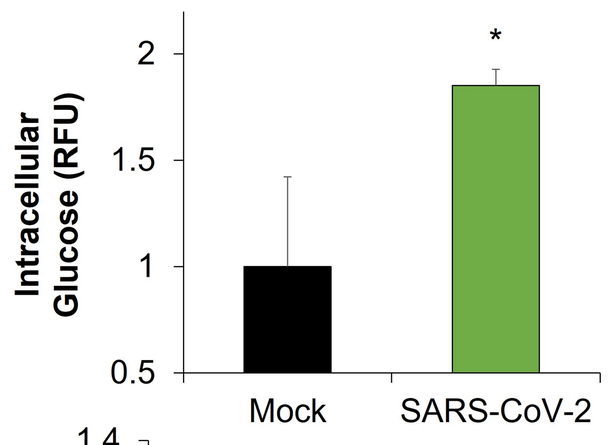

F

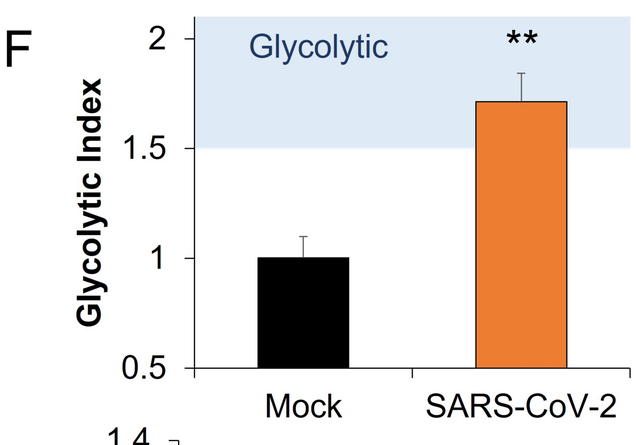

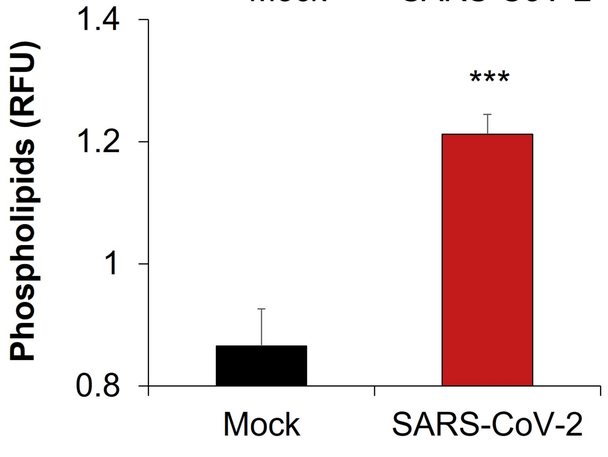

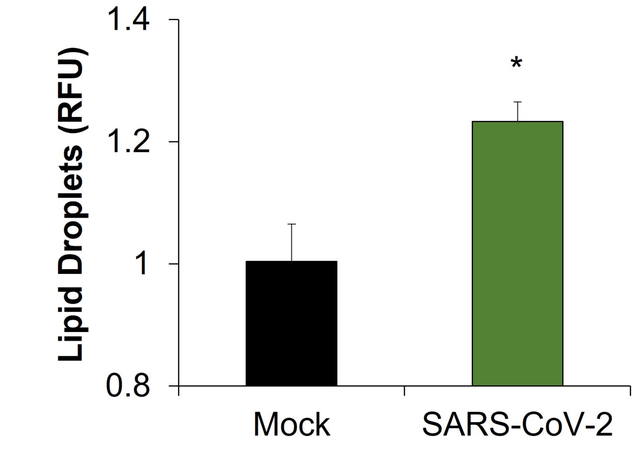

A

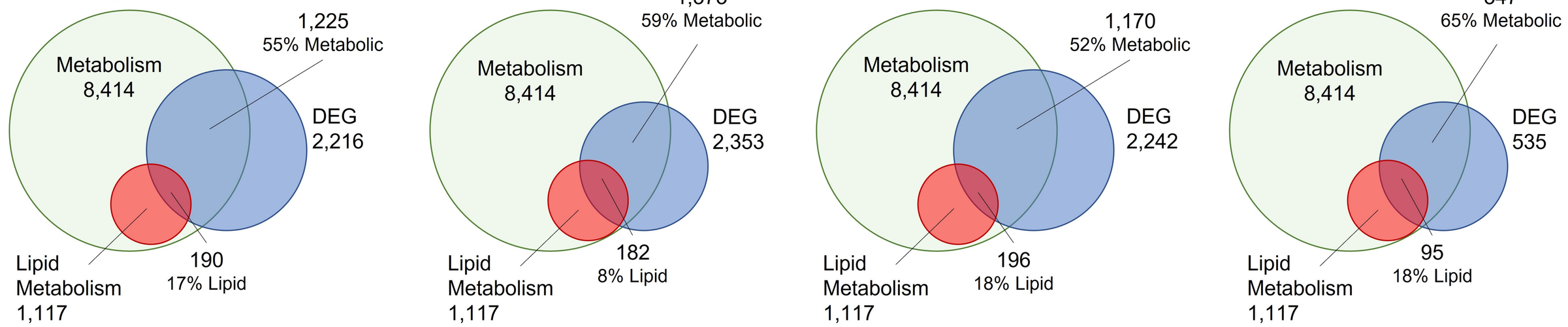
COVID-19
Bronchoalveolar Lavage
Fluid Epithelium
Metabolism
8,414
1,225
55% Metabolic
DEG
2,216
190
17% Lipid
Lipid
Metabolism
1,117
COVID-19 Lung
Autopsy#
1,373
59% Metabolic
182
8% Lipid
SARS-CoV-2 Infected
Small Airway Epithelium
1,170
52% Metabolic
196
18% Lipid
SARS-CoV-2 Infected
Bronchial Epithelium
347
65% Metabolic
95
18% Lipid

B

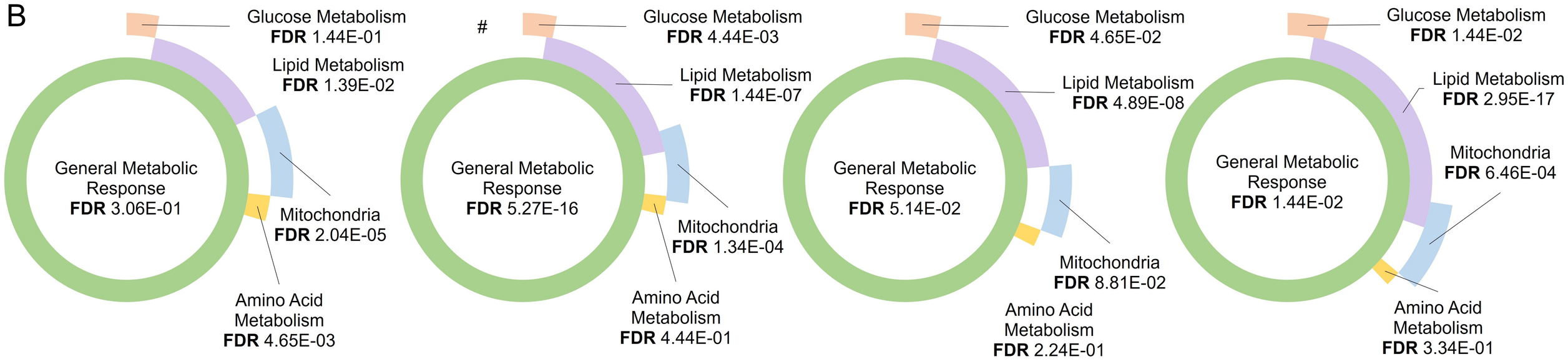
Glucose Metabolism
FDR 1.44E-01
Lipid Metabolism
FDR 1.39E-02
General Metabolic
Response
FDR 3.06E-01
Mitochondria
FDR 2.04E-05
Amino Acid
Metabolism
FDR 4.65E-03
#
Glucose Metabolism
FDR 4.44E-03
Lipid Metabolism
FDR 1.44E-07
General Metabolic
Response
FDR 5.27E-16
Mitochondria
FDR 1.34E-04
Amino Acid
Metabolism
FDR 4.44E-01
Glucose Metabolism
FDR 4.65E-02
Lipid Metabolism
FDR 4.89E-08
General Metabolic
Response
FDR 5.14E-02
Mitochondria
FDR 8.81E-02
Amino Acid
Metabolism
FDR 2.24E-01
Glucose Metabolism
FDR 1.44E-02
Lipid Metabolism
FDR 2.95E-17
General Metabolic
Response
FDR 1.44E-02
Mitochondria
FDR 6.46E-04
Amino Acid
Metabolism
FDR 3.34E-01

C

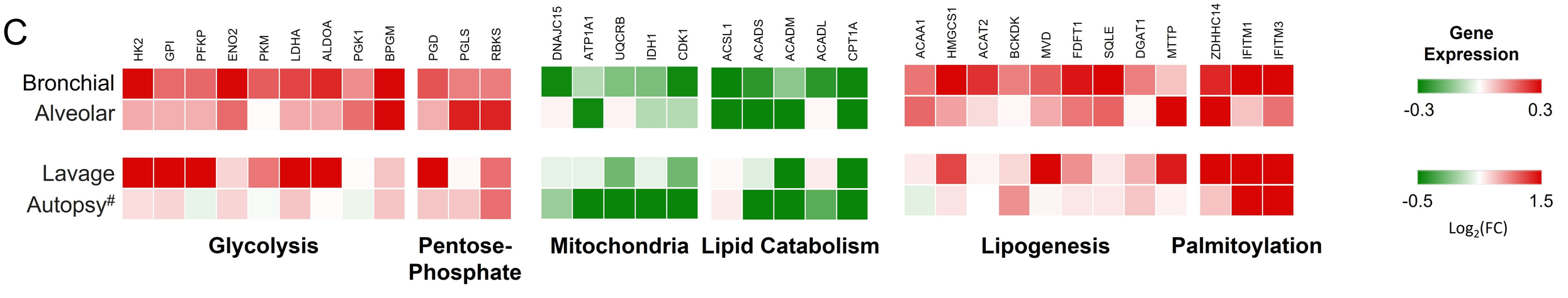
HK2
GPI
PFKP
ENO2
PKM
LDHA
ALDOA
PGK1
BPGM
PGD
PGLS
RBKS
DNAJC15
ATP1A1
UQCRB
IDH1
CDK1
ACSL1
ACADS
ACADM
ACADL
CPT1A
ACAA1
HMGCS1
ACAT2
BCKDK
MVD
FDFT1
SQLE
DGAT1
MTTP
ZDHHC14
IFITM1
IFITM3
Bronchial
Alveolar
Lavage
Autopsy#
Glycolysis
Pentose-
Phosphate
Mitochondria
Lipid Catabolism
Lipogenesis
Palmitoylation
Gene
Expression
-0.3
0.3
-0.5
1.5
Log2(FC)

D

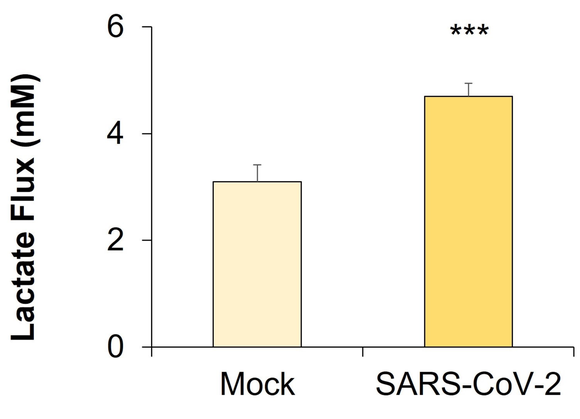
Lactate Flux (mM)
6
4
2
0
***
Mock
SARS-CoV-2

E

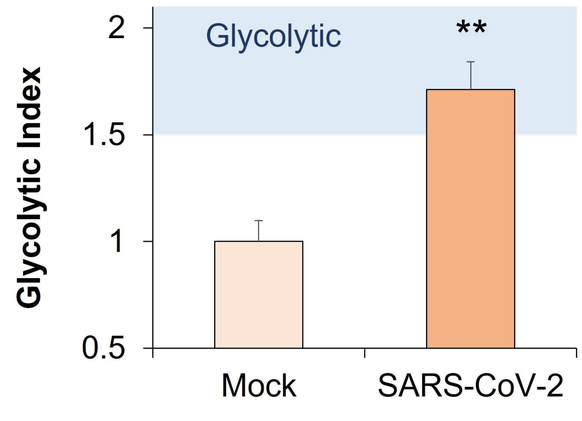
Glycolytic Index
2
1.5
1
0.5
Glycolytic
**
Mock
SARS-CoV-2

F

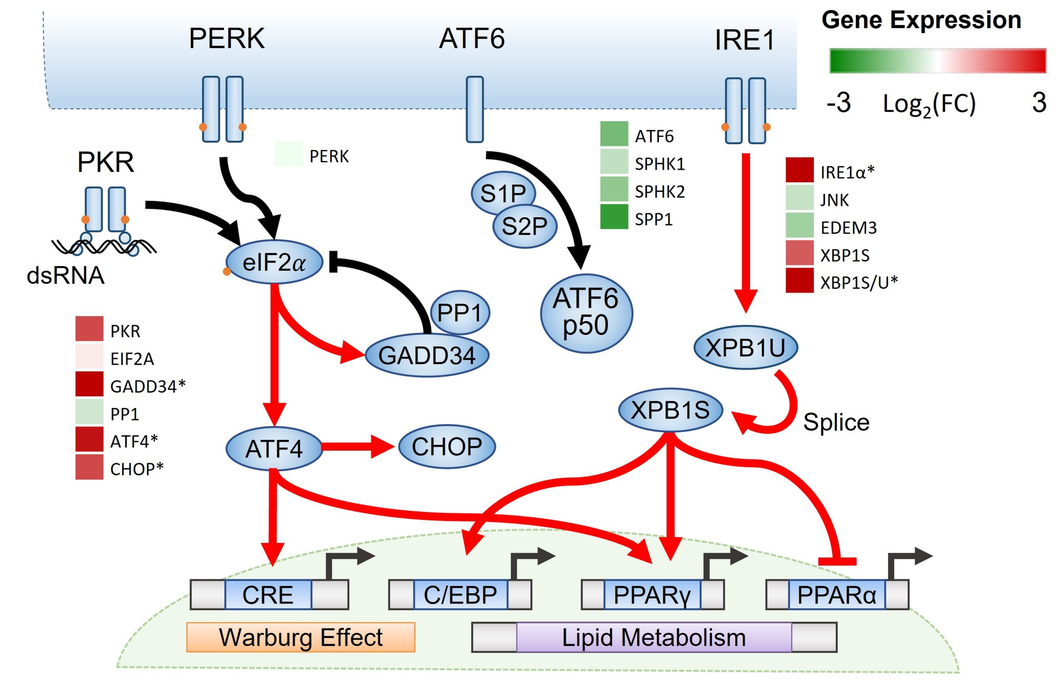
ER Stress Response
PERK
ATF6
IRE1
Gene Expression
-3
Log2(FC)
3
PKR
dsRNA
PERK
eIF2α
S1P
S2P
ATF6
SPHK1
SPHK2
SPP1
IRE1α*
JNK
EDEM3
XBP1S
XBP1S/U*
PP1
GADD34
ATF6
p50
XPB1U
XPB1S
Splice
PKR
EIF2A
GADD34*
PP1
ATF4*
CHOP*
ATF4
CHOP
CRE
C/EBP
PPARγ
PPARα
Warburg Effect
Lipid Metabolism

G

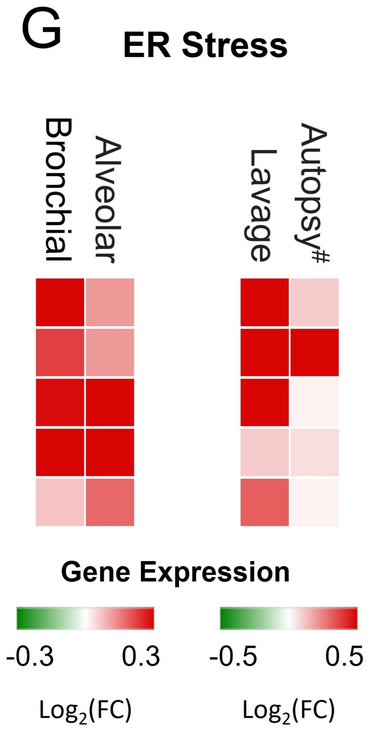
ER Stress
Bronchial
Alveolar
Autopsy#
Lavage
Gene Expression
-0.3
0.3
-0.5
0.5
Log2(FC)
Log2(FC)

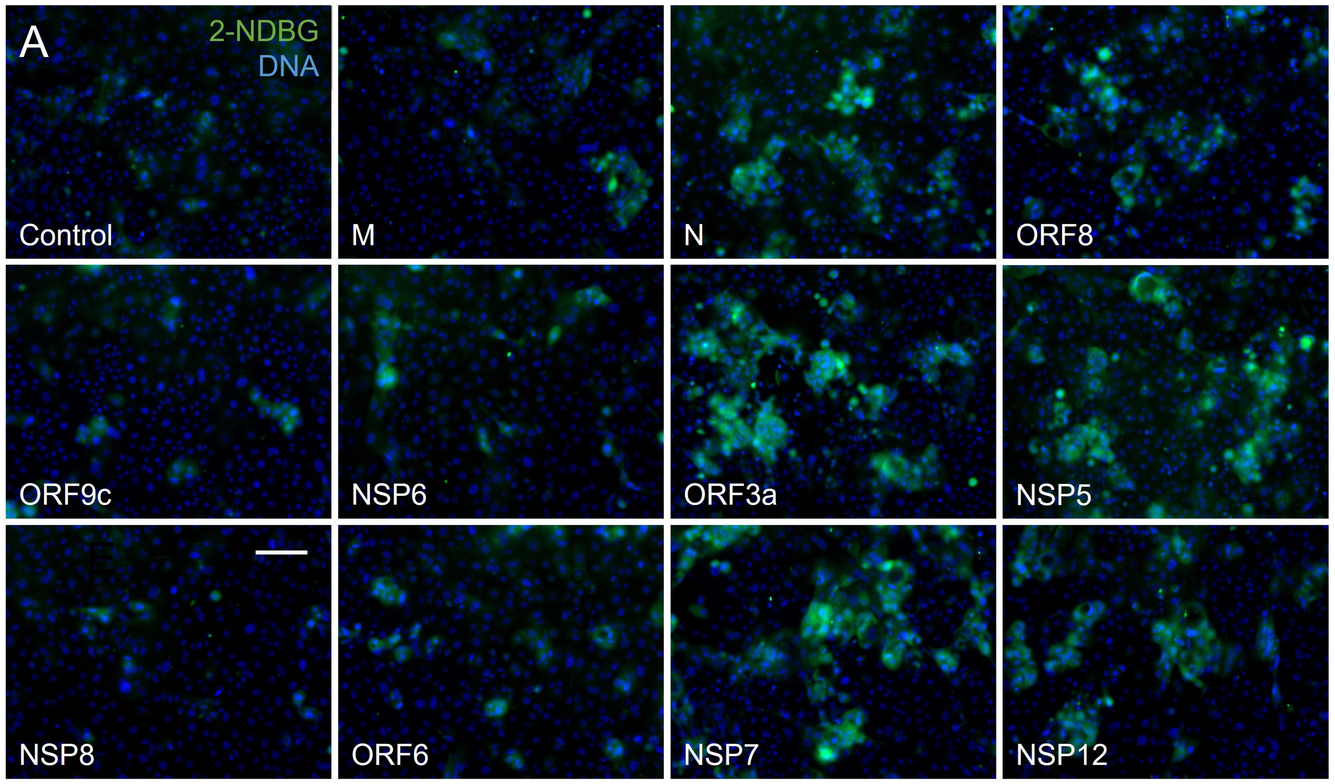
A
2-NDBG
DNA
Control
M
N
ORF8
ORF9c
NSP6
ORF3a
NSP5
NSP8
ORF6
NSP7
NSP12

B

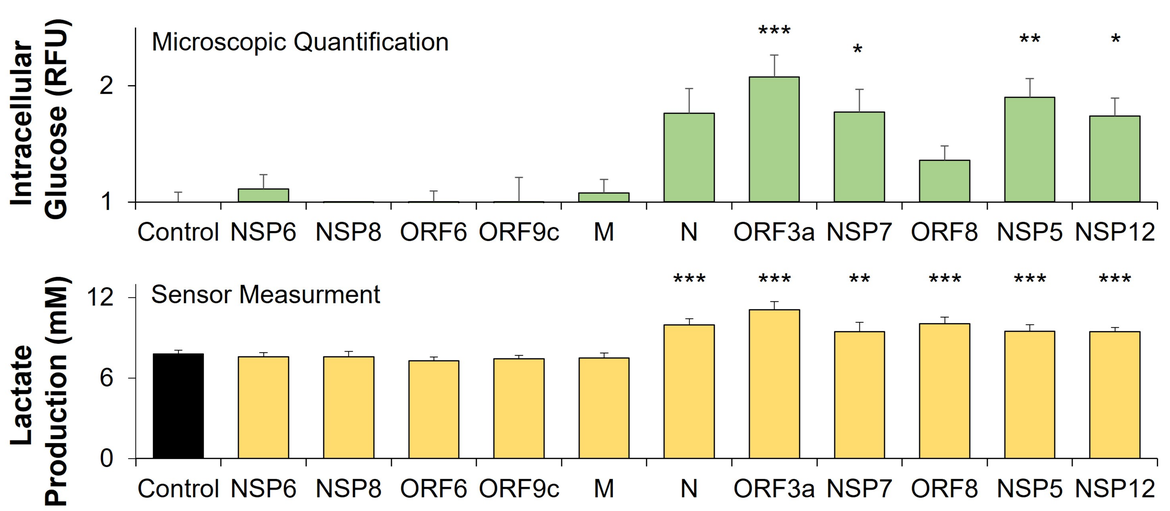
Microscopic Quantification
Intracellular Glucose (RFU)
Sensor Measurment
Lactate Production (mM)
Control NSP6 NSP8 ORF6 ORF9c M N ORF3a NSP7 ORF8 NSP5 NSP12

C

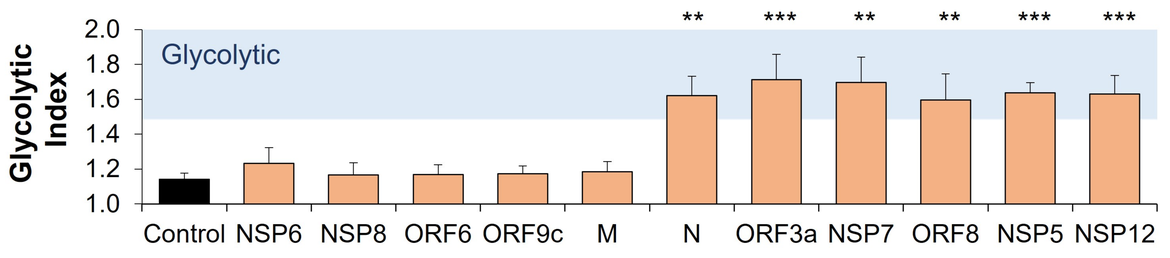
Glycolytic
Glycolytic Index
Control NSP6 NSP8 ORF6 ORF9c M N ORF3a NSP7 ORF8 NSP5 NSP12

D

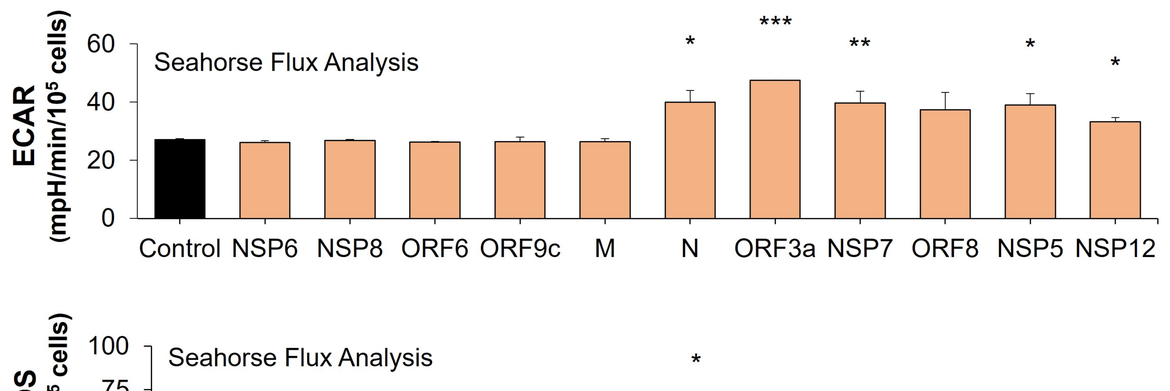
Seahorse Flux Analysis
ECAR (mpH/min/10⁵ cells)
Control NSP6 NSP8 ORF6 ORF9c M N ORF3a NSP7 ORF8 NSP5 NSP12

E

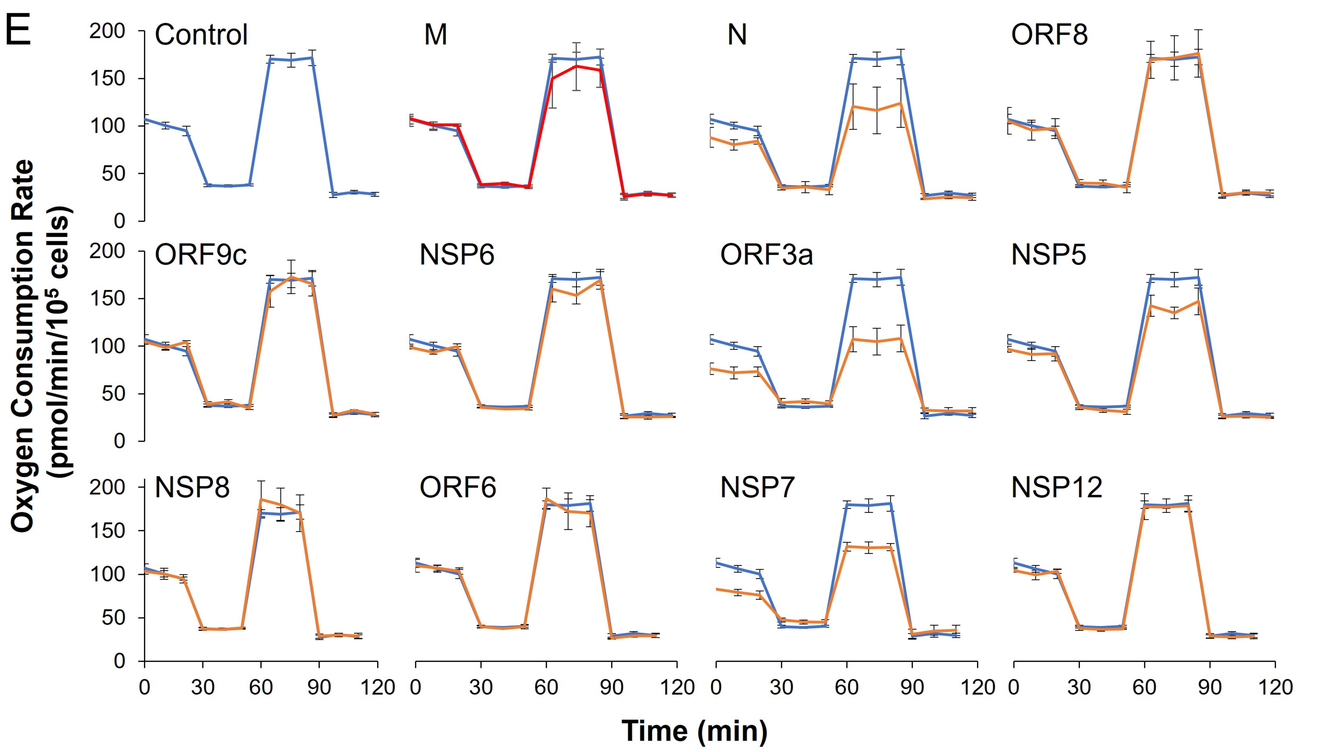
Control
M
N
ORF8
ORF9c
NSP6
ORF3a
NSP5
NSP8
ORF6
NSP7
NSP12
Oxygen Consumption Rate (pmol/min/10⁵ cells)
Time (min)

F

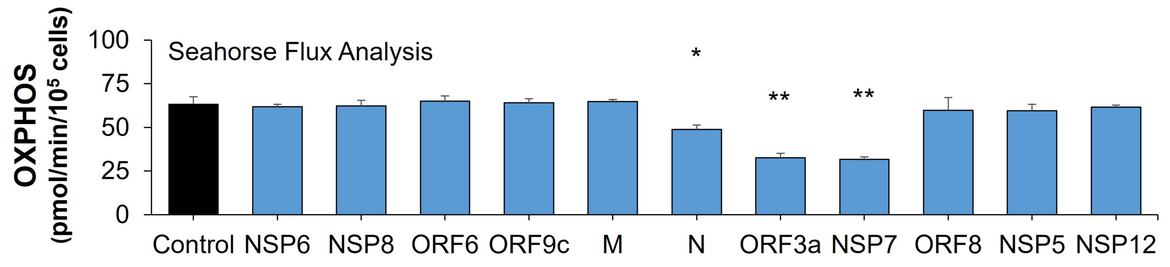
Seahorse Flux Analysis
OXPHOS (pmol/min/10⁵ cells)
Control NSP6 NSP8 ORF6 ORF9c M N ORF3a NSP7 ORF8 NSP5 NSP12

G

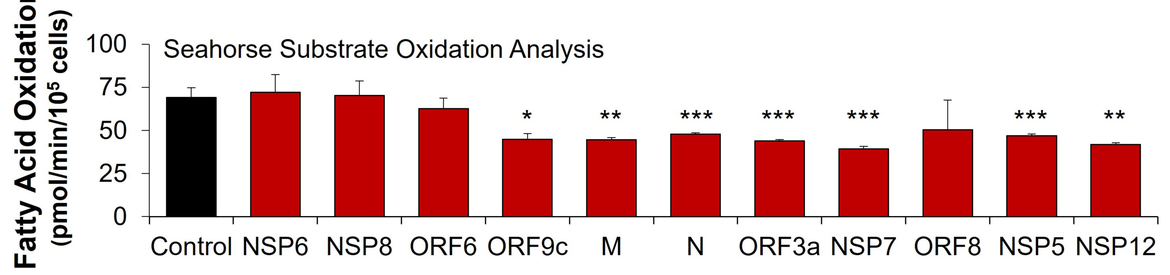
Seahorse Substrate Oxidation Analysis
Fatty Acid Oxidation (pmol/min/10⁵ cells)
Control NSP6 NSP8 ORF6 ORF9c M N ORF3a NSP7 ORF8 NSP5 NSP12

H

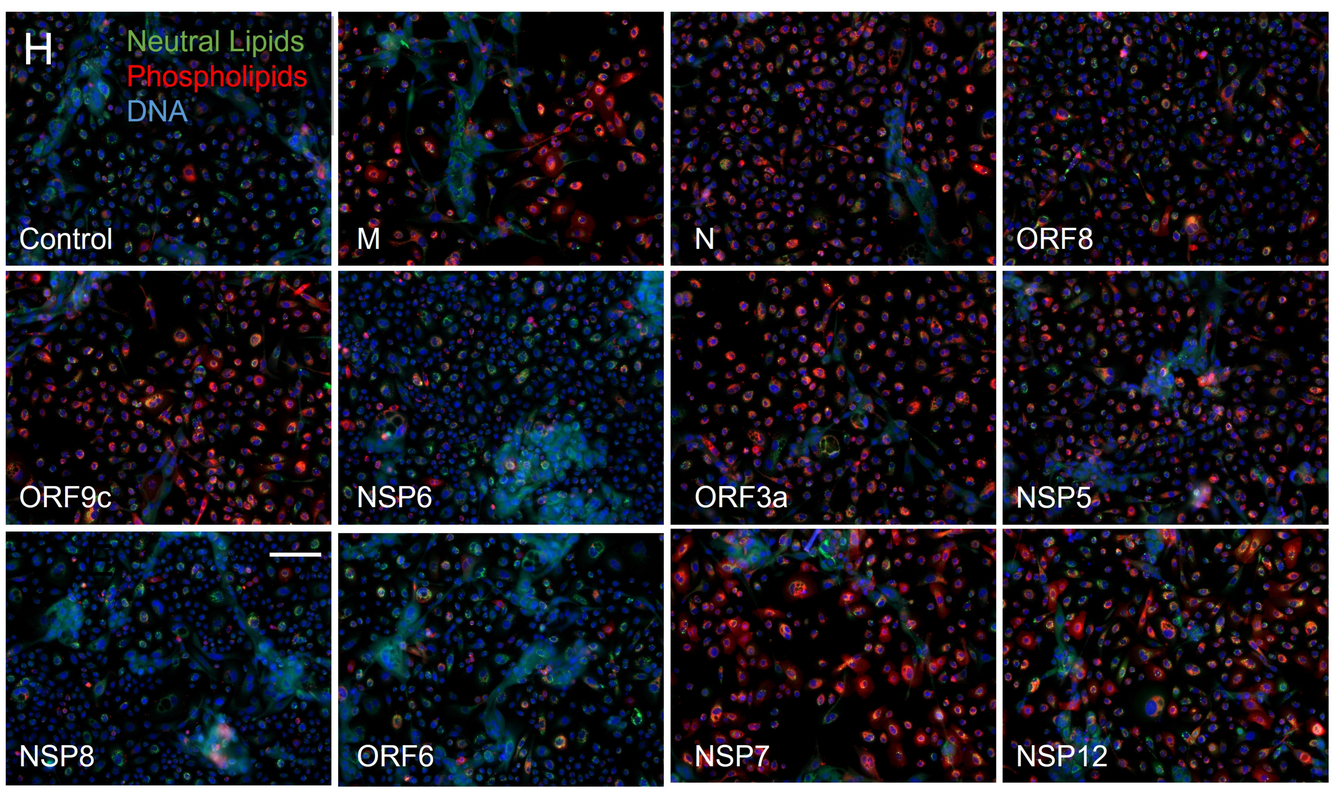
Neutral Lipids
Phospholipids
DNA
Control
M
N
ORF8
ORF9c
NSP6
ORF3a
NSP5
NSP8
ORF6
NSP7
NSP12

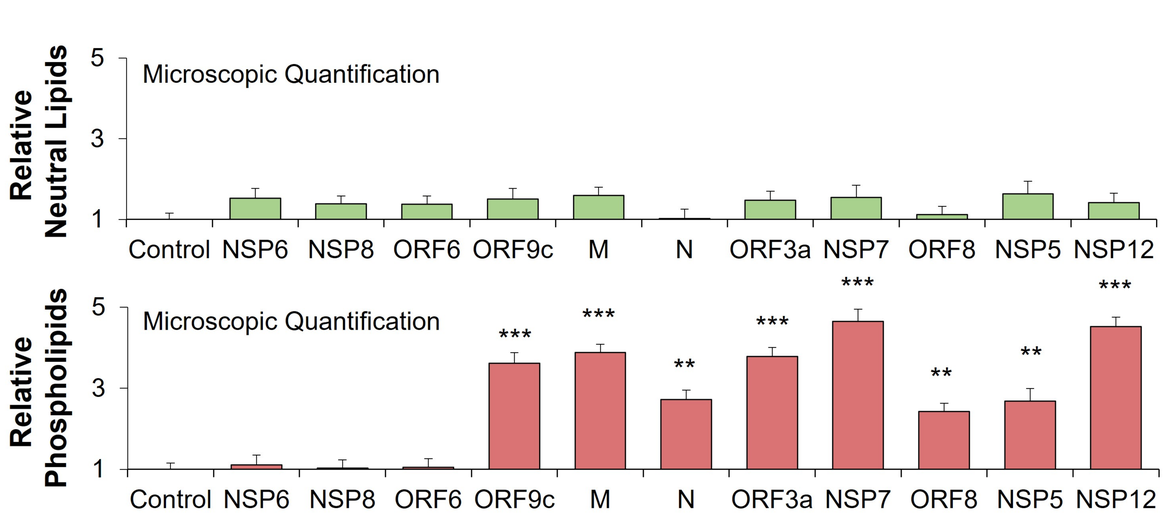
Microscopic Quantification
Relative Neutral Lipids
Microscopic Quantification
Relative Phospholipids
Control NSP6 NSP8 ORF6 ORF9c M N ORF3a NSP7 ORF8 NSP5 NSP12

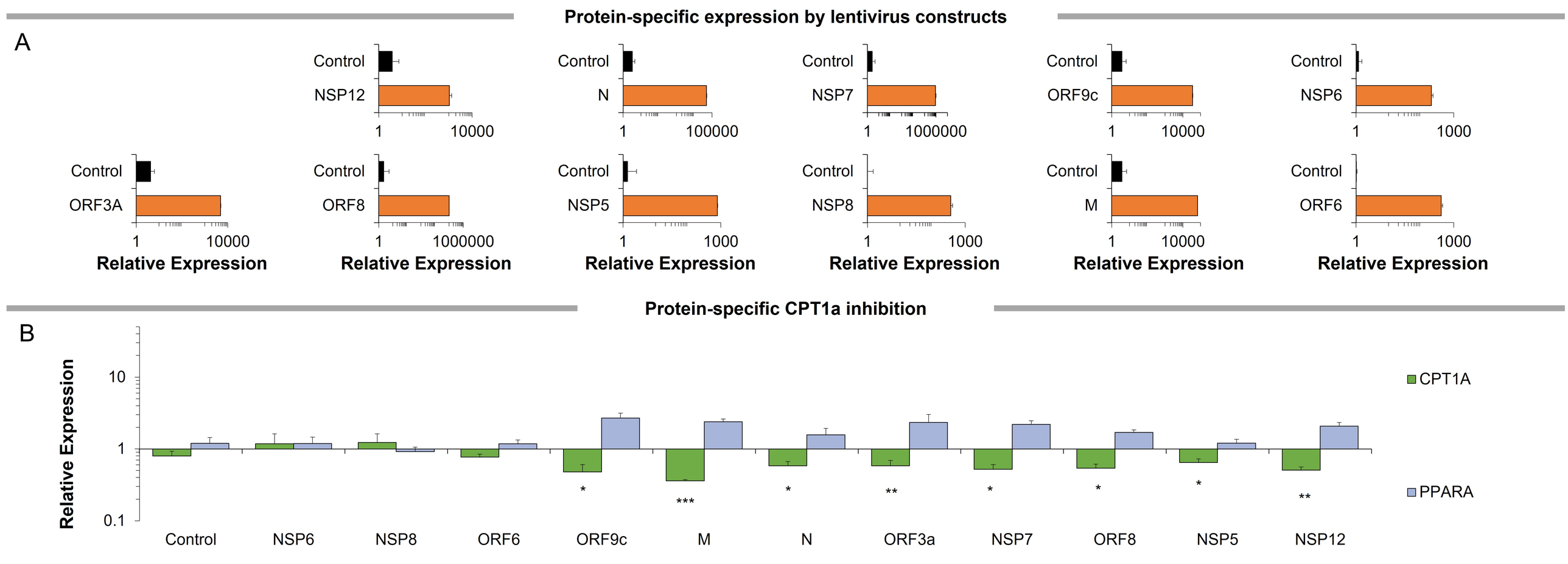
Protein-specific expression by lentivirus constructs
A
Control
NSP12
1
10000
Control
N
1
100000
Control
NSP7
1
1000000
Control
ORF9c
1
10000
Control
NSP6
1
1000
Control
ORF3A
1
10000
Relative Expression
Control
ORF8
1
1000000
Relative Expression
Control
NSP5
1
1000
Relative Expression
Control
NSP8
1
1000
Relative Expression
Control
M
1
10000
Relative Expression
Control
ORF6
1
1000
Relative Expression
Protein-specific CPT1a inhibition
B
Relative Expression
10
1
0.1
CPT1A
PPARA
*
***
*
**
*
*
*
**
Control
NSP6
NSP8
ORF6
ORF9c
M
N
ORF3a
NSP7
ORF8
NSP5
NSP12

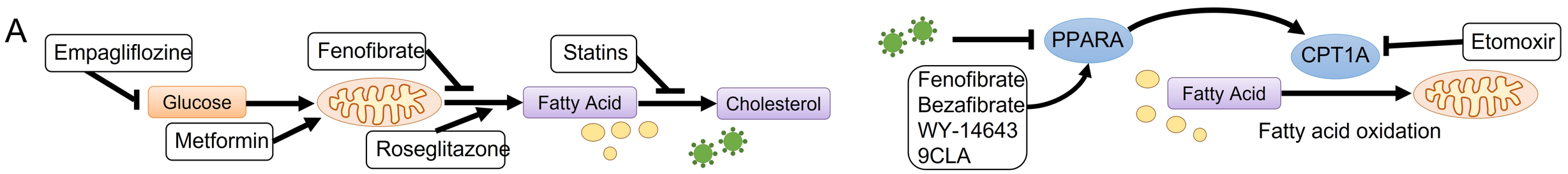

Metabolic Intervention in SARS-CoV-2 Infected Bronchial Epithelium

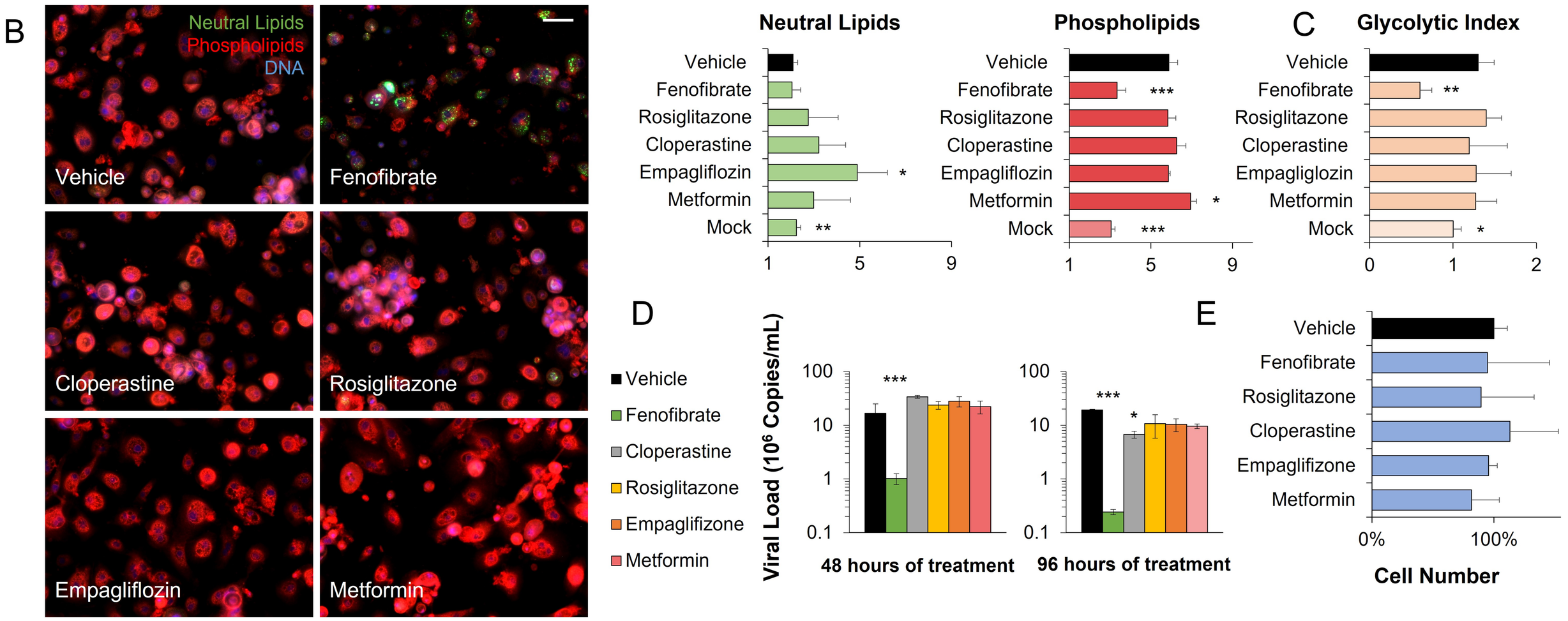

Myriad PPARα Agonists Show Antiviral Lipid Catabolism Effect

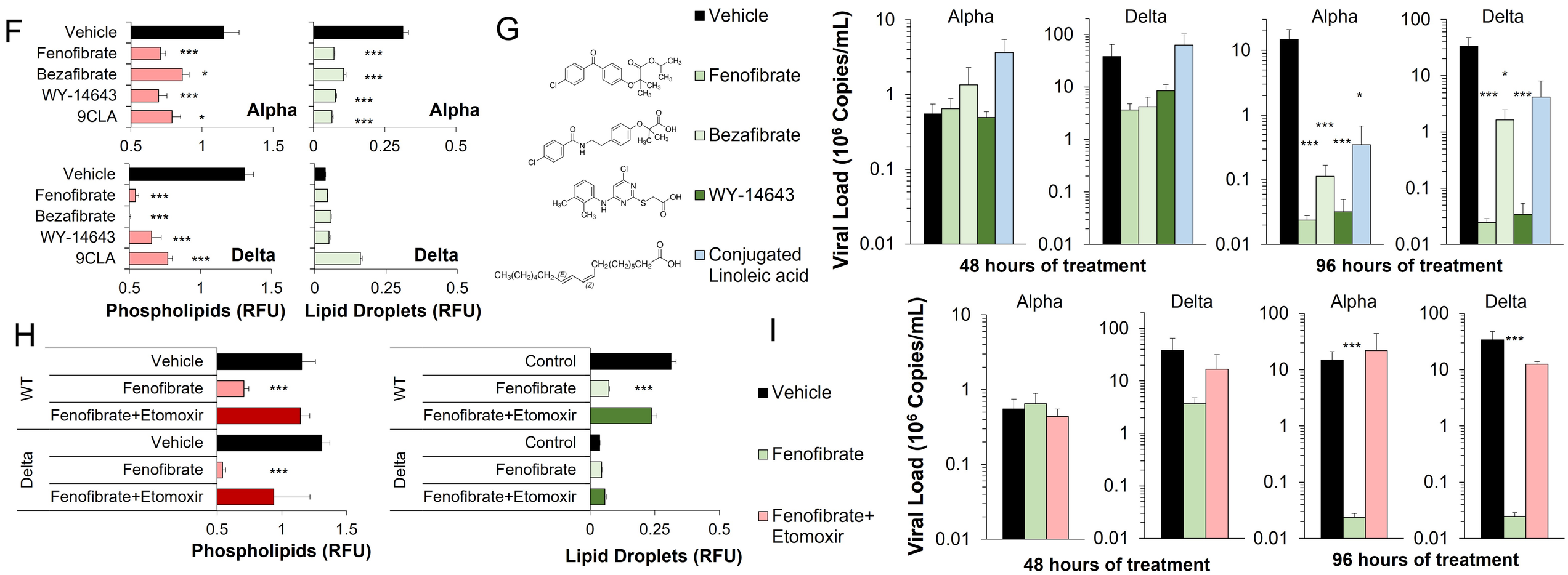

PPARα-dependent Antiviral Lipid Catabolism

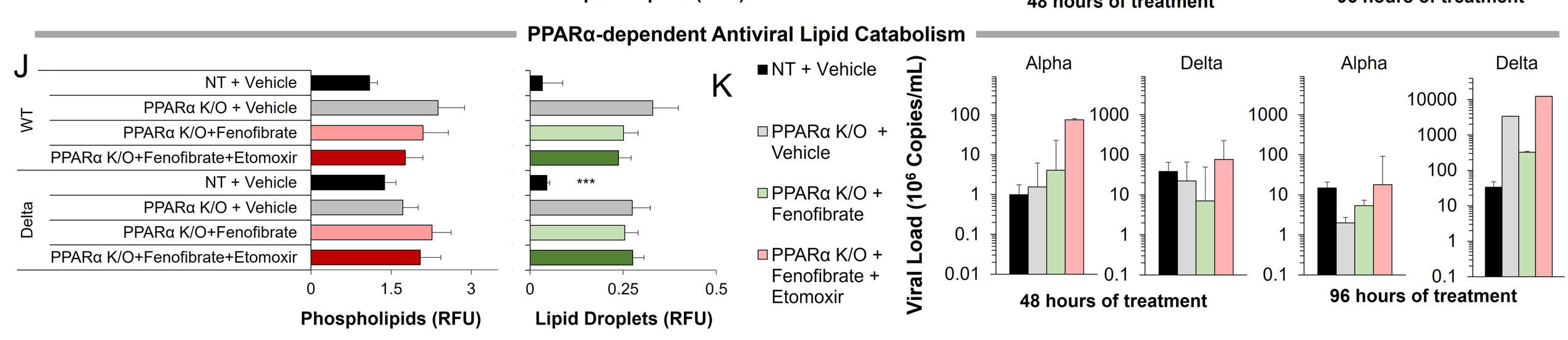

A

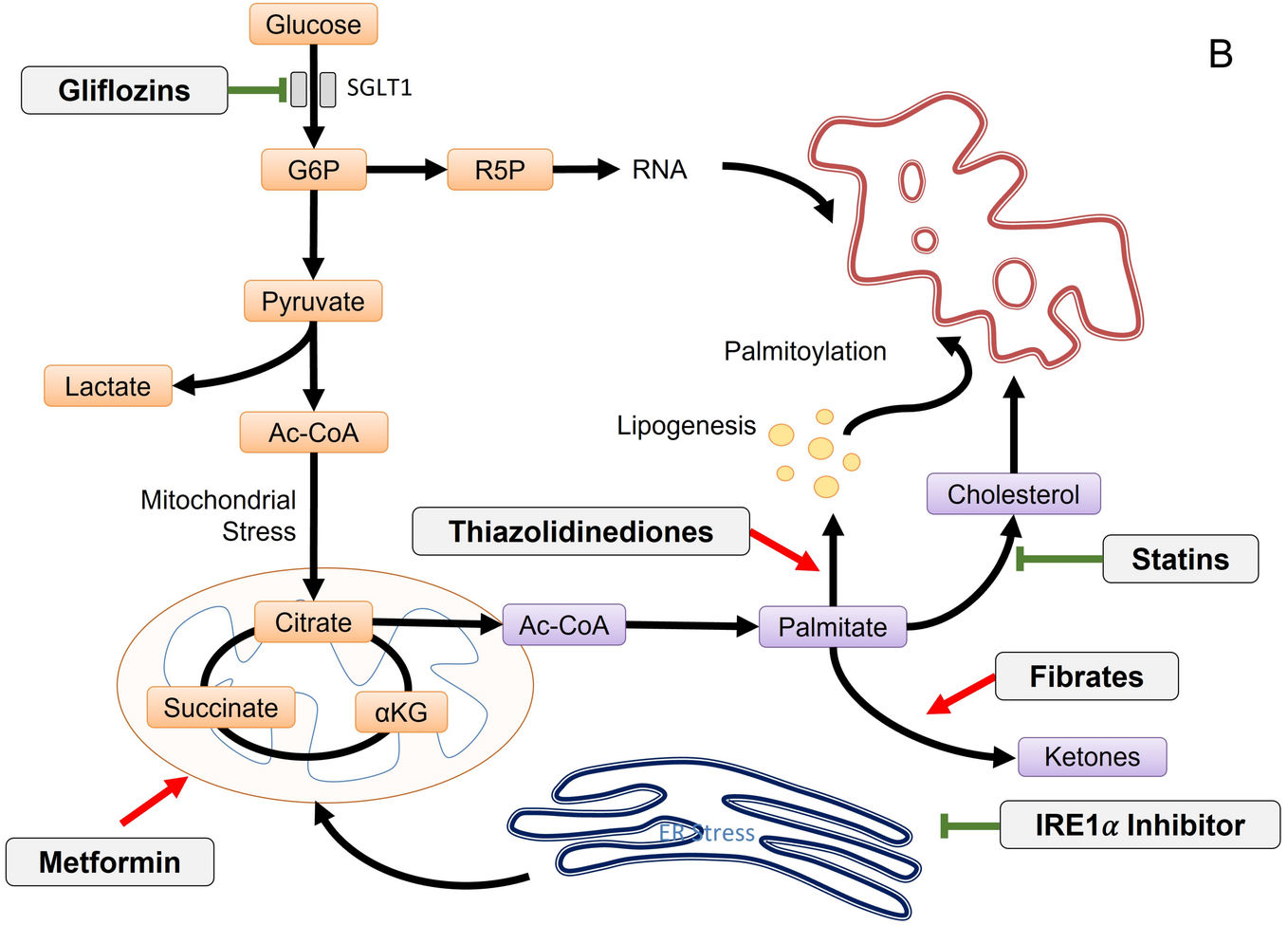

B

Drug Name	Indication	Therapeutic Target
Cloperastine (Hustazol®)	Cough Suppressant	SGLTI/II inhibitor
Empagliflozin (Jardiance®)	Type II Diabetes	SGLTII inhibitor
Metformin (Fortamet®)	Type II Diabetes	AMPK activator
Simvastatin (Zocor®)	Dyslipidemia	HMGCR inhibitor
Pravastatin (Pravachol®)	Dyslipidemia	HMGCR inhibitor
Fenofibrate (TriCor®)	Dyslipidemia	PPARα agonist
Bezafibrate (Bezalip®)	Dyslipidemia	PPARα agonist
Rosiglitazone (Avandia®)	Type II Diabetes	PPARγ agonist
Telmisartan (Micardis®)	Hypertension	IRE1α inhibitor

C

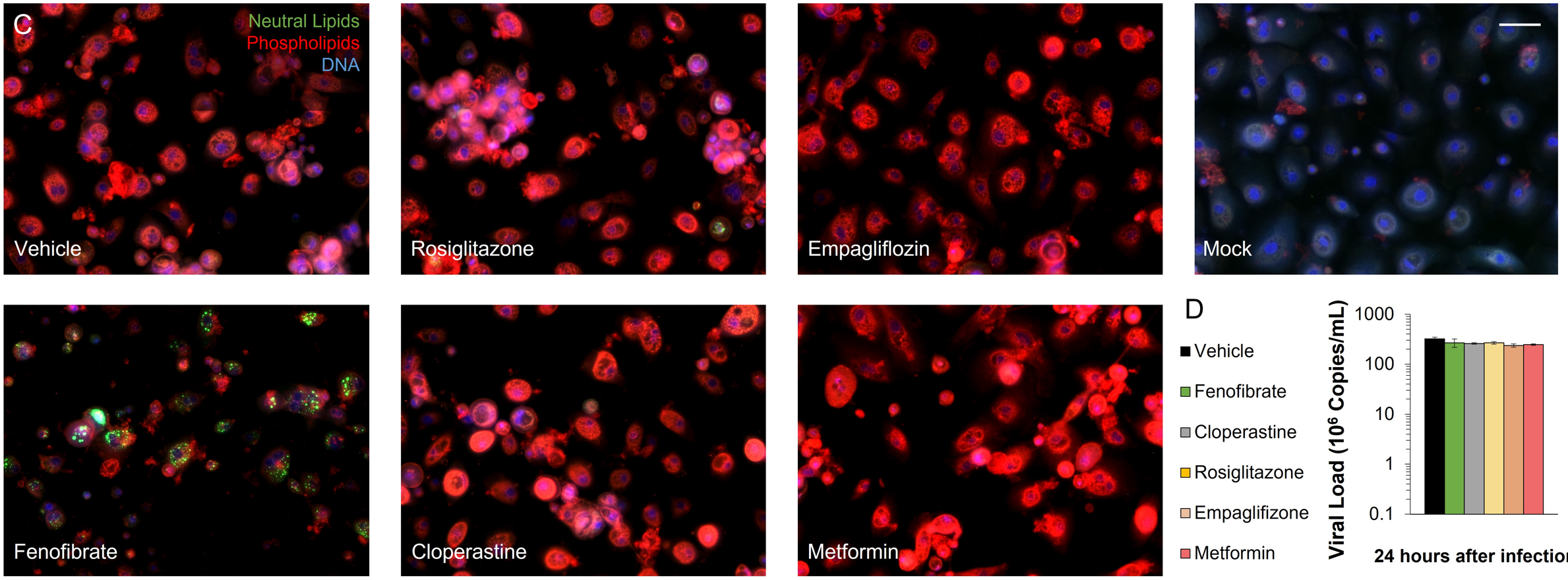

D

SARS-CoV-2 (Alpha)

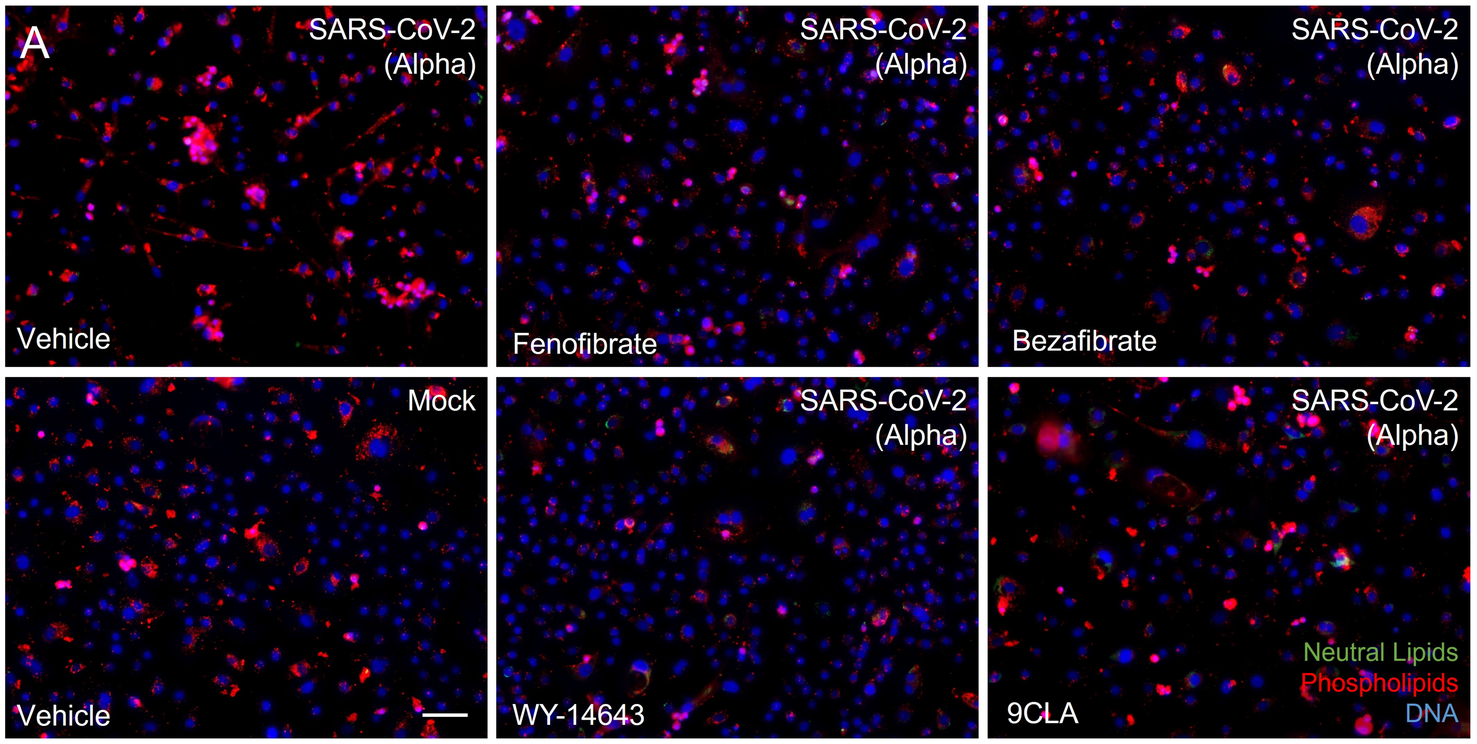

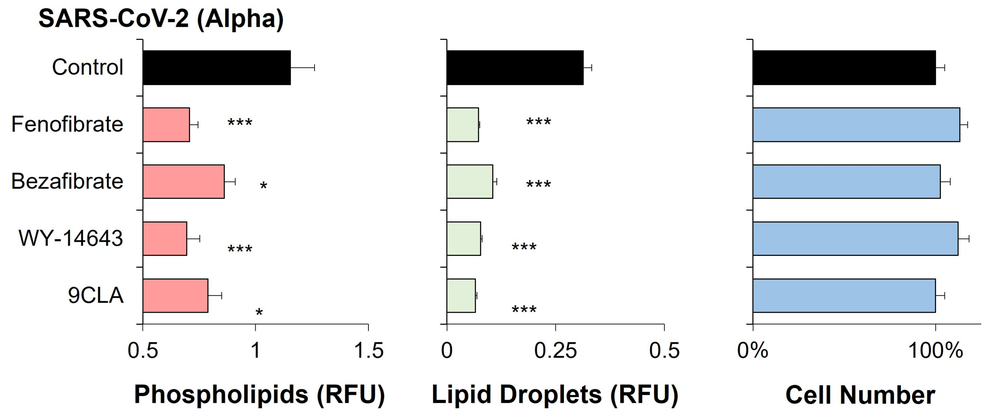

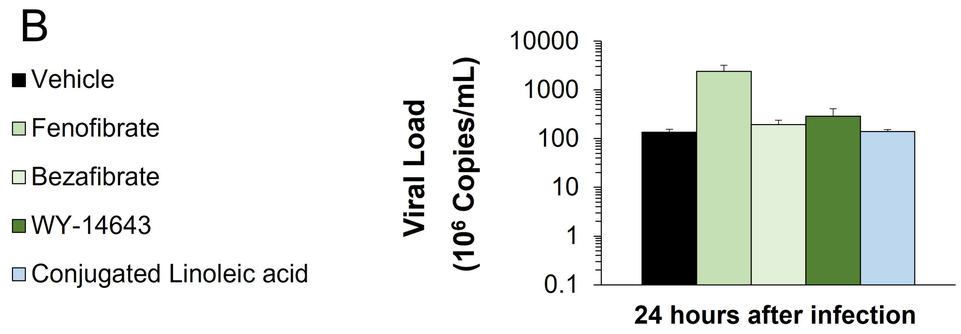

SARS-CoV-2 (Delta)

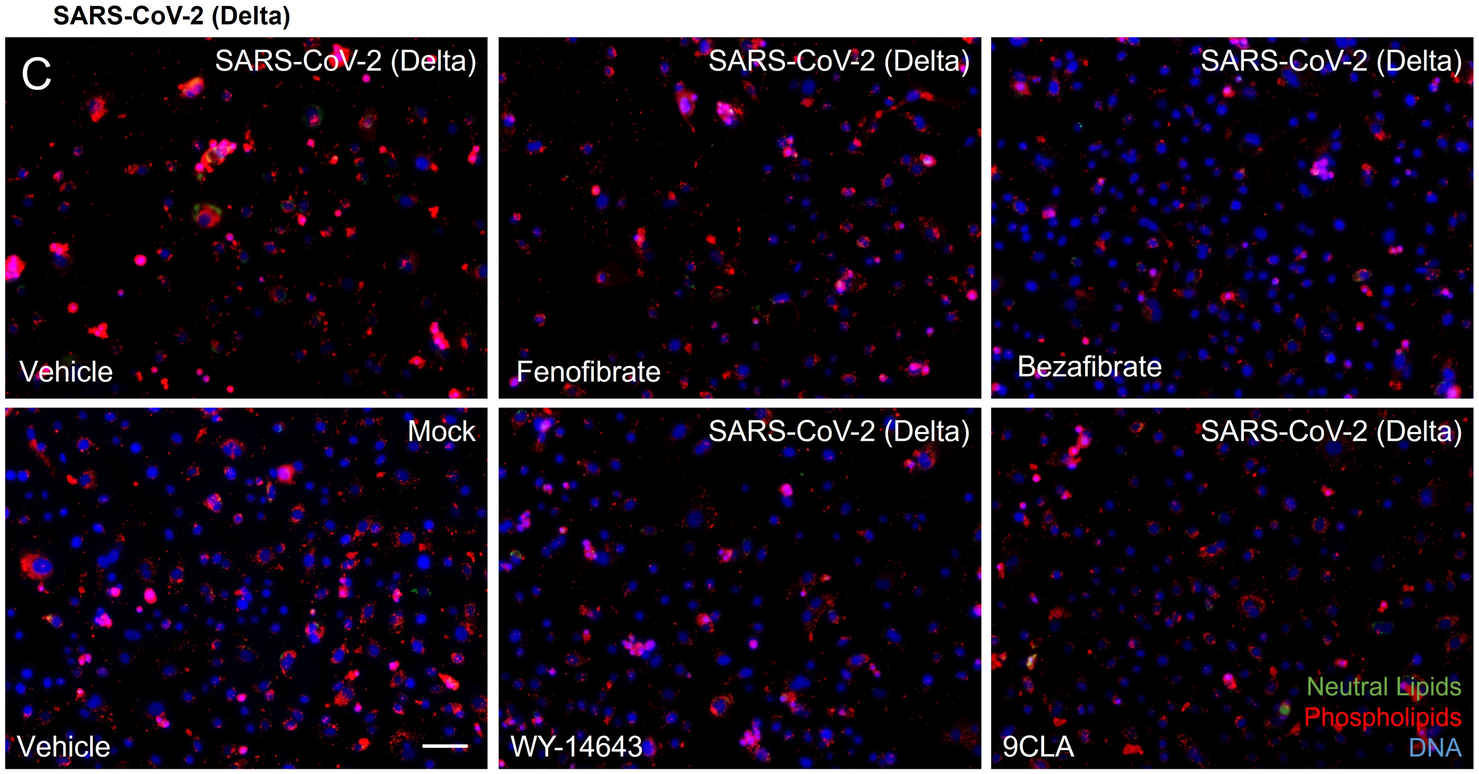

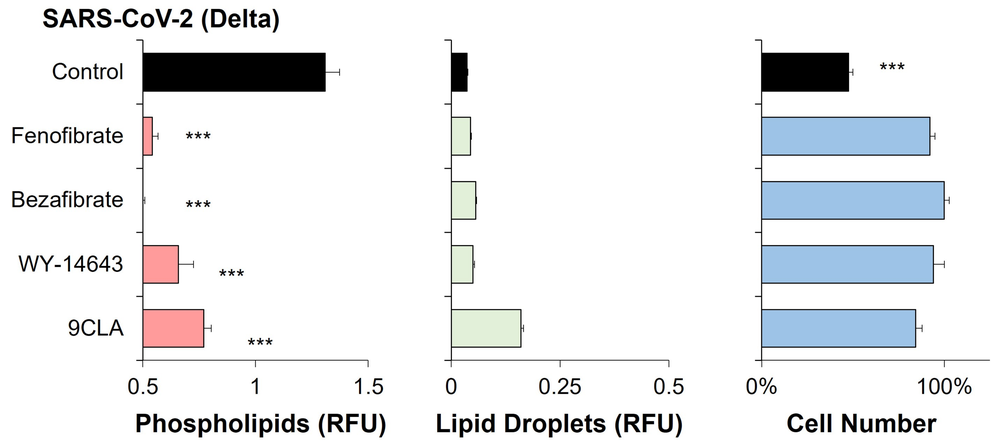

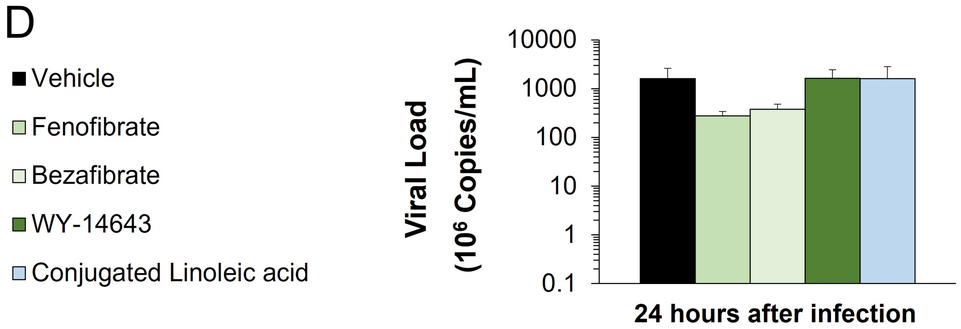

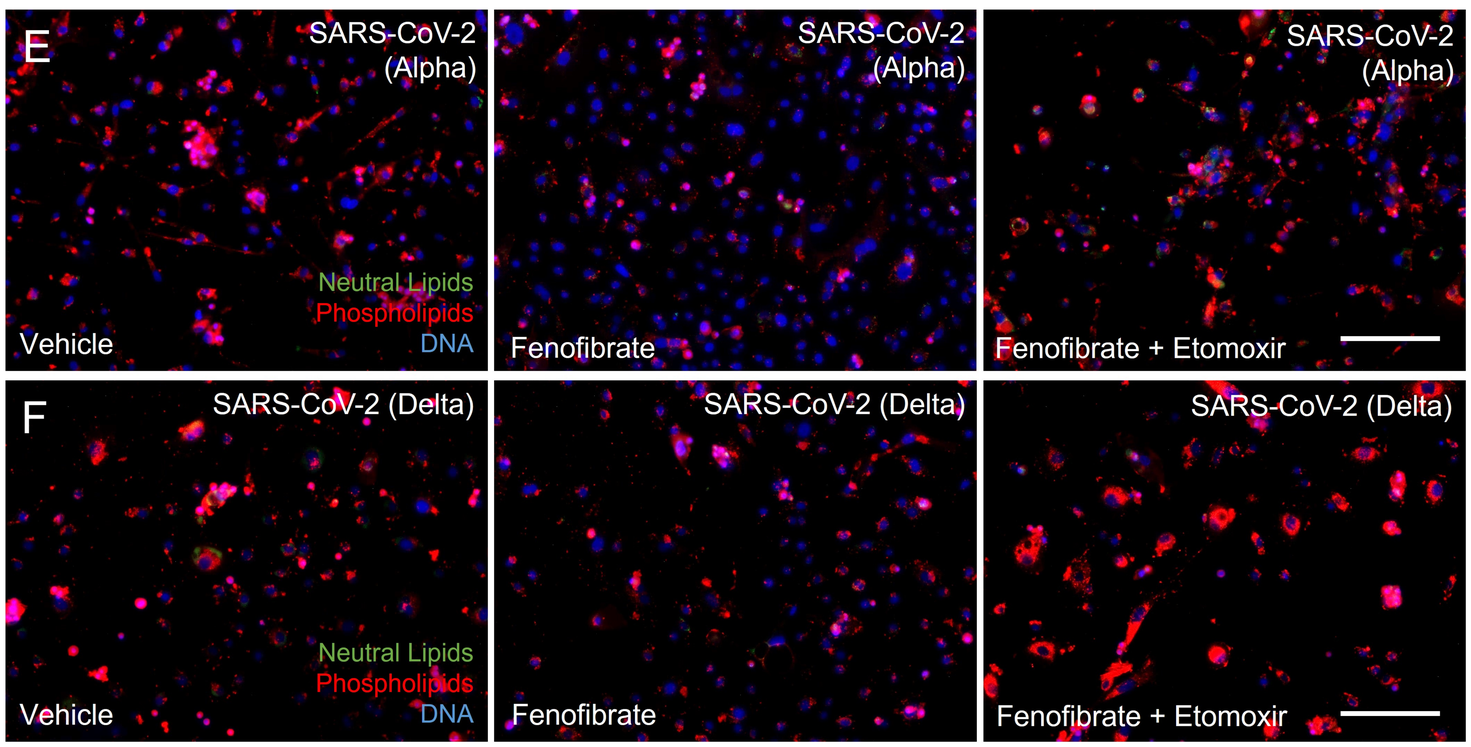

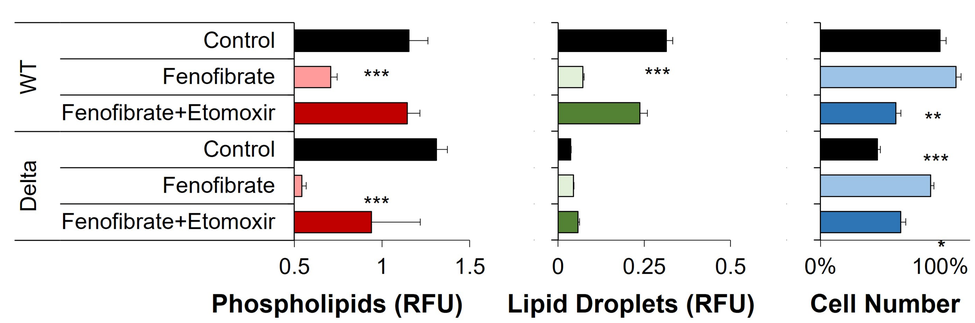

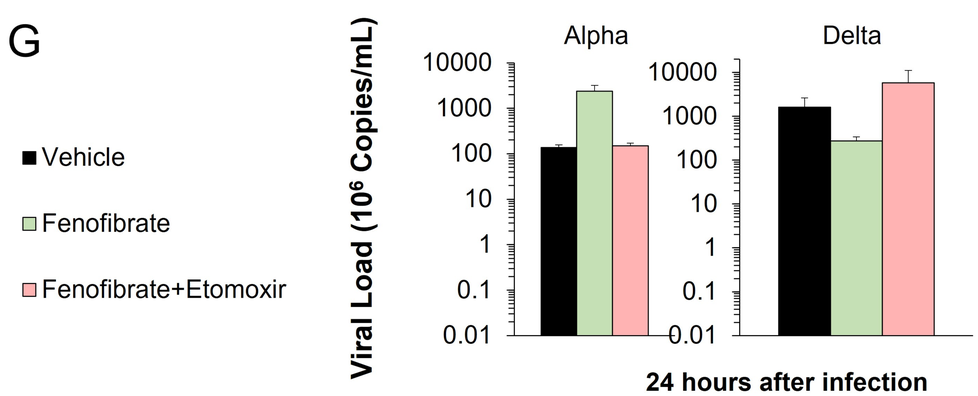

A

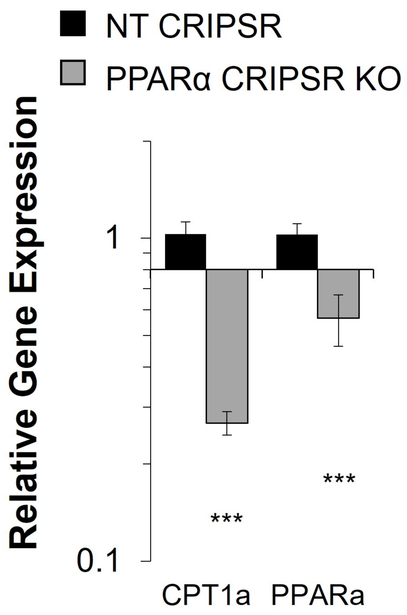
NT CRIPSR
PPARα CRIPSR KO
Relative Gene Expression
1
0.1
***
***
CPT1a
PPARa

B

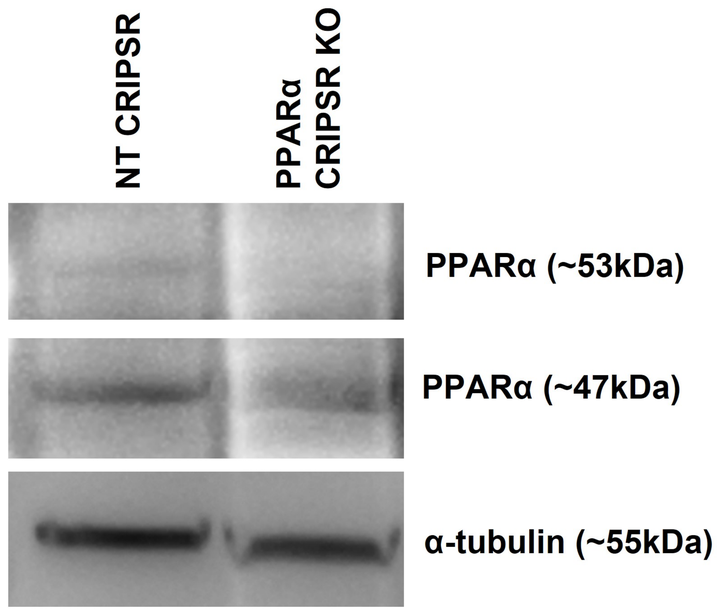
NT CRIPSR
PPARα CRIPSR KO
PPARα (~53kDa)
PPARα (~47kDa)
α-tubulin (~55kDa)

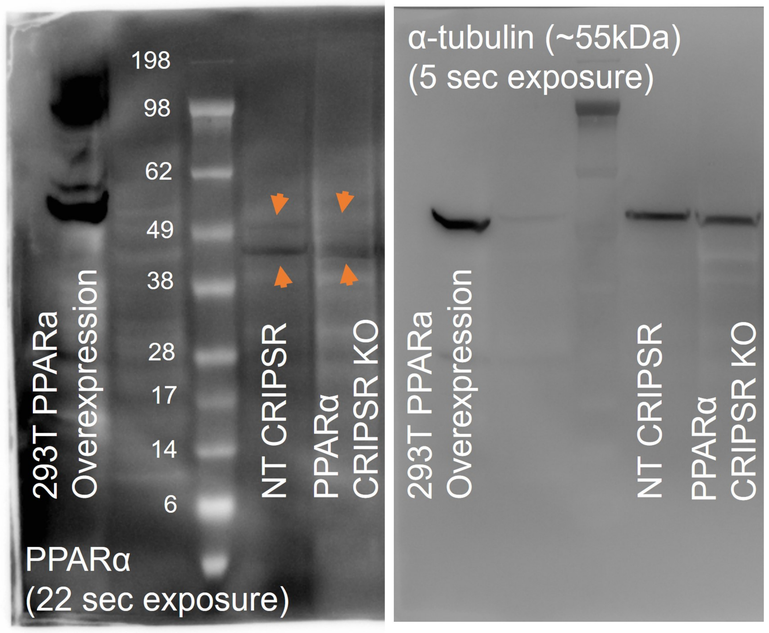
198
98
62
49
38
28
17
14
6
293T PPARa Overexpression
NT CRIPSR
PPARα CRIPSR KO
PPARα
(22 sec exposure)
α-tubulin (~55kDa)
(5 sec exposure)
293T PPARa Overexpression
NT CRIPSR
PPARα CRIPSR KO

C

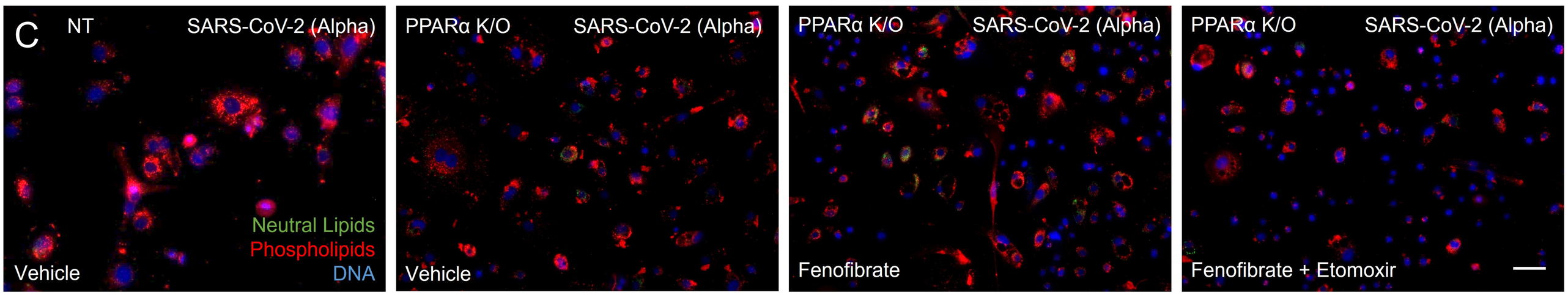
NT
SARS-CoV-2 (Alpha)
Neutral Lipids
Phospholipids
DNA
Vehicle
PPARα K/O
SARS-CoV-2 (Alpha)
Vehicle
PPARα K/O
SARS-CoV-2 (Alpha)
Fenofibrate
PPARα K/O
SARS-CoV-2 (Alpha)
Fenofibrate + Etomoxir

D

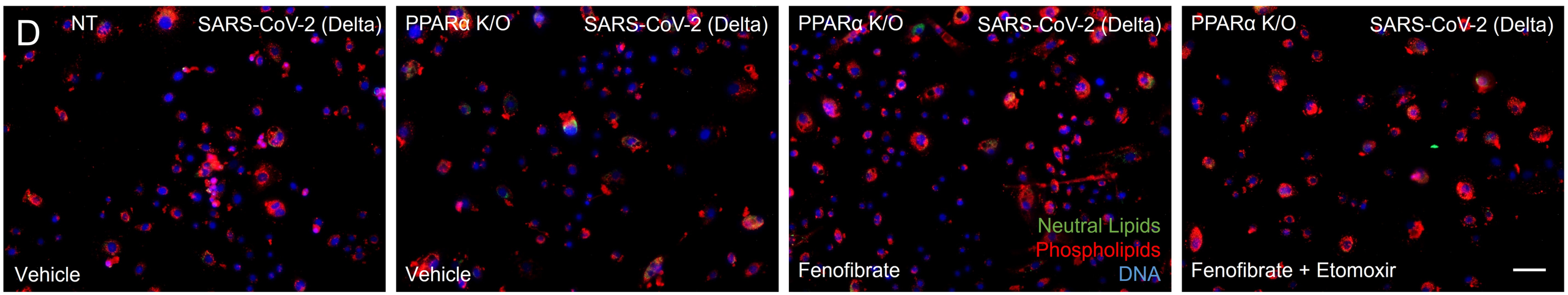
NT
SARS-CoV-2 (Delta)
Vehicle
PPARα K/O
SARS-CoV-2 (Delta)
Vehicle
PPARα K/O
SARS-CoV-2 (Delta)
Neutral Lipids
Phospholipids
DNA
Fenofibrate
PPARα K/O
SARS-CoV-2 (Delta)
Fenofibrate + Etomoxir

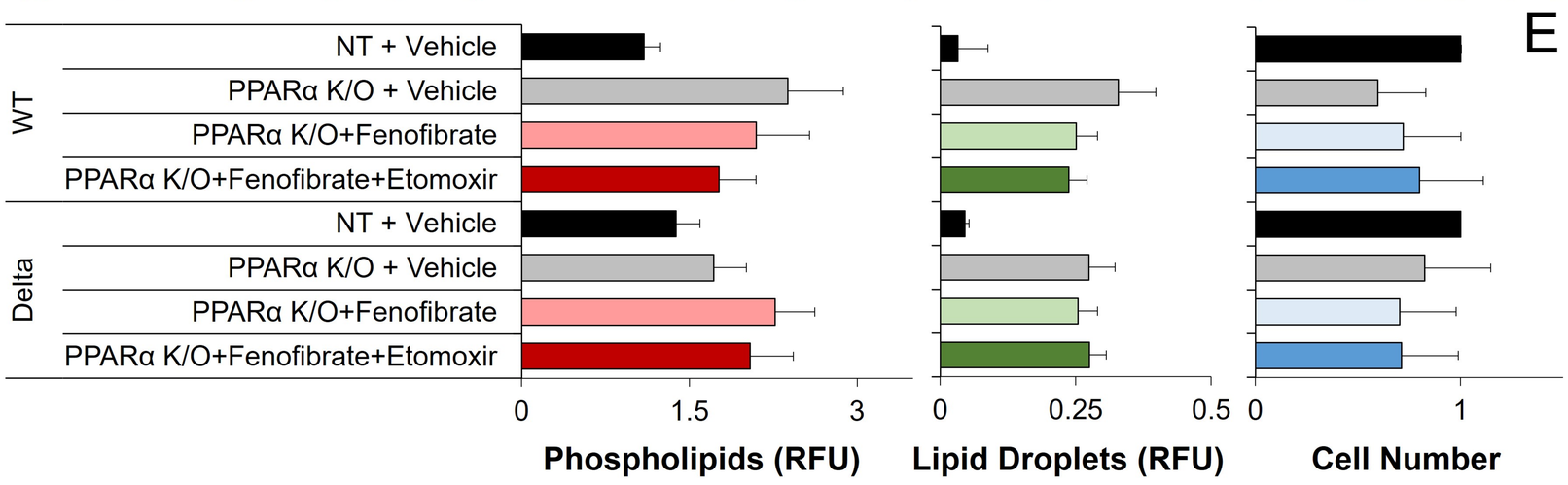
WT
NT + Vehicle
PPARα K/O + Vehicle
PPARα K/O+Fenofibrate
PPARα K/O+Fenofibrate+Etomoxir
Delta
NT + Vehicle
PPARα K/O + Vehicle
PPARα K/O+Fenofibrate
PPARα K/O+Fenofibrate+Etomoxir
0
1.5
3
Phospholipids (RFU)
0
0.25
0.5
Lipid Droplets (RFU)
0
1
Cell Number

E

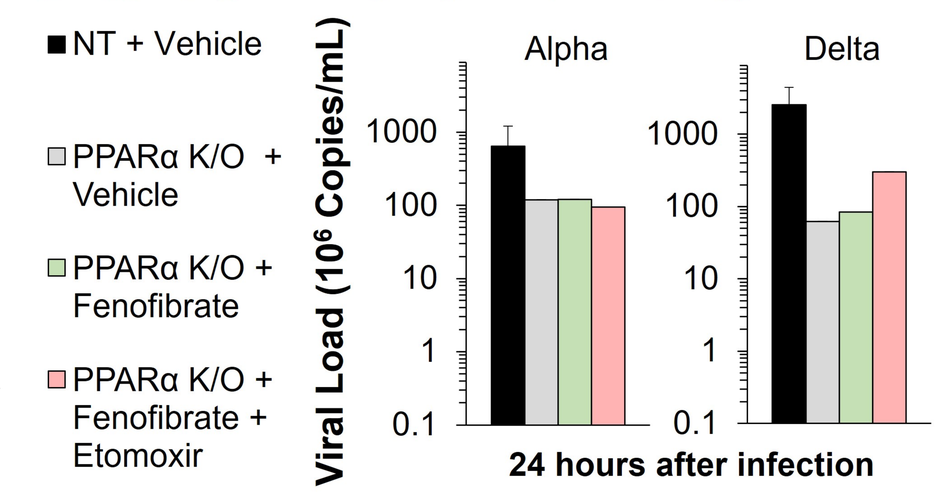
NT + Vehicle
PPARα K/O + Vehicle
PPARα K/O + Fenofibrate
PPARα K/O + Fenofibrate + Etomoxir
Viral Load (10⁶ Copies/mL)
Alpha
Delta
1000
100
10
1
0.1
24 hours after infection

A

COVID-19 Severity in Patients under Metabolic Treatments

Hospitalization Duration

B

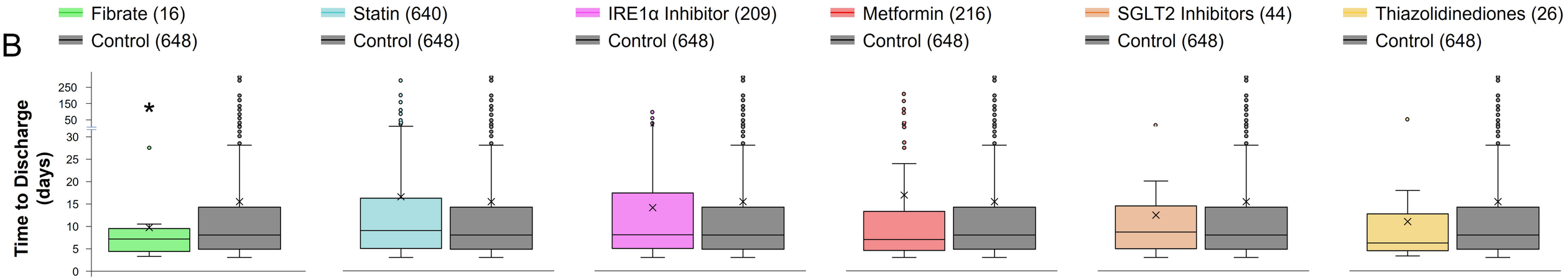

Disease Severity Biomarkers

C

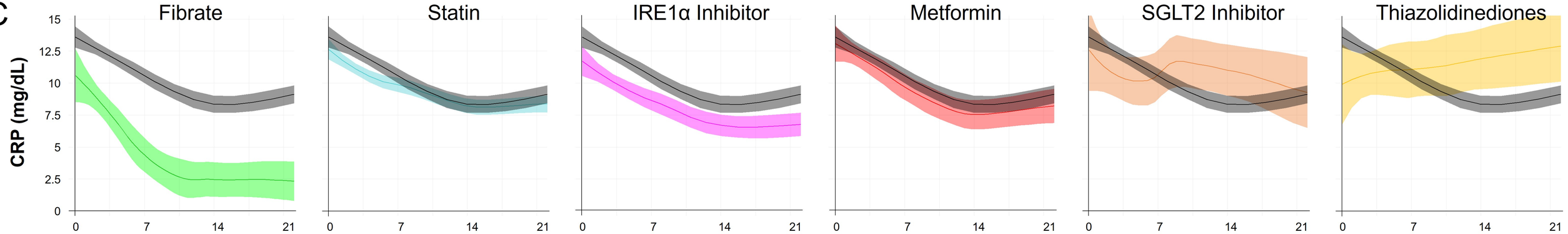

D

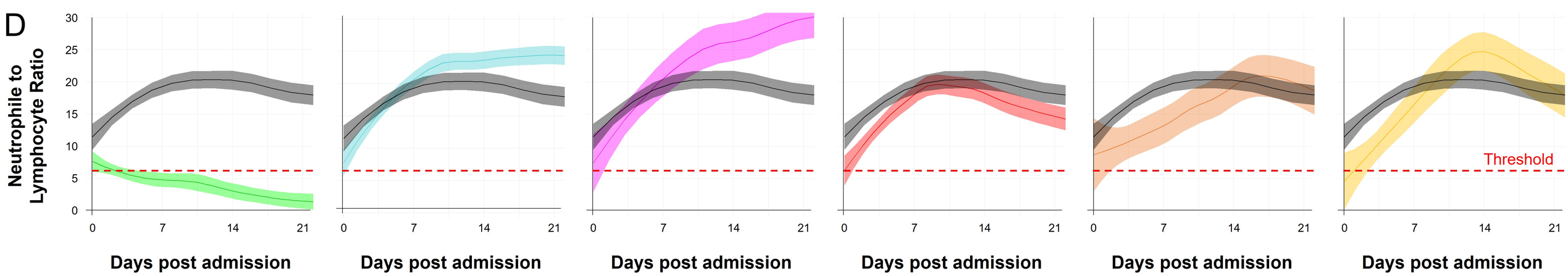

28-Days Mortality

E

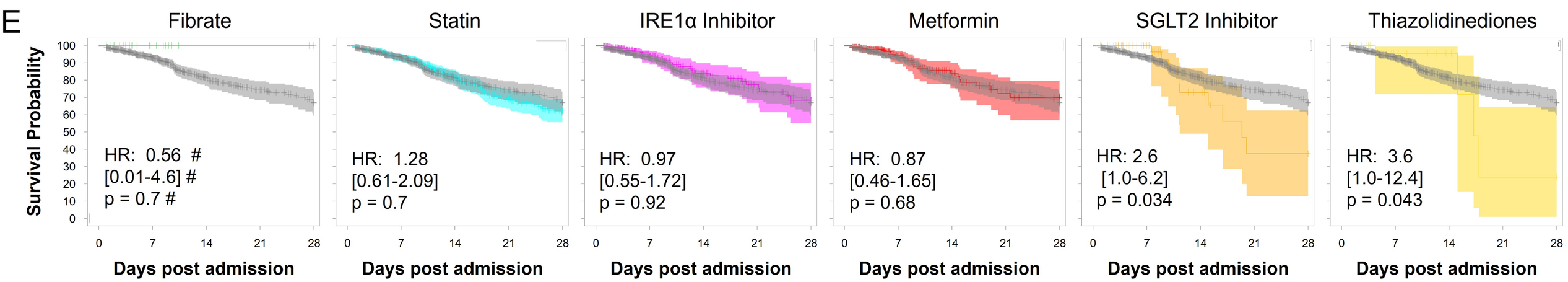

Admissions to COVID ward/ICU
N=4,480

COVID-19 patients
N=4,000

COVID-19 patients with complete electronic records
N=3,815

COVID-19 patients matching inclusion criteria
N=3,410

Adult COVID-19 patients
(Non-missing age > 18)
N=3,233

At-risk COVID-19 patients
(age > 30)
N=2,806

High-risk COVID-19 patients
(age > 45, hospitalization > 3 days)
N=1,438

Unique medical records
(hospital visits)
N(10 yrs)=532,493
N(5 yrs)=249,939
N(1 yr)=51,483

Relative risk (representation) analysis
(Wald test)

Any metabolic regulating drug used
N(10 yrs)=158,211 (29.71%)
N(5 yrs)=82,037 (32.82%)
N(1 yr)=18,267 (35.48%)

No metabolic regulating drug used
N=1,691

Any metabolic regulating drug used
N=1,115
(39.74%)

Fibrates
N=21
(0.75%)

Statins
N=924
(32.93%)

Thiazolidinediones
N=37
(1.32%)

SGLT2 inhibitors
N=54
(1.92%)

Ire1α inhibitors
N=278
(9.91%)

Metformin
N=321
(11.44%)

Clinical outcomes assessment

Dynamic changes in the inflammation and immunoinflammatory stress markers
(Lowess)

Time-to-event and risk analysis
(Kaplan-Meir and adjusted mixed-effect Cox)

No metabolic regulating drug used
N=648

In-hospital use of metabolic regulating drug
N=790
(54.94%)

Fibrates
N=16
(1.11%)

Statins
N=640
(44.51%)

Thiazolidinediones
N=26
(1.81%)

SGLT2 inhibitors
N=44
(3.06%)

Ire1α inhibitors
N=209
(14.53%)

Metformin
N=216
(15.02%)

Immune Markers

Fibrate (16) | Control (648)
Statin (640) | Control (648)
IRE1α Inhibitor (209) | Control (648)
Metformin (216) | Control (648)
SGLT2 Inhibitors (44) | Control (648)
Thiazolidinediones (26) | Control (648)

A
Neutrophils (10^9 Cells/L)
15
12.5
10
7.5
5
2.5
0
UNL

B
Lymphocytes (10^9 Cells/L)
4
3
2
1
0
LNL

C
Monocytes (10^9 Cells/L)
0.6
0.4
0.2
0
UNL

D
Platelets (10^9 /L)
400
300
200
LNL

0 7 14 21
Days after admission

Lipotoxicity Induce Inflammation in Lung Epithelial Cells

E
Neutral Lipids
Phospholipids
DNA
Control
Rosiglitazone
Rosiglitazone + Fenofibrate

F
Relative Expression
50
5
0.5
5000
500
50
5
0.5
CCL20 CXCL1 CXCL2 CXCL5 GCSF IL-1b NFKB2 SAA2
IL-6 IL-8 TNFa
Control
Rosi
Rosi + FF

Interventional Study

A

- Presumptive positive lab test for SARS-CoV-2

Within 48 hours of admission:

- Requiring supp. oxygen
- Room air SaO2 <93%
- PaO2/FiO2 < 300
- SOFA < 5
- Lesions in chest CT

Sampling the Intervention Group

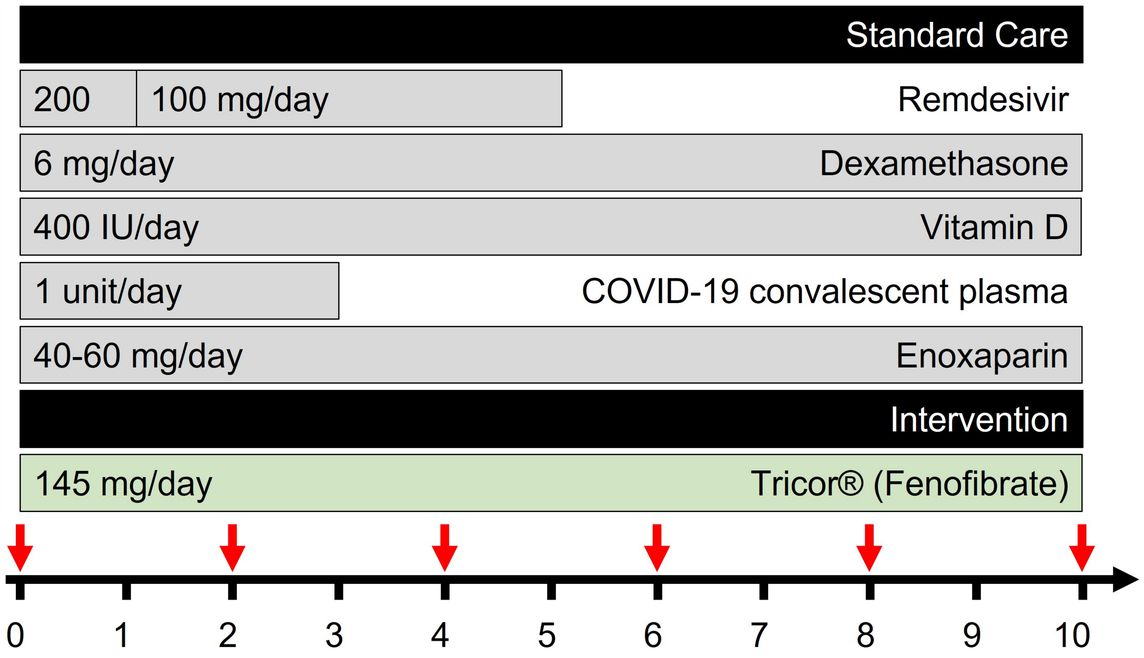

B

Drug	Nanocrystallized Fenofibrate **(TriCor®)**
Chemical Structure	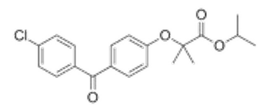
Clinical Use	Dyslipidemia (hypertriglyceridemia)
Dose	145 mg/day
Cmax	7.9 ± 1.6 µg/mL
Tmax	2.3 ± 0.7 hrs

C

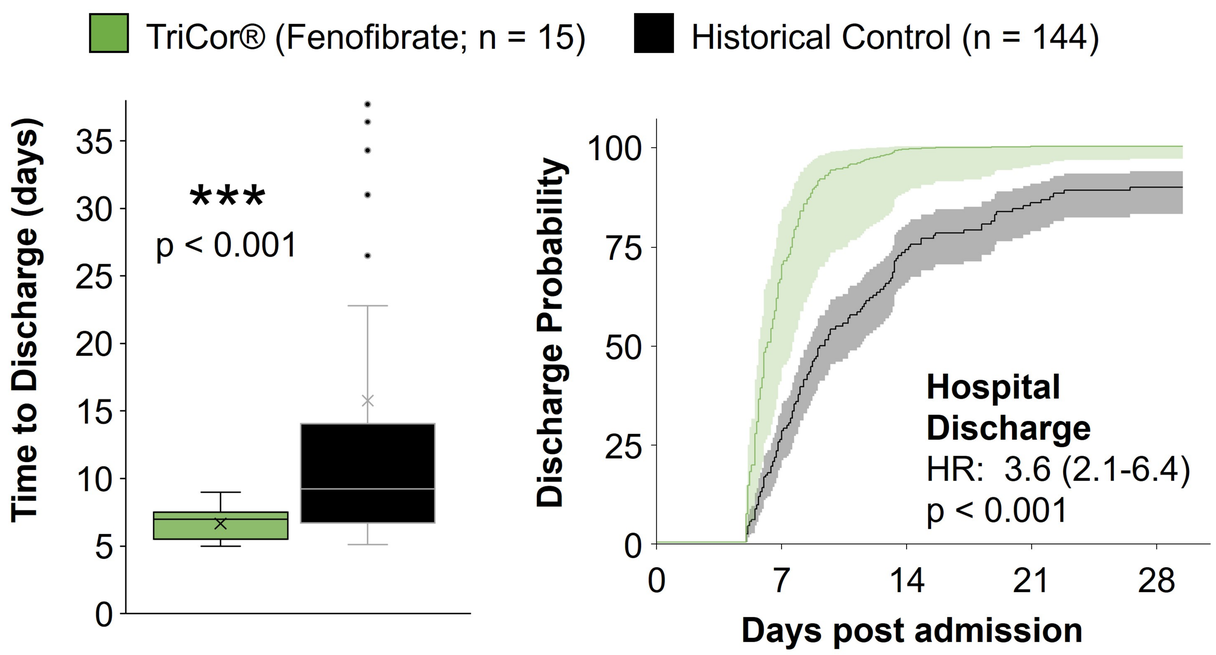

D

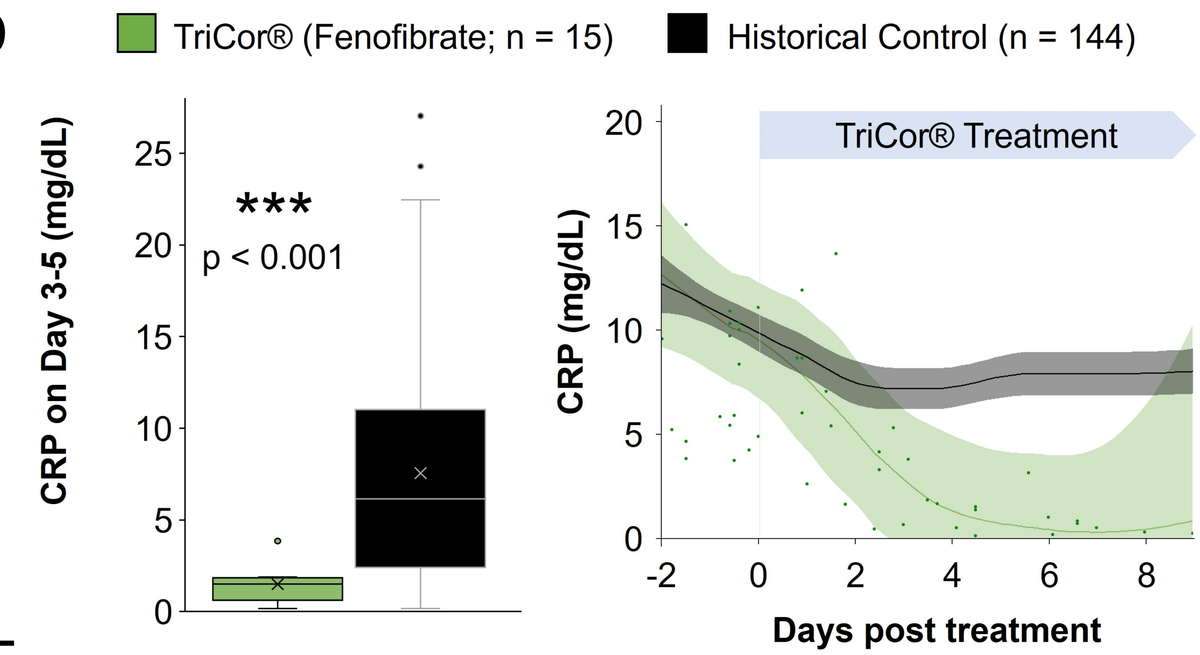

E

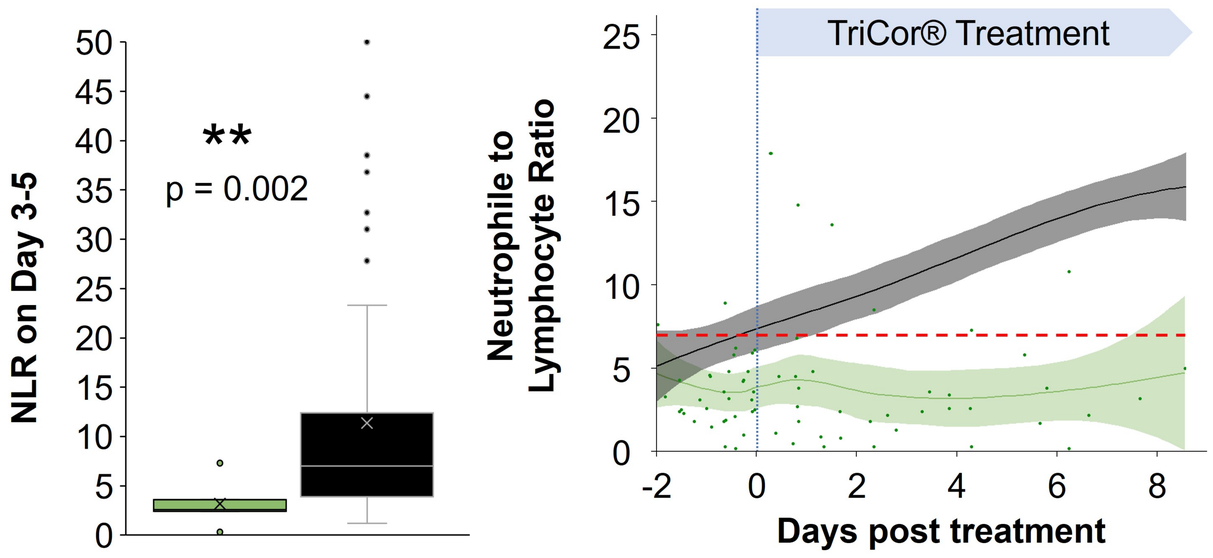

F

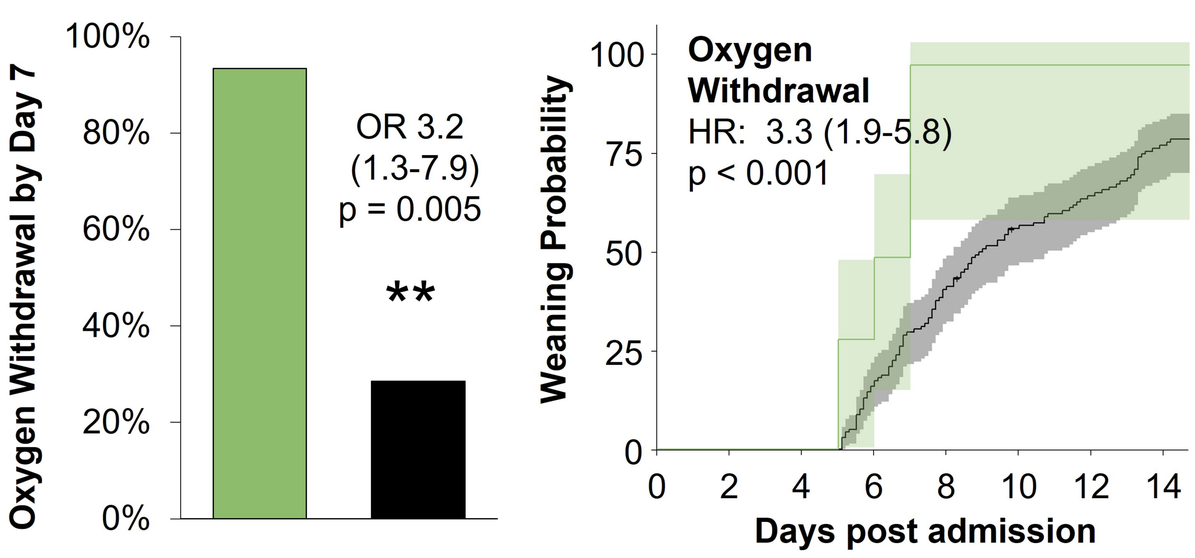

G

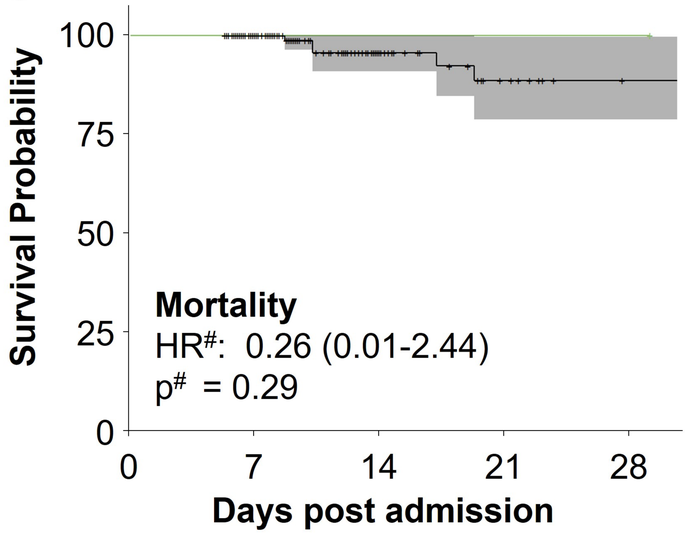

H

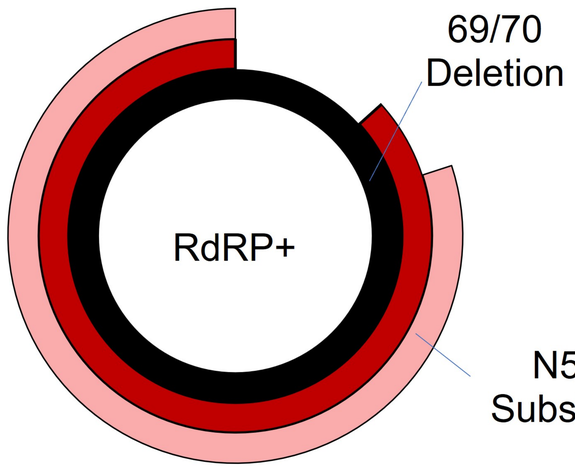

I

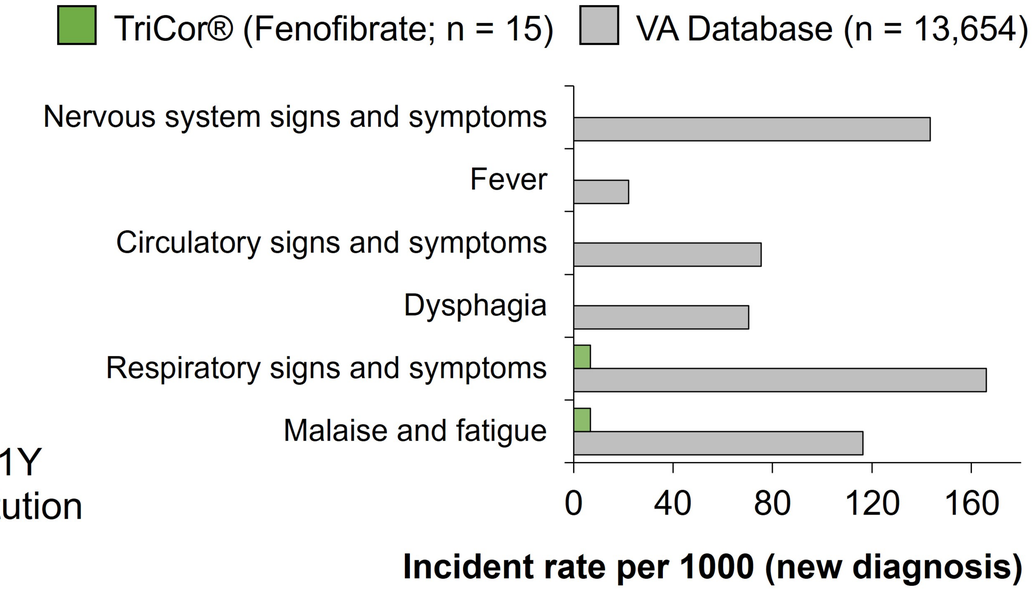

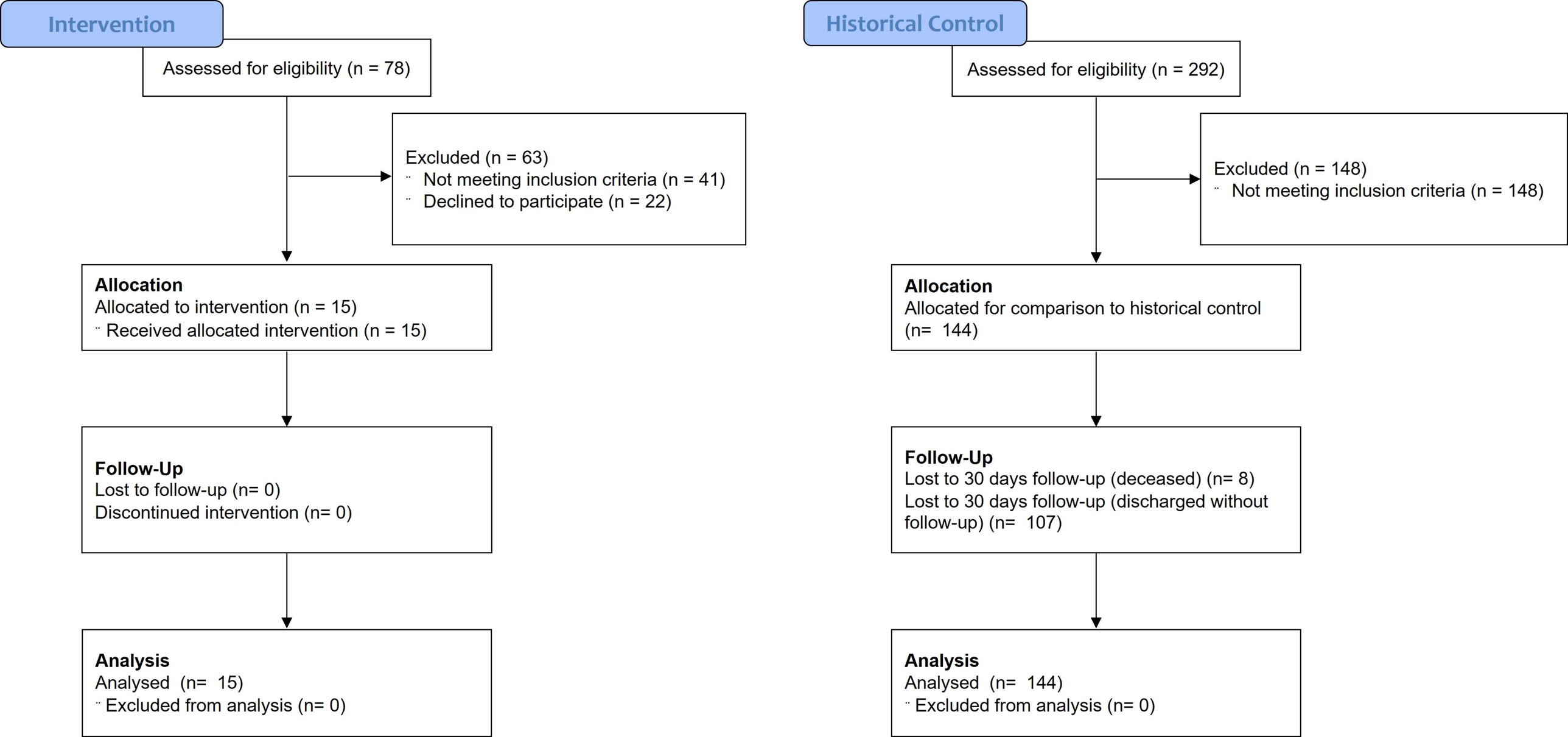
Intervention
Assessed for eligibility (n = 78)
Excluded (n = 63)
Not meeting inclusion criteria (n = 41)
Declined to participate (n = 22)
Allocation
Allocated to intervention (n = 15)
Received allocated intervention (n = 15)
Follow-Up
Lost to follow-up (n= 0)
Discontinued intervention (n= 0)
Analysis
Analysed (n= 15)
Excluded from analysis (n= 0)
Historical Control
Assessed for eligibility (n = 292)
Excluded (n = 148)
Not meeting inclusion criteria (n = 148)
Allocation
Allocated for comparison to historical control (n= 144)
Follow-Up
Lost to 30 days follow-up (deceased) (n= 8)
Lost to 30 days follow-up (discharged without follow-up) (n= 107)
Analysis
Analysed (n= 144)
Excluded from analysis (n= 0)

A

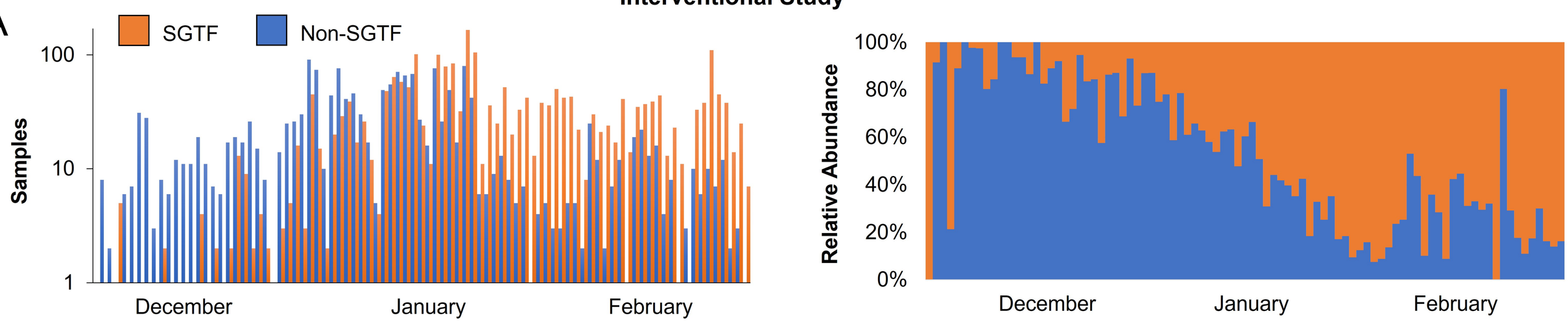

B

C

Period	Odds Ratio (95%CI)	p value
16-31 Dec	4.02 (0.05-316.61)	0.36
1-15 Jan	2.33 (0.17-32.2)	0.59
16-31 Jan	1.43 (0.33-6.24)	0.75
1-15 Feb	0.78 (0.12-4.02)	1
16-28 Feb	1.2 (0.09-16.67)	1

D